The Dissertation Committee for Lauren Avery Mitchell Certifies that this is the approved version of the following dissertation:

Functional Polymers: Polyoxanorbornene-Based Block Copolymers for the Separation of *f*-Elements and Luminescent Conducting Metallopolymers

Committee:

Bradley J. Holliday, Supervisor

Richard A. Jones

Simon M. Humphrey

Sheldon Landsberger

Christopher J. Ellison

Functional Polymers: Polyoxanorbornene-Based Block Copolymers for the Separation of *f*-Elements and Luminescent Conducting Metallopolymers

by

Lauren Avery Mitchell, BSCh

Dissertation

Presented to the Faculty of the Graduate School of

The University of Texas at Austin

in Partial Fulfillment

of the Requirements

for the Degree of

Doctor of Philosophy

The University of Texas at Austin

May 2014

Dedication

To my family,

for supporting me even though you aren't quite sure what I am doing.

Acknowledgements

Dr. Brad Holliday's continued enthusiasm for science even in the face of failure has inspired me to push further and find success in my projects. I would not have made it without his guidance and inspiration. In addition I would like to thank my committee for their help and support, Dr. Simon Humphrey, Dr. Richard Jones, Dr. Sheldon Landsberger, and Dr. Christopher Ellison.

Everyone in the Holliday group has contributed to my success. I'd like to thank Josh Biberdorf, Travis Hesterberg, Kristen Milum, Michelle Mejía, Monica Villa, and Kate Edelman for teaching me technique. I'd also like to thank Lauren Lytwak, Jordan Dinser, Sarah Moench, Kristin Suhr, and Kate Crawford for their help and friendship.

I would like to thank Rachel Butorac and Vincent Lynch for introducing me to and teaching me X-ray crystallography, it has been one of my most enjoyed activities in graduate school. Josh Katstien and Joon Cho in the Ellison group have been so kind in assisting me with GPC. Issac Arnquist in the Holcombe lab was kind enough to assist me with ICP-MS. Minh Nguyen has been a great help in his advice on various projects as well as running XPS for me.

I am grateful to my husband Dan Mitchell and the rest of my family for being there for me when I was stressed. I would like to thank Dan for listening to my practice talks, listening to me complain, and generally supporting my endeavors. I would like to thank my father for seeming genuinely interested in what I do. I would like to thank my mom and my sister for being proud of me.

FUNCTIONAL POLYMERS: POLYOXANORBORNENE-BASED BLOCK COPOLYMERS FOR THE SEPARATION OF *F*-ELEMENTS AND LUMINESCENT CONDUCTING METALLOPOLYMERS

Lauren Avery Mitchell, Ph.D.

The University of Texas at Austin, 2014

Supervisor: Bradley J. Holliday

A new polymeric material with a polyoxanorbornene backbone and carbamoylmethylphosphine oxide, CMPO, ligand pendant groups has been synthesized, characterized, and studied. The ability of the material to selectively partition actinides utilizing a biphasic extraction strategy was tested. The polymeric materials had significantly higher (> 5-25 times) ability to extract Th^{4+} than the monomeric system. The molecular weight of the material affected the extraction and separation abilities. The lower molecular weight material extracted more ions, but was less discriminate for thorium(IV) over cerium(III), lanthanum(III), and europium(III), than the higher molecular weight material. Structural modifications to this system were made by creating block copolymers. The influence of additional functionalities, created by the addition of new polymeric blocks, was investigated. The ability of the material to selectively partition actinides utilizing both solid-liquid and liquid-liquid extraction strategies was tested. Extraction efficiencies comparable to liquid-liquid extractions were achieved in the solid-liquid extractions. The extraction behavior of the materials was significantly altered by the incorporation of new blocks. The incorporation of glycol chains into the system caused an increase in the uptake of thorium(IV) over the homopolymers. The

incorporation of blocks of glycol chains and blocks of cross-linked hydroxcoumarian increased the selectivity significantly ($X_{Th/Eu}$ 2.3 – 4.5 times higher) over the homopolymer. These materials show tremendous promise as modular polymeric scaffolds.

A novel emissive tetradentate platinum complex with electropolymerizable ethylenedioxythiophene groups has been synthesized and characterized. This material has been developed for use as the active layer in polymer light-emitting diodes. Electropolymerization offers ease of processing by depositing thin films directly onto an electrode during the polymerization process. Additionally because the emitter is covalently bound in the polymer, it cannot aggregate as is the case with some small molecule emitters. The platinum complex displayed emission peaks at 510 nm and 544 nm. Electropolymerization resulted in a conductive and emissive thin film, with an emission maximum at 453 nm.

Table of Contents

List of Tables

List of Figures

List of Schemes

SEPARATION OF *f*-ELEMENTS

Chapter 1: Influence of CMPO Platform on Liquid-Liquid *f*-element Extractions

INTRODUCTION

One of the issues that continues to plague the furtherance of nuclear technologies is the disposal of spent fuel. Currently spent fuel rods in the United States remain in storage at the reactor site, since no long term storage or disposal plan has been implemented.[1] As of 2013, the United States has generated approximately 68,000 MTHM (metric tons of heavy metal) of used nuclear fuel, with an estimated growth of 2,000 MTHM per year.[2] Many of the radionuclides in the spent fuel will decay to stable isotopes within approximately 300 years, yet others will continue to be radioactive for a millennia.[3] This makes engineering a burial system that will last the lifetime of the radioactivity unfeasible.

A proposed solution to this issue is a process termed partitioning and transmutation, whereby the various elements in the fuel are separated and then buried as less hazardous waste or transmuted into less harmful isotopes.[4] Transmutation, however, requires that those elements with high neutron cross sections first be removed. One of the most difficult of these separations involves partitioning of actinides and lanthanides.

Demonstrated in the transuranic extraction (TRUEX) process was the ability of the carbomylmethylphosphine oxide (CMPO) ligand to selectively bind to actinides over lanthanides see Figure 1.1.[5–7] Reprocessing spent fuel begins with the dissolution of the fuel rods in nitric acid. In the TRUEX process actinides are sequestered from the aqueous acidic media into an organic medium by chelation through the carbonyl and phosphoryl oxygens of three CMPO ligands.[7]

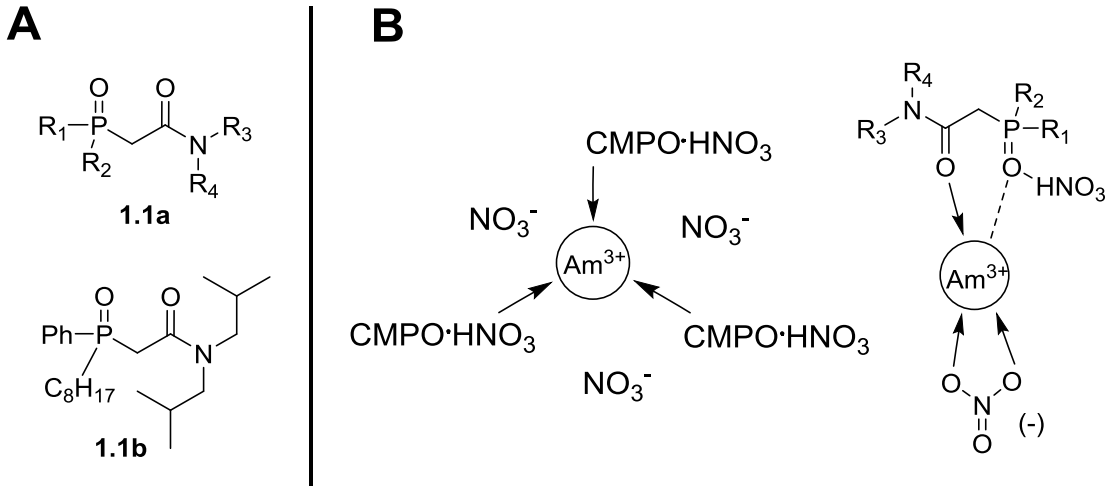

Figure 1.1: (A) **1.1a** general form carbamoylmethylphosphine oxide (CMPO) ligand, **1.1b** *n*-octyl(phenyl)-*N*,*N*-diisobutyl-methylcarbamoyl phosphine oxide (B) Proposed solution structure of americium(III) CMPO complex in nitric acid.[8]

Efforts to improve separation factors have currently focused on preorganizing several CMPO moieties onto a small molecule substrate. In this effort a variety of different small molecule platforms have been developed. Herein is a review of the current mutli-CMPO systems present in the literature. Discussed will be the varying effects each type of platform has on the extraction properties of the system.

LINEAR OLIGOMER SYSTEMS

The simplest system which covalently binds two or more CMPO units together is the linear oligomer system, shown in Figure 1.2.[8–10] Unlike the other systems which typically have 3-4 CMPO units, the linear systems vary more widely with 2-5 CMPO units. Many of these systems are structurally very similar to calixarenes, with methyl linked phenols. The linear oligomer systems have been studied for their ability to extract thorium(IV) and europium(III), the results are summarized in Table 1.1

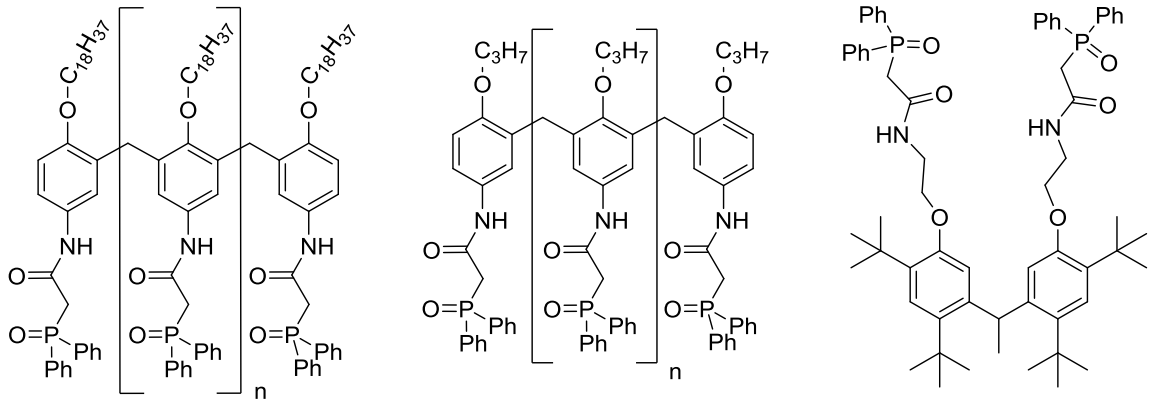

Figure 1.2: CMPO-derivatized linear compounds.[8–10]

Compounds **1.2a** and **1.2b** both show discrimination for thorium(IV) over europium(III). The importance of the chelate effect is observed in the comparison of the performance of these two materials. Compound **1.2b**, which has three CMPO arms binds to significantly more thorium(IV) than compound **1.2a**, which has only two CMPO arms. Unlike many other materials, the increased uptake of throium(IV) is not accompanied by an increase in the uptake of the lanthanide europium(III). This results in an increase in extraction as well as separation efficiency by the addition of a third CMPO unit.

Compounds **1.3a** – **1.3d** vary only in the length of the alkyl chain on the phenol from compounds **1.2a** – **1.2b**. This difference has resulted in drastically different chelation properties. While compound **1.2a** was able to extract 17% of the present thorium(IV) at 1 : 1 (ligand : Th^{4+}), the shortening of the alkyl chain resulted in a decrease to 6% for compound **1.3b** at 10 : 1 (ligand : Th^{4+}). A similar trend was observed for compounds **1.2b** and **1.3b**, where compound **1.2b** extracted 78% of the thorium at 1 : 1 (ligand :

Th^{4+}), and compound **1.3b** extracted only 18% with a higher concentration of ligand (10 : 1, ligand : Th^{4+}). Additionally compounds **1.3a** and **1.3b** extracted increased amounts of europium(III) than their counterparts with shorter alkyl chains, compounds **1.2a** and **1.2b**. Decreasing the length of the alkyl chain resulted overall in a decrease in both the extraction and separation efficiencies.

Table 1.1: Extraction (% E) of thorium(IV) and europium(III) by linear oligomer compounds.

# CMPOs	Ligand	Equiv of ligand in organic phase	% Th	% Eu
2	**1.2a**[8]	1	17	
		10		< 3
3	**1.2b**[8]	1	78	
		10		< 3
2	**1.3a**[10]	10	6	
		100		4
3	**1.3b**[10]	10	18	
		100		24
4	**1.3c**[10]	1	35	
		10		56.5
5	**1.3d**[10]	1	31	
		10		38.1
2	**1.4**[9]	10	4	6

Equal volumes organic/aqueous phases, organic phase: CH_2Cl_2, aqueous phase: 1 M HNO_3, $C_M = 10^{-4}$ M.

When the number of repeat units is increased in system **1.3** an increase is observed in the extraction of both thorium(IV) and europium(III). This increase continues from dimer to tetramer, but decreases again for the pentamer. The separation efficiency decreases from dimer to tetramer, and then increases again for the pentamer.

The switch to a different linear oligomer platform, **1.4**, gave vastly different extraction values than the dimers **1.2a** and **1.3a**. Compound **1.4** extracted small quantities of europium(III), yet it is not discriminate; at equal ligand concentrations, complex **1.4** actually showed an increased selectivity for europium(III).

Table 1.2: Distribution coefficients for the extraction of Eu(III) and Am(III) for select linear oligomer systems.

# CMPOs	Ligand	D_{Am}	D_{Eu}	$S_{Am/Eu}$
2	**1.2a**[8]	1.8	1.2	1.50
3	**1.2b**[8]	17	13	1.31

Equal volumes organic/aqueous phases, organic phase: nitrophenyl hexyl ether, $C_L = 10^{-3}$ M, aqueous phase: 1 M HNO_3.

Compounds **1.2a** and **1.2b** were also tested for their ability to selectively chelate americium(III), see Table 1.2. The extraction efficiencies are described by the distribution coefficient, D_M, defined in equation 1.1, where $\Sigma[M_{org}]$ represents the concentration of cations in the organic layer and $\Sigma[M_{aq}]$ the cations in the aqueous layer.

$$D_M = \Sigma[M_{org}]/ \Sigma[M_{aq}] \qquad (1.1)$$

The separation efficiencies are described by $S_{M1/M2}$, defined by equation 1.2.

$$S_{M1/M2} = D_{M1} / D_{M2} \qquad (1.2)$$

These systems were found to be selective for americium(III) over europium(III). The increase from 2 to 3 CMPOs resulted in a slight decrease for the selectivity, but resulted in a large increase in the affinity for americium(III).

Generally the linear systems displayed increased extraction efficiencies with additional CMPO moieties which may be due to an increased chelate effect. Also the

linear systems displayed increased extraction and separation efficiencies with longer alkyl chains on the platform, possibly due to an increase in solubility.

MACROCYCLIC PLATFORMS

Calixarenes

CMPO derivatized calixarenes are among the most widely studied of CMPO platform systems. The appendage of the CMPO moiety can be made on the upper wide rim, or on the lower narrow rim, see Figure 1.3. Attachment of groups larger than ethyl to R_2 on the narrow rim fixes the molecule into a single conformation. By contrast tetramethyl ethers have been shown to have the flexibility to adopt cone, partial cone, 1,2-alternate, or 1,3-alternate conformations.[11] The size of calixarene cycles can vary from three phenyl rings to more than eight.[12] As the number of phenyls is increased the flexibility of the system increases affecting the preorganization properties.

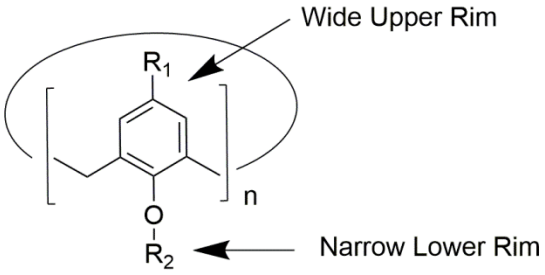

Figure 1.3: General form of calixarenes illustrating wide and narrow rims.

Wide Rim

The wide rim (wr) calixarenes, shown in Figure 1.4, generally have larger binding cavities than the narrow rim calixarenes.[8,10,13,14] Additionally the wide rim calixarenes

have been more extensively studied than the narrow rim calixarenes. Summarized in Table 1.3 are extractions performed with thorium(IV) and europium(III). To easily compare the separation efficiencies, $X_{Th/Eu}$, was calculated using equation 1.3, where % Th is the percentage of thorium(IV) extracted from a 10^{-4} M solution of thorium(IV) by a 10^{-4} M solution of ligand, and % Eu is the percentage of europium(III) extracted from a 10^{-4} M solution of europium(III) by a 10^{-3} M solution of ligand.

$$X_{Th/Eu} = (\%\ Th) / (\%\ Eu) \qquad (1.3)$$

Compounds **1.5a** – **1.5f** vary in the length of the alkyl chain on the narrow rim, from C_{10} to C_{18}. Although the amount of thorium(IV) extracted between these systems varied, the increase in chain length does not cause any trend in the extraction data. The selectivity for the systems did not vary greatly and ranged for $X_{Th/Eu}$ from 0.75 to 1.08. Compounds **1.7e** and **1.7f** also varied in the length of the alkyl chain on the narrow rim, with compound **1.7e** containing methyl groups and compound **1.7f** containing propyl groups. This variation did not cause significant changes in the amount of thorium(IV) extracted, however, unlike compounds **1.5a** – **1.5f**, the increase in chain length did cause significant differences in the selectivity for thorium(IV). Compound **1.7e**, with methyl chains displayed much higher selectivties ($X_{Th/Eu}$ = 1.7) than compound **1.7f**, with propyl chains ($X_{Th/Eu}$ = 0.97). The selectivity for compound **1.7f** fell within the range seen for complexes **1.5a** – **1.5f**, but the selectivity for compound **1.7e** is much higher. Compounds **1.5a** – **1.5f** and **1.7f** all have groups larger than ethyl on the narrow rim. These large groups are likely limiting the possible conformations of the molecule. In contrast, complex **1.7e** contains groups smaller than ethyl and can thus likely adopt more conformations. Conformational differences may explain the differences in selectivity between these compounds.

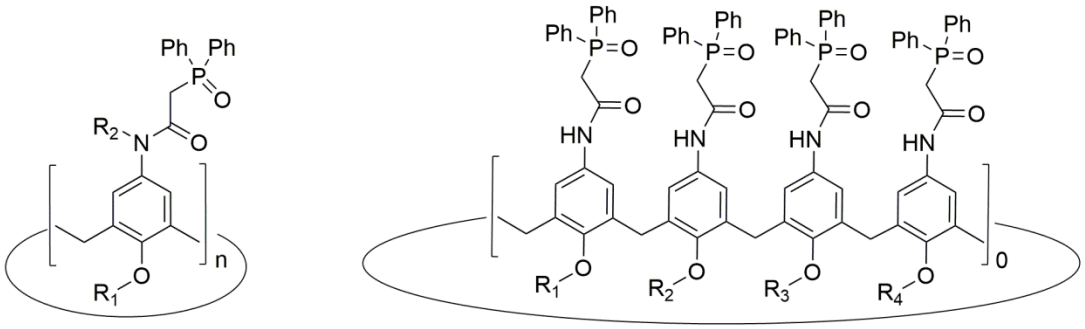

1.5a n=4 R_1= C_5H_{11}, R_2 = H
1.5b n=4 R_1 = $CH_2CH(C_4H_9)_2$, R_2 = H
1.5c n=4 R_1 = $C_{10}H_{21}$, R_2 = H
1.5d n=4 R_1 = $C_{12}H_{25}$, R_2 = H
1.5e n=4 R_1 = $C_{14}H_{29}$, R_2 = H
1.5f n=4 R_1 = $C_{16}H_{33}$, R_2 = H
1.5g n=4 R_1 = $C_{18}H_{37}$, R_2 = H
1.5h n=5 R_1 = $C_{14}H_{29}$, R_2 = H
1.5i n=4 R_1 = C_5H_{11}, R_2 = CH_3

1.7a R_1 = CH_3, R_2 = CH_3, R_3 = CH_3, R_4 = C_3H_7
1.7b R_1 = CH_3, R_2 = C_3H_7, R_3 = CH_3, R_4 = C_3H_7
1.7c R_1 = CH_3, R_2 = CH_3, R_3 = C_3H_7, R_4 = C_3H_7
1.7d R_1 = CH_3, R_2 = C_3H_7, R_3 = C_3H_7, R_4 = C_3H_7
1.7e R_1 = CH_3, R_2 = CH_3, R_3 = CH_3, R_4 = CH_3
1.7f R_1 = C_3H_7, R_2 = C_3H_7, R_3 = C_3H_7, R_4 = C_3H_7

1.6a R = $CH_2CH(C_4H_9)_2$
1.6b R = $C_{10}H_{21}$
1.6c R = $C_{18}H_{37}$

1.8

1.9

Figure 1.4: Calixarenes derivatized with CMPO at the wide rim.[8,10,13,14]

Compounds with mixed length chains out perform their single chain length counterparts. Compounds **1.6a** – **1.6c** have mixed alkyl systems on the narrow rim. Complex **1.6b** contains two C_{10} chains and two methyl groups, while complex **1.5c** contains four C_{10} chains. Comparing the two, compound **1.6b** extracts more thorium(IV) than **1.5c** and is also more discriminate for thorium(IV) over europium(III). This trend holds true with the two other pairs of compounds with the same R group, **1.6a** and **1.5b**,

and **1.6c** and **1.5g**. For all three pairs the replacement of two R groups with methyl groups increases the extraction and separation efficiencies. Compounds **1.7a** – **1.7d** examine this further by probing the placement and ratio of mixed chain lengths. All of the mixed systems, compounds **1.7a** – **1.7d**, extract more thorium(IV) than their homogenous counterparts **1.7e** and **1.7f**. The **1.7** system that was found to be the most discriminate for thorium(IV) was not a mixed system, but the homogenous system **1.7e** with four methyl groups at the narrow rim. The selectivity decreases as more of the methyl groups are replaced by longer chains, (**1.7e** (4 methyls) > **1.7a** (3 methyls) > **1.7b** (2 methyls) > **1.7d** (1 methyl) > **1.7f** (0 methyl)). The placement of the methyl groups was found to be significant, compounds **1.7b** and **1.7c** both have two methyl groups and two propyl alkyl groups on the narrow rim. In compound **1.7b** the methyl and propyl groups are alternated, while in compound **1.7c** the methyl groups are placed right next to each other. Compound **1.7c** was found to extract slightly more thorium(IV) than compound **1.7b**, but complex **1.7b** was found to be significantly more discriminate for thorium(IV) than compound **1.7c**. The selectivity for compound **1.7c**, with only two methyl groups, is comparable to that of compound **1.7f**, which contains four propyl groups on the narrow rim. This indicates that appending methyl groups *trans* to one another on the narrow rim is preferential to methyls being *cis* to one another.

The number of phenyl groups in the macrocycle also influences the extraction properties. The length of the alykyl chain is C_{14} for calixarenes **1.5e** and **1.5h**, but the two vary in the number of phenyl groups in the macrocycle; **1.5e** has four phenyls, while compound **1.5h** has five phenyls. The tetramer, **1.5e**, extracted slightly more thorium(IV) than the pentamer, **1.5h**. A similar trend was observed for the linear analogs **1.3c** and

1.3d, which also had a decrease in the uptake of thorium(IV) from the tetramer to the pentamer.

Table 1.3: Extraction (% E) of thorium(IV) and europium(III) by select macrocyclic compounds.

# CMPOs	Type	Ligand	% Th ($C_L = 10^{-4}$ M)	% Eu ($C_L = 10^{-3}$ M)	$X_{Th/Eu}$
4	Calixarene (wr)	**1.5a**[8]	39	47	0.83
4	Calixarene (wr)	**1.5b**[8]	26	24	1.08
4	Calixarene (wr)	**1.5c**[8]	53	68	0.78
4	Calixarene (wr)	**1.5d**[8]	63	68	0.93
4	Calixarene (wr)	**1.5e**[8]	54	72	0.75
4	Calixarene (wr)	**1.5f**[8]	51.5	69.5	0.74
4	Calixarene (wr)	**1.5g**[8]	50	59	0.85
5	Calixarene (wr)	**1.5h**[8]	46	-	-
4	Calixarene (wr)	**1.5i**[14]	9	9	1.00
4	Calixarene (wr)	**1.6a**[8]	32	20	1.60
4	Calixarene (wr)	**1.6b**[8]	39	40	0.98
4	Calixarene (wr)	**1.6c**[8]	43	49	0.88
4	Calixarene (wr)	**1.7a**[10]	69	45	1.53
4	Calixarene (wr)	**1.7b**[10]	66	48	1.38
4	Calixarene (wr)	**1.7c**[10]	70	73	0.96
4	Calixarene (wr)	**1.7d**[10]	66	60	1.10
4	Calixarene (wr)	**1.7e**[10]	60	35	1.71
4	Calixarene (wr)	**1.7f**[10]	61.8	64	0.97
4	Calixarene (nr)	**1.10a**[15]	76	16	4.75
4	Calixarene (nr)	**1.10b**[15]	81	12.5	6.48
4	Calixarene (nr)	**1.10c**[15]	96	68	1.41
4	Cavitand	**1.15a**[16]	24	11[a]	2.18[a]
4	Cavitand	**1.15b**[16]	17	9[a]	1.88[a]

Equal volumes organic/aqueous phases, organic phase: CH_2Cl_2, aqueous phase: 1 M HNO_3, $C_M = 10^{-4}$ M. (a) $C_L = 10^{-4}$ M.

Compounds **1.5a** and **1.5i** vary in the amide; **1.5a** is a secondary amide, while **1.5i** is a tertiary amide. This small synthetic difference causes large changes in the amount of

thorium(IV) extracted. Complex **1.5a** extracted 39% of the present thorium(IV), while complex **1.5i** only extracted 9%. Complex **1.5i** ($X_{Th/Eu}$ = 1.00) does show a modest increase in the selectivity for thorium(IV) over complex **1.5a** ($X_{Th/Eu}$ = 0.83).

A study of the distribution coefficient as a function of ligand concentration was performed and a log-log plot revealed a linear relationship between the two variables. For the extraction of thorium(IV) compounds **1.5b** and **1.5c** have linear plots with slopes of approximately 1, revealing a 1 : 1 complex. Compound **1.6c** does not have a linear plot, suggesting the formation of complexes with multiple stoichiometries. For europium(III) complexes **1.5b**, **1.5c**, **1.6c**, **1.7c**, **1.7e**, and **1.7f** have slopes of approximately 2, suggesting that the europium(III) complexes are extracted by two ligands. CPK-models examined by Böhmer and coworkers reveal that this stoichiometry is possible.[10]

Extraction studies with americium(III) and europium(III) were also performed for complexes **1.5a**, **1.8** and **1.9**, see Table 1.4.[13,17] Compound **1.5a** displayed high extraction and separation efficiencies with americium(III) (D_{Am} = 150, $S_{Am/Eu}$ = 4.05). Attempts were made by Böhmer and coworkers to improve this by increasing the number of CMPOs in close proximity using dendrimer type compounds, see structure **1.8**.[13] Despite the fact that there are more CMPOs available for binding the extraction and separation efficiencies decreased from **1.5a** to **1.8**. Other attempts by Böhmer and coworkers to improve upon **1.5a** included the incorporation of adamantyl groups into the system in an effort to increase the solubility and thus extraction efficiency of the system, see compound **1.9**.[17] Unfortunately, this led to an even larger decrease in the extraction and separation efficiencies from compound **1.5a**.

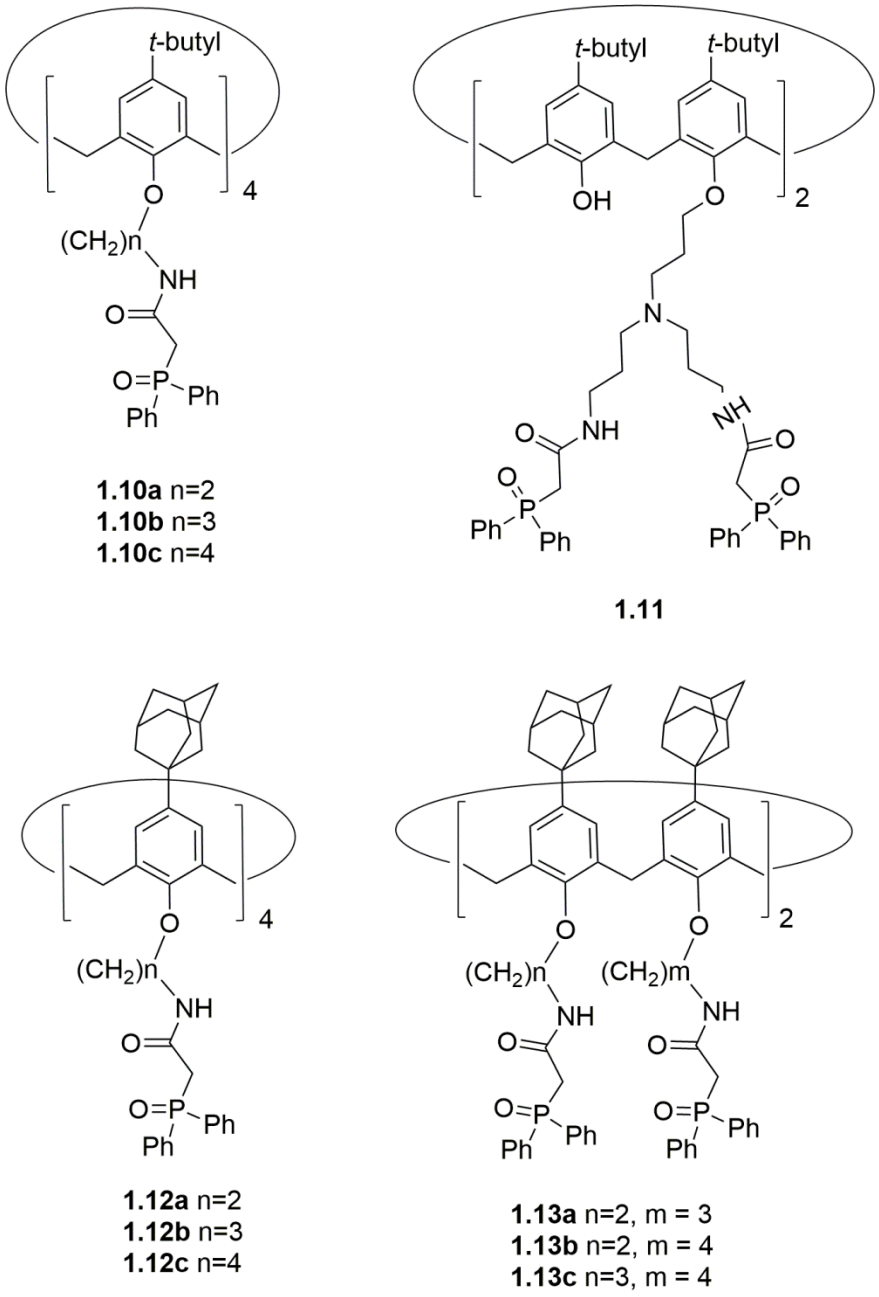

Figure 1.5: Calixarenes derivatized with CMPO at the narrow rim.[13,15,17]

Narrow Rim

Fewer compounds with CMPO on the narrow rim (nr) have been studied than those with CMPO on the wide rim, see Figure 1.5.[13,15,17] These compounds have been studied in extractions with thorium(IV), americium(III), and europium(III), see Tables 1.3 and 1.4.

Similar to the wide rim compound **1.5a**, compound **1.10a** extracted significantly larger amounts of americium(III) than the dendrimer and adamatyl compounds **1.11** and **1.12a** – **1.12c**, and **1.13a** – **1.13c**. Unlike the wide rim system the *tert*-butyl analog **1.10a** was not the most selective for americium(III) over europium(III). In the narrow rim system the dendrimer compound **1.11** is the most selective followed by the adamatyl compound **1.12a**, with **1.10a** being the third most selective.

Compounds **1.10a** – **1.10c** all extract high amounts of thorium(IV) (76 – 96 %), higher than most of the other macrocycles. These materials are also very selective for thorium(IV) over europium(III). Compounds **1.10a** and **1.10b** are the most selective materials for thorium(IV) represented in Table 1.3.

Compounds **1.10a** – **1.10c** vary in the length of the alkyl spacer between the phenol backbone and the CMPO moiety. It was observed that the longer the spacer, the more the thorium(IV) uptake was increased. Complex **1.10c**, with the propyl linkage, extracted nearly quantitative amounts of thorium at a ligand : Th^{4+} ratio of 1 : 1. The most selective material was **1.10b**, with a ethyl linkage, followed by **1.10a**, with a methyl linkage, followed by **1.10c**, with a propyl linkage. It was proposed by Böhmer and coworkers that both the size of the cavity and the flexibility of the ligand system influence the extraction and separation efficiencies.[15] The most flexible compound, **1.10c**, extracted the most material, but the large cavity made it less selective.

Compounds **1.12a** – **1.12c**, also vary in the length of the alkyl spacer between the backbone and the CMPO moiety. These complexes did not show any trend between the amount of americium(III) extracted and the length of the alkyl chain. The selectivity for americium(III) over europium(III) decreased with the increasing length of the alkyl chain, **1.12a** ($(CH_2)_2$) **>** **1.12b** ($(CH_2)_3$) > **1.12c** ($(CH_2)_4$). Compounds **1.13a** – **1.13c** also ranged in the length of the alkyl spacer between the phenol backbone and the CMPO moiety. In this system there were alkyl spacers of varying lengths within a single molecule. The increasing lengths of the alkyl chains caused no trend in the selectivity of these materials, but did cause an increase in the amount of americium(III) extracted. Generally the systems with mixed length alkyl chains, **1.13a – 1.13c** displayed lower extraction and separation values than the analogous systems, **1.12a** – **1.12c**, with homogenous chain lengths.

The europium(III) distribution coefficient as a function of ligand concentration was studied for compounds **1.10b** and **1.10c**. Plots of the log of the distribution coefficient verses the log of the ligand concentration had a linear slope near 1, suggesting that europium(III) is extracted in as a 1 : 1 complex for the narrow rim calixarenes. This is in contrast to the wide rim calixarenes, most of which extract europium(III) as a 2 : 1 (ligand : Eu^{3+}) complex.

Cyclotriveratrylene

Cyclotriveratrylenes, also known as CVTs are cyclic structures composed of phenyls linked by methyl spacers. They are similar to calixarenes except that the methyl linkages occur at the 1 and 2 positions on the phenyl rings for cyclotriveratrylenes, while the methyl linkages are at the 1 and 3 positions for calixarenes. Additionally, while the

size of calixarenes are varied with 3 or more phenyls, cyclotriveratrylenes are generally only 3 phenyls.

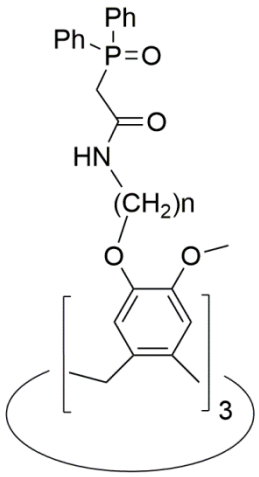

1.14a n = 0
1.14b n = 3
1.14c n = 6

Figure 1.6: Cyclotriveratrylene derivatized with CMPO.[18]

Three CMPO-derivatized CVT macrocycles were synthesized by Verboom and coworkers, see Figure 1.6.[18] The extraction data for americium(III) and europium(III) for these three materials is summarized in Table 1.4. All three materials were found to be selective for americium(III) over europium(III), although they were less selective than some calixarene and cavitands.

The three complexes vary in the length of the alkyl spacer between the macrocycle and the CMPO moiety. Compound **1.14a** has no spacer; CMPO is bound directly to the macrocycle. This rigid conformation is likely the cause of the low extraction values observed for this compound. Increasing the spacer, and creating more flexibility in compounds **1.14b** and **1.14c** increased the extraction efficiency. This is similar to what was observed for calixarenes **1.8a** – **1.8c**, which also displayed an

increased uptake with increased chain length. The selectivity is similar for all three materials ranging from $S_{Am/Eu}$ = 1.4 - 1.6, with the smallest cavity, **1.14a**, being the most selective.

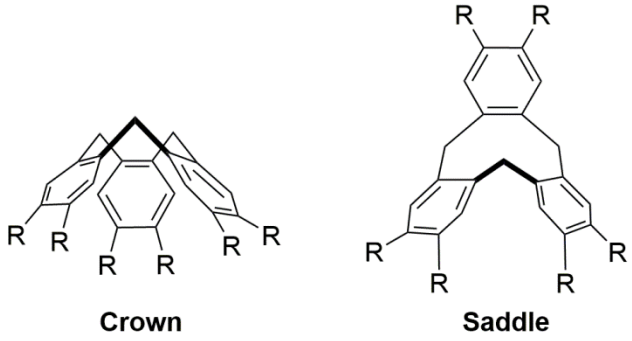

Figure 1.7: Cyclotriveratrylene conformers.[19]

The stoichiometry of the complexes was examined by plotting the log of the distribution coefficient verses the log of the ligand concentration. Compound **1.14a** displayed a linear relationship with a slope of approximately 0.8 for complexation with americium(III) and europium(III). This could indicate a stoichiometry of 5 : 4 metal to ligand ratio, although Verboom and coworkers consider this unlikely for such a rigid ligand.[18] It is possible that complexes with "saddle geometry" have been formed, see Figure 1.7. The slope of the logD vs log[L] plots for compounds **1.14b** and **1.14c** with americium(III) and europium(III) was approximately 1.3. This indicates a metal to ligand ratio of 4 : 5, although a mixture of 1 : 1 and 2 : 3 would also produce the same slope. Although the exact nature of the complexation is still unknown, it is suggested that more than one ligand is participating in complexation with the metal cations for all three cyclotriveratrylene compounds.

Cavitand

Cavitands are very similar to calixarenes, the main difference being that the phenyls in calixarenes are connected in only one position, but are connected in two

Table 1.4: Distribution coefficient for the extraction of Eu(III) and Am(III) for select macrocycles.

# CMPOs	Type	Ligand	D_{Am}	D_{Eu}	$S_{Am/Eu}$
4	Calixarene (wr)	**1.5a**[13, a]	150	37	4.05
8	Calixarene (wr)	**1.8**[13, a]	7.5	2.4	3.13
4	Calixarene (wr)	**1.9**[17, b]	1.9	1.2	1.58
4	Calixarene (nr)	**1.10c**[13, a]	63	48	1.31
4	Calixarene (nr)	**1.11**[13, a]	0.88	0.38	2.32
4	Calixarene (nr)	**1.12c** [17, b]	0.66	0.47	1.40
4	Calixarene (nr)	**1.12d**[17, b]	0.33	0.24	1.38
4	Calixarene (nr)	**1.12c**[17, b]	2.4	2.8	0.86
4	Calixarene (nr)	**1.13a**[17, b]	0.27	0.25	1.08
4	Calixarene (nr)	**1.13b**[17, b]	0.44	0.38	1.16
4	Calixarene (nr)	**1.13c**[17, b]	1.2	1.8	0.67
3	CVT	**1.14a**[18, c]	0.08	0.05	1.60
3	CVT	**1.14b**[18, c]	2.95	1.95	1.51
3	CVT	**1.14c**[18, c]	1.38	1.02	1.35
4	Cavitand	**1.15a**[16, c]	0.83	0.36	2.31
4	Cavitand	**1.15b**[16, c]	0.26	0.08	3.25

Equal volumes organic/aqueous phases, aqueous phase: 3 M HNO_3, organic phase: (a) nitrophenyl hexyl ether, (b) CH_2Cl_2 (c) nitrobenzene, $C_L = 10^{-3}$ M.

positions for cavitands. This additional connectivity increases the rigidity of the system. It also lessens the effect that substituents have on the conformation of the structure.

The cavitands **1.15a** and **1.15b**, shown in Figure 1.8, were studied for their ability to extract thorium(IV) and europium(III), the results are summarized in Table 1.3.[20] It was found that the cavitands extracted very low amounts of thorium(IV) when compared

to the calixarenes. Both cavitands **1.15a** and **1.15b** were found to be selective for thorium(IV) over europium(III). The selectivity is among the higher of the macrocycles studied ($X_{Am/Eu}$ = 1.88 – 2.18, $S_{Am/Eu}$ = 2.31 – 3.25). They do not outperform the narrow rim calixarenes, but they are more selective than any of the wide rim calixarenes. Compound **1.15a** which contains a secondary amide was found to be more selective than compound **1.15b** which contains a tertiary amide. This is the opposite of what was observed for the alkylation of the amide for compounds **1.5a** and **1.5i**. For both pairs though, the amount of thorium(IV) extracted was decreased from the secondary to the tertiary amide.

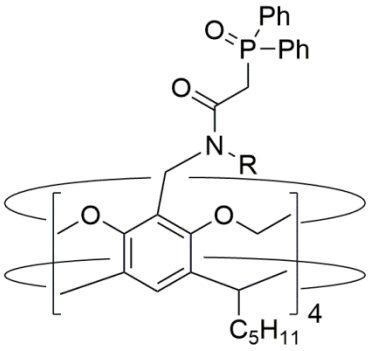

1.15a R = H
1.15b R = C_3H_7

Figure 1.8: CMPO-derivatized cavitands.[20]

It was determined by logD vs log[L] plots that compounds **1.8a** and **1.8b** form 1 : 1 complexes with europium(III) when excess metal is present and 2 : 1 ligand to metal complexes when excess ligand is present. The 2 : 1 complexes have been shown by infrared spectroscopy to only bind through the phosphoryl oxygens rather than the amide carbonyls.

C_3-SYMMETRIC PLATFORMS

Triphenoxymethane

It has been demonstrated that when all three phenol oxygens of triphenoxymethane (TPM) are substituted that the structure adopts an "all up" conformation, see Figure 1.9.[21] This conformer exists exclusively in both solution and solid states. The locked arrangement ensures that the attached CMPO units will all be pre-organized for cooperative binding.

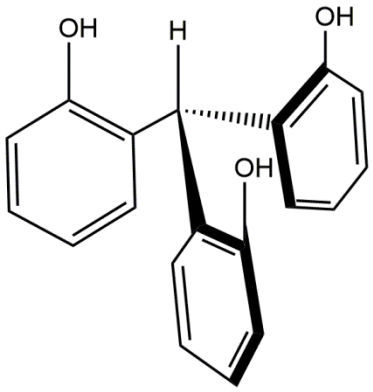

Figure 1.9: The "all up" conformation of triphenoxymethane.[21]

Scott and coworkers tethered three CMPOs to the triphenoxymethane platform, see Figure 1.9, complex **1.16a** and confirmed by X-ray crystallography that all three CMPO arms are in the "all up" conformation.[22] At a ratio of 1 : 1 (ligand : Th^{4+}) the system performs comparably to calixarene systems, see Table 1.5. At higher concentrations of the ligand, 10 : 1 (ligand : Th^{4+}), **1.16a** binds to 98% of the present thorium(IV). The material is much more selective than the calixarene systems, at a ligand concentration of 10 : 1 (ligand : Eu^{3+}), **1.16a** binds to only 3% of the present europium(III), while the calixarene systems bind to significantly more (9-73%).

Scott and coworkers examined the influence of varying the alkyl group on the ortho positions of the triphenoxymethane system, see Figure 1.9.[9] Compound **1.16a** has *t*-butyl substituents, compound **1.16b** has *t*-pentyl substituents, and compound **1.16c** has one methyl and one *t*-butyl substituent. The bulkier groups increase the solubility, as all three compounds (**1.16a** – **1.16c**) were found to be soluble in common organic solvents, but only **1.16b** was found to be soluble in 1-octanol. The affinity for thorium(IV) was found to be high for all three compounds (**1.16a** – **1.16c**), with all extracting over 98% of the thorium(IV) present at a ligand : Th^{4+} ratio of 10 : 1. The affinity for europium(III) was found to be low for all three compounds (< 4% extracted). Although the introduction of new alkyl groups changed the solubility of the complexes, it did not significantly alter the extraction or separation abilities.

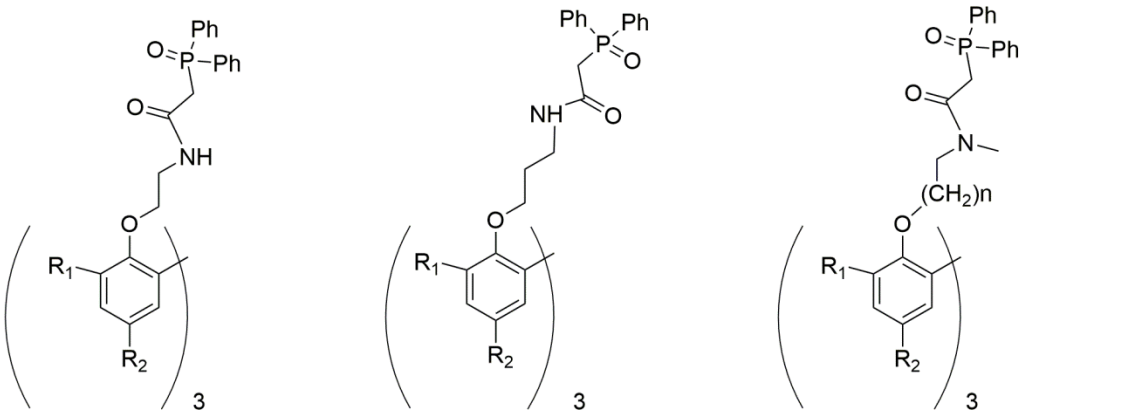

1.16a) $R_{1,2} = C(CH_3)_3$
1.16b) $R_{1,2} = C(CH_3)_2CH_2CH_3$
1.16c) $R_1 = CH_3$, $R_2 = C(CH_3)_3$

1.16d) $R_{1,2} = C(CH_3)_3$
1.16e) $R_{1,2} = C(CH_3)_2CH_2CH_3$

1.16f) n=2, $R_{1,2} = C(CH_3)_3$
1.16g) n=1, $R_{1,2} = C(CH_3)_2CH_2CH_3$

Figure 1.10: CMPO-derivatized triphenoxymethanes.[9,22]

Table 1.5: Extraction Percentage (% E) for compounds **1.16a** - **1.16c**.

# CMPOs	Ligand	Equiv of ligand in organic phase	% Th	% Eu
3	**1.16a**	1	40	-
		10	98	3
3	**1.16b**	10	100	2
3	**1.16c**	10	99	4

Equal volumes organic/aqueous phases, organic phase: CH_2Cl_2, aqueous phase: 1 M HNO_3, $C_M = 10^{-4}$ M.

The cavity size can have a direct effect on the systems' affinity for various cations and is directly influenced by the length and flexibility of the arms. To probe this, Scott and coworkers synthesized compounds **1.16d** and **1.16e**, which are identical to systems **1.16a** and **1.16b** except that there is a three carbon spacer between the phenol and the CMPO groups instead of a two carbon spacer. Extraction values for thorium(IV) remained the same between the different arm lengths, but the affinity for europium(III) increased for the longer spacer. Thus the increased arm length resulted in a less selective material.

The influence of alkylating the amide was examined; as seen in compounds **1.16f** and **1.16g**. Just as was seen in the case of the cavitands, the amount of thorium(IV) extracted decreased when moving from the secondary to the tertiary amide.

Compound**1.16a** was also studied for americium(III) selectivites, see Table 1.6. It was found to have moderate separation efficiencies ($S_{Am/Eu}$ = 1.5 – 1.7). The americium(III) distribution coefficient was found to be an order of magnitude higher than any other C_3 platform system at 3 M HNO_3 with a lower concentration of ligand than was used in the other C_3 platform studies.

Trialkylbenzene

The trialkylbenzene (TAB) platforms consist of a central benzene ring ligated at the 2, 4, and 6 positions. Three CMPO derivatized trialkylbenzene compounds have been reported by Reinhoudt *et al.*, see Figure 1.11.[23] Compounds **1.17a** - **1.17b** have moderate americium(III) distribution coefficients (1.0 – 2.0) at relatively low ligand concentrations ($C_L \approx 0.03$ M), see Table 1.6. This value drops significantly (0.02 – 0.16) when the amide is alkylated for compounds **1.17c** and **1.17d**. This is similar to what was observed for the calixarene and triphenoxymethane systems which also saw a decrease in the amount of actinides extracted when moving from secondary to tertiary amides. The selectivity for americium(III) over europium(III) increased minimally from the secondary to tertiary amine. The increased selectivity for the actinide over europium(III) was also observed for compounds **1.5a** and **1.5i**, but not for compounds **1.3a** and **1.3i**.

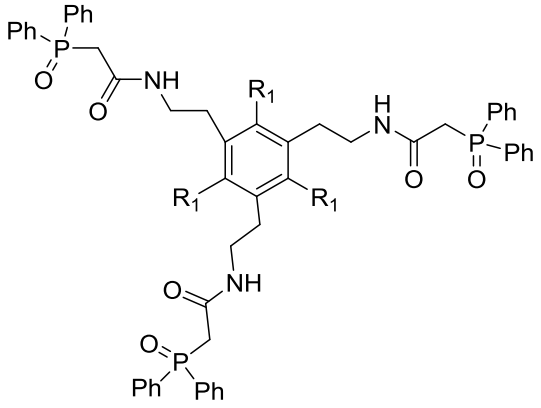

1.17a R_1 = Me
1.17b R_1 = Et

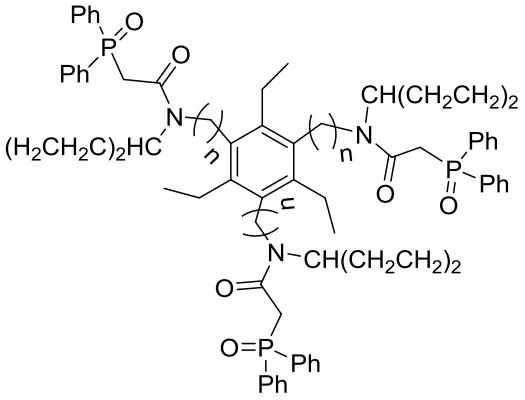

1.17c n=2
1.17d n=1

Figure 1.11: CMPO-derivatized trialkylbenzene.[23]

Compounds **1.17a** and **1.17b** differ in the alkyl group at the 1, 3 and 5 positions. Compound **1.17a** has methyl substituents, while compound **1.17b** has ethyl substituents. The longer alkyl chain increases the solubility of the compound. Complex **1.17b** is soluble in trichloroethylene (TCE) and 1-octanol, while complex **1.17a** is only soluble in TCE. The affinity for thorium(IV) for compound **1.17b** increases when extraction are performed in 1-octanol versus TCE. In TCE, **1.17a** is more selective than **1.17b**. Comparing **1.17a** in TCE and **1.17b** in 1-octanol, **1.17b** is more selective.

Compounds **1.17c** and **1.17d** differ in the length of the spacer between the platform and the CMPO ligand. Compound **1.17d**, which has a shorter spacer, has higher affinities for americium(III) and higher selectivities for americium(III) over europium(III) than compound **1.17c**, which has a longer spacer. This is true in TCE and 1-octanol, as well as at 1 M HNO_3 and at 3 M HNO_3.

Tripodands

A large number of CMPO-derivatized tripodands have been studied. In these compounds three CMPO moieties are bound to a central carbon atom. The tripodands are the most flexible of the C_3-symmetric complexes. These compounds can be broken up into two classes of systems, those which have imide groups tethered to the central carbon and those which have alkyl chains tethered to the central carbon.

Imide Tripodands

The imide tripodands (ImT) can be seen in Figure 1.12.[18,24] The results of extractions with the imide tripodands are given in Table 1.6. The imide tripodands generally display

Table 1.6: Extraction Percentage (% E) for compounds **1.16a** - **1.19f**.

Type	Conc	Ligand	$[HNO_3]$ / Organic Solvent	D_{Am}	D_{Eu}	$S_{Am/Eu}$
TPM	10^{-4}	**1.16a**[18]	1 / nitrobenzene	0.27	0.16	1.69
			3 / nitrobenzene	2.82	1.82	1.54
TAB	3.5×10^{-2}	**1.17a**[23]	1 / TCE	2.0	1.2	1.67
TAB	3.1×10^{-2}	**1.17b**[23]	1 / TCE	1.0	0.7	1.43
			1 / Octanol	1.28	0.66	1.94
TAB	3.0×10^{-2}	**1.17c**[23]	1 / TCE	0.02	0.01	2.0
TAB	3.2×10^{-2}	**1.17d**[23]	1 / TCE	0.16	0.07	2.29
ImT	10^{-3}	**1.18a**[24]	1.37 / *n*-Octanol	0.0068	0.0035	1.94
			2.70 / *n*-Octanol	0.0017	0.0011	1.55
			1 / TCE	0.64	0.33	1.94
ImT	10^{-3}	**1.18b**[24]	1.37 / *n*-Octanol	0.0089	0.0042	2.11
			2.70 / *n*-Octanol	0.0019	0.0011	1.72
			1 / TCE	0.52	0.27	1.93
ImT	10^{-4}	**1.18c**[18]	1 / nitrobenzene	0.13	0.08	1.63
			3 / nitrobenzene	0.11	0.06	1.83
ImT	1.27×10^{-3}	**1.18d**[24]	0.01 / nitrobenzene	414	346	1.20
			1 / nitrobenzene	0.0978	0.0568	1.72
			3 / nitrobenzene	0.0276	0.0205	1.35
AlT	10^{-3}	**1.19a**[24]	1.37 / *n*-Octanol	0.0069	0.0036	1.92
			2.70 / *n*-Octanol	0.0021	0.0013	1.62
AlT	10^{-3}	**1.19b**[24]	1.37 / *n*-Octanol	0.0045	0.0024	1.88
			2.70 / *n*-Octanol	0.011	0.0067	1.64
AlT	4.9×10^{-2}	**1.19c**[23]	1 / TCE	1.4	0.68	2.06
			3 / *n*-Octanol	1.7	0.71	2.39
AlT	4.4×10^{-2}	**1.19d**[23]	1 / TCE	1.1	0.50	2.20
			3 / *n*-Octanol	0.87	0.41	2.12
AlT	4.6×10^{-2}	**1.19e**[23]	1 / TCE	3.2	1.5	2.13
			3 / *n*-Octanol	3.7	1.5	2.47
AlT	3.2×10^{-2}	**1.19f**[23]	1 / TCE	0.18	0.087	2.07
			3 / *n*-Octanol	0.13	0.075	1.73

Equal volumes organic/aqueous phases, aqueous phase: 3 M HNO_3. TPM: triphenoxymethane, TAB: trialkylbenzene, ImT: imide tripodands, AlT: alkyl tripodands.

low distribution coefficients compared to the other platform systems. The separation factors are moderate ($S_{Am/Eu}$ = 1.3 – 1.9) and comparable to many of the other systems.

Complexes **1.18a** and **1.18b** are soluble in 1-octanol, but have extremely low distribution coefficients in this solvent. The switch to TCE vastly improved the distribution coefficients, yet compared to other compounds these values still not very high (D_{Am} = 0.0276 – 0.64).

Between complexes **1.18a** and **1.18b**, the americium(III) distribution coefficients increase with a longer alkyl chain on the imide. The longer chain also causes an increase in the separation efficiencies. In complex **1.18c**, the ether linkage between the central carbon and the CMPO moieties is replaced with an alkyl linkage and the alkyl chain on the imide is replaced with a *p-tert*-butylphenyl. These alterations result in a complex that has separation factors similar to compounds **1.8a** and **1.8b**, but decreased americium(III) distribution coefficients.

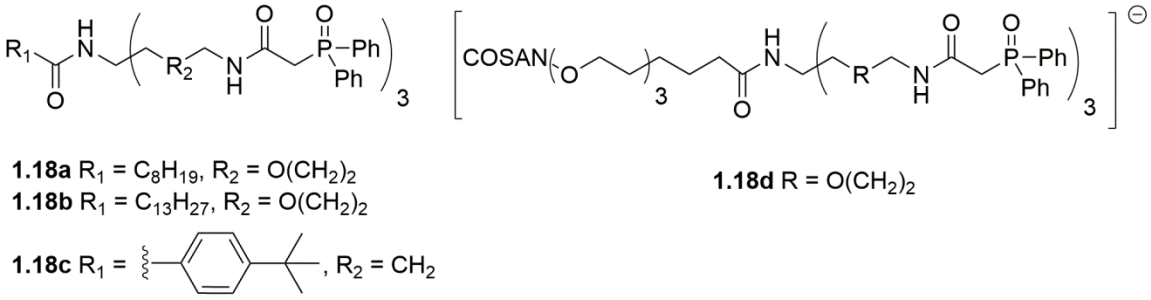

Figure 1.12: CMPO-derivatized imide tripodands.[18,24]

Compound **1.18d** has a cobalt *bis*(dicarbollide), COSAN, moiety attached. COSAN has been shown to have synergistic effects on the separation of americium(III) and europium(III).[25] At extremely low acid concentrations (0.01 M HNO_3) the distribution coefficients for **1.18d** are extremely high (D_{Am} = 414) but as the

concentration of acid is increased to 1 M, the distribution coefficients plummet (D_{Am} = 0.0978). The strong dependence of extraction values on acidic concentration has been commonly seen in COSAN systems.[26, 27]

Using a log-log plot, Verboom and coworkers plotted the americium(III) distribution coefficient as a function of the ligand concentration and observed a linear relationship between the two variables. The slope of the line was 1.5 indicating a metal to ligand stoichiometry of 2 : 3.

Alkyl Tripodands

The alkyl tripodands (AlT) can be seen in Figure 1.12.[23,24] The results of chelation tests with these materials are summarized in Table 1.6. These materials have similar separation efficiencies as compared to the imide tripodands.

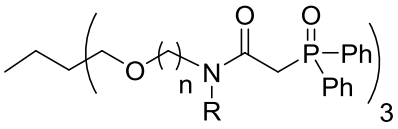

1.19a n=3, R = H
1.19b n=2, R = H
1.19c n=3, R = $CH_2(CH_2)_2CH_3$
1.19d n=3, R = $CH_2(CH_2)_6CH_3$
1.19e n=3, R = $CH(CH_2CH_3)_3$
1.19f n=3, R = $CH(CH_3)_2CH_2CH_3$

Figure 1.12: CMPO-derivatized alkyl tripodands.[23,24]

As in other systems, the length of the spacer between the CMPO moiety and the platform was investigated. Compound **1.19a** has a five atom spacer, while compound **1.19b** has a four atom spacer. Both compounds have very low americium(III) distribution

coefficients. Compound **1.19a** extracted slightly more americium(III) at lower acid concentrations, while compound **1.19b** extracted slightly more americium(III) at higher acid concentrations. The separation efficiencies were nearly identical for these two compounds. Altering the length of the spacer between the CMPO moiety and the platform has a noticeable impact on the extraction properties for most systems. It is possible that the influence is minimal in this particular system because the system already has a large degree of flexibility. While in other systems a longer spacer significantly alters the flexibility and thus the size of the binding pocket, in the tripodand systems the flexibility is not very hindered and thus longer spacers do not substantially alter the binding site.

The switch between secondary and tertiary amides was investigated. Unlike many of the other systems, which displayed a decrease in the affinity for the actinides from the seconday to tertiary amides, the alkyl tripodands display a significant increase in the americium(III) distribution coefficients when the amide is alkylated. The tertiary amides, **1.19c** – **1.19f**, have americium(III) distribution coefficients 2-3 orders of magnitude higher than the secondary amides, **1.19a** and **1.19b**. Reinhoudt and coworkers attribute the increased americium distribution coefficients to an increase in solubility of the tertiary amides over the secondary amides. There is a modest increase in the selectivity from the secondary to the tertiary amides.[23] Between the tertiary amides **1.19c** – **1.19f** there is little difference in the separation efficiencies, but there are large differences in the distribution coefficients. The differences in the distribution coefficients may only be a factor of the different concentrations of ligand used in each extraction.

CONCLUSION

The attachment of many CMPOs into a single system has shown many beneficial chelation properties. There are large variances in the performance of systems depending on the type of platform utilized. It was observed that for the americium(III)/europium(III) extractions that the wide rim calixarene systems were the most selective, with an average $S_{Am/Eu}$ of 2.92, and median $S_{Am/Eu}$ of 3.13. This system also included the most selective material overall in solutions of greater than 1 M HNO_3, compound **1.5a** ($S_{Am/Eu}$ = 4.05). The median $S_{Am/Eu}$ factors follow the order: wide rim calixarenes > cavitand > alkyl tripodands > trialkylbenzene > imide tripodands > triphenoxymethane > CVT > linear oligomers > narrow rim calixarenes. In addition to being the most selective, the wide rim calixarenes also include the compound with the highest overall americium(III) distribution coefficient, and generally have high distribution coefficients. Although the alkyl tripodands and cavitand systems have high selectivities, they do not have high distribution coefficients.

The least selective system, the narrow rim calixarenes, had the lowest average and lowest median separation factor, and included the least selective material overall, compound **1.13c**. The americium(III) distribution coefficients varied widely for the narrow rim calixarenes.

For the extractions with thorium(IV), the highest performing materials for each system were compared. The materials with the highest affinities for thorium(IV) follow the order: the narrow rim calixarene **1.10c** (%Th = 96, $X_{Th/Eu}$ = 1.41) > the linear oligomer **1.2b** (%Th = 78, $X_{Th/Eu}$ > 26) > the wide rim calixarene **1.7c** (%Th = 70, $X_{Th/Eu}$ = 0.96) > the cavitand **1.15a** (%Th = 24, $X_{Th/Eu}$ = 2.18). The materials with the highest selectivity for thorium(IV) over europium(III) for each platform type were ranked and ordered: the linear oligomer **1.2b** ($X_{Th/Eu}$ > 26, %Th = 78) > the narrow rim calixarene

1.10b ($X_{Th/Eu}$ = 6.48, %Th = 81) > the cavitand **1.15a** ($X_{Th/Eu}$ = 2.18, %Th = 24) > the wide rim calixarene **1.7e** ($X_{Th/Eu}$ = 1.71, %Th = 60).

For all of the systems it was found that alkylating the amide of the CMPO system resulted in a decreased uptake of the actinides, except for the alkyl tripodands which experienced a large increase in the uptake of americium(III) after alkylating. The selectivity did not vary greatly between the secondary and tertiary amides for any of the systems and one was not found to be consistently higher.

The length of alkyl chains on the platforms generally had no influence on the extraction behavior of the systems. Some systems did observe differences in extraction behavior when longer alkyl chains were appended to the platform, but the longer chains did not cause any consistent increase or decrease in the extraction or separation behavior.

For the systems which studied varying the number of CMPO moeities, the calixarenes and the linear systems, it was generally seen that more CMPO moeities lead to increased separation and extraction efficiencies up to 4 CMPO moeities. For both the linear oligomer systems and the calixarene systems, the move from tetramer to pentamer did not increase the extraction efficiencies. Additionally the calixarene species **1.8**, with 8 CMPO moeities, was out performed by the calixarene **1.5a**, with only 4 CMPO moeities.

The influence of the length of the spacer between the platform and the CMPO moiety was studied for many systems. For all of the systems either no trend was observed or there was a decrease in the selectivity with a longer spacer between the platform and the CMPO moiety. In some cases the extraction efficiency increased, in some it decreased, and in some there was no trend observed for a longer spacer between the platform and the CMPO moiety.

Chapter 2: Separation of *f*-Elements Using CMPO Functionalized Ring-Opening Metathesis Polymers

INTRODUCTION

Spent nuclear fuel contains many radioisotopes with half lives on the order of 10^3 years. This makes engineering a burial system that contains the material for the life of the radioactivity very difficult.[3] The transmutation of the long lived products in a fast reactor can create more energy and less high level waste.[4,28] This however, requires the separation of the various components in the fuel into separate waste streams. This is a difficult task, especially for obtaining selectivity between the lanthanides and actinides when considering the chemical similarities of these two classes of ions.

CMPO, carbamoylmethylphosphine oxide, based ligands have shown discrimination between these two classes of materials, by taking advantage of the slightly softer nature of the actinides.[29] In the 1980s, Horwitz *et al.* developed CMPO for the TRUEX process (TRansUranic Extraction), whereby actinides are selectively sequestered into the organic phase by CMPO during a liquid-liquid extraction from acidic media.[5,7,30,31] This work revealed that the bidentate CMPO binds predominately in a 3 : 1 fashion to the actinides with the remaining coordination sphere of the metal ion occupied by water and nitrate ligands.[7]

In the 1990s a series of CMPO-derivatized platform systems were developed to take advantage of cooperative binding with high local concentration or to enable ease of separation. To provide systems with the 3 : 1 stoichiometry, many groups bound together three CMPO ligands in a single molecule using various organic support structures. In 1996 Böhmer *et al.* developed a CMPO calixarene system.[8] In 1997 Reinhoudt *et al.* developed the first CMPO cavitand systems.[20] Then in 2002 Scott *et al.* developed CMPO tripod systems based on a C_3-symmetric triphenoxymethane platform.[22] These

research groups consistently observed an increased separation and extraction efficiency as compared a molecules with a single CMPO. Additionally, in 1995 Vandergrift *et al.* bound CMPO to magnetic particles to eliminate the organic phase required in typical separations.[32]

Although the extraction properties of these tri-ligand systems are high, these systems would be difficult to synthetically modify. The properties of block polymers can be easily modified by substituting the ratio of blocks or choosing different blocks entirely. ROMP, ring-opening metathesis polymerization, has been shown to easily create block copolymers.[33] By creating a ROMP active CMPO containing monomer, a wide range of block copolymer systems can easily be synthesized. This will support future efforts to modify the properties of a CMPO containing material to create a high performing, single phase extraction system. Herein, I will discuss the synthesis and characterization of a CMPO containing ROMP active monomer, the corresponding homopolymers, and the extraction properties of each. Figure 2.1 shows a schematic of extraction of actinides by a polymeric CMPO material.

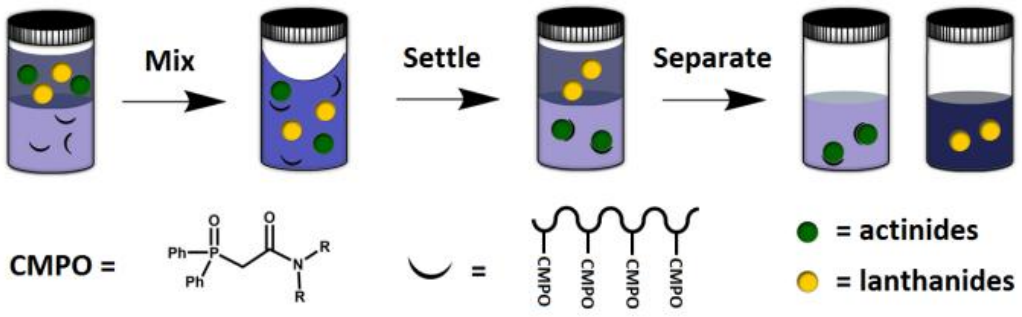

Figure 2.1: Schematic showing actinides selectively sequestered from an aqueous phase into an organic phase by a CMPO containing material.

RESULTS AND DISCUSSION

Synthesis and Characterization

A series of CMPO tethered polymers were synthesized largely through modified literature procedures.[8,34] Compound **2.4** was prepared through a condensation between the Diels-Alder product **2.1** and ethylenediamine. An X-ray crystal structure has been obtained of the product, see Figure 2.2. First attempts at this reaction were performed with 1,3-diaminopropane and resulted in the formation of **2.2**. An X-ray crystal structure was obtained of this material, see Figure 2.3. Literature searches revealed that this compound is an intermediate in the synthesis of phloeodictine A1, which has been shown to have antimicrobial properties, as well as exhibiting significant cytotoxicity towards KB human naso-pharyngeal carcinoma cells.[35] This synthetic route eliminated 3 steps from previously published routes.[35] It was found later that by lowering the reaction temperature, **2.3** could be synthesized.

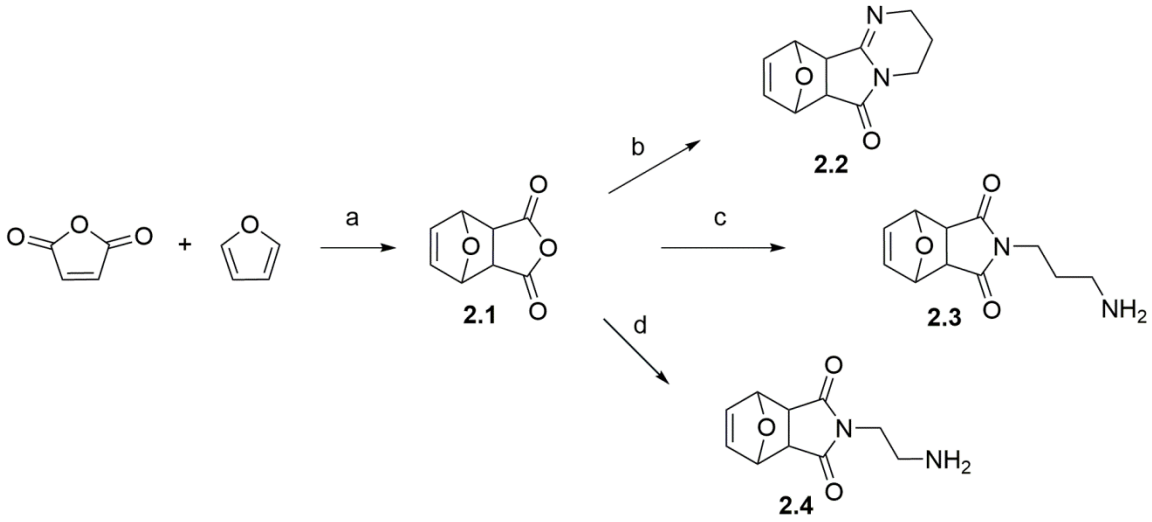

Scheme 2.1: Synthesis of ROMP functionalized amines, **2.1– 2.4**.

(a) benzene, RT, 18 h, 81.5% (b) 1,3-diaminopropane, 70 °C, 2 h, 23.5% (c) 1,3-diaminopropane, RT, 2 h, 12.1% (d) 1,2-diaminoethane, 70 °C, 2 h, 9.9%.

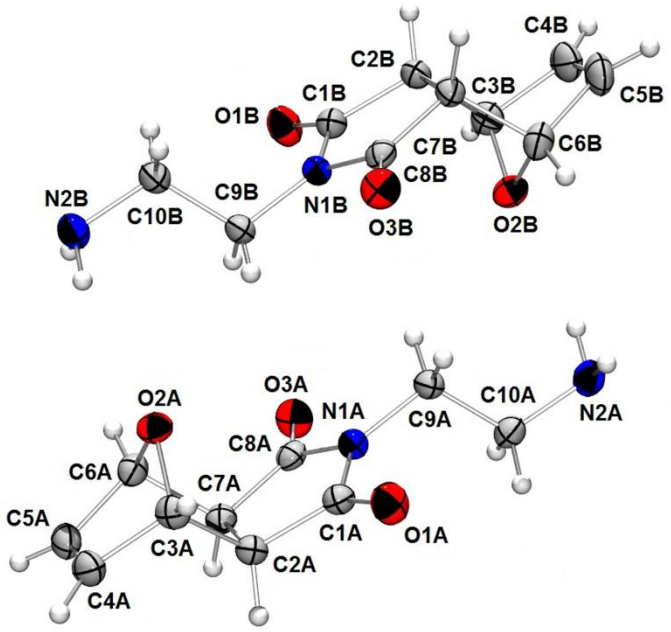

Figure 2.2: Molecular structure of **2.4**.

Two independent molecules of **2.4** showing the atom labeling scheme. Displacement ellipsoids are shown at the 50% probability level.

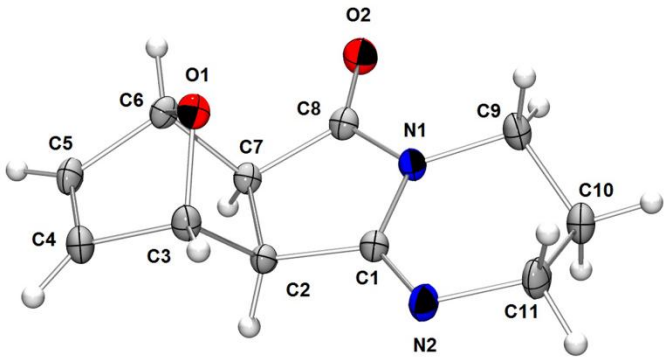

Figure 2.3: Molecular structure of **2.2**.

The atom labeling scheme is shown. Displacement ellipsoids are shown at the 50% probability level.

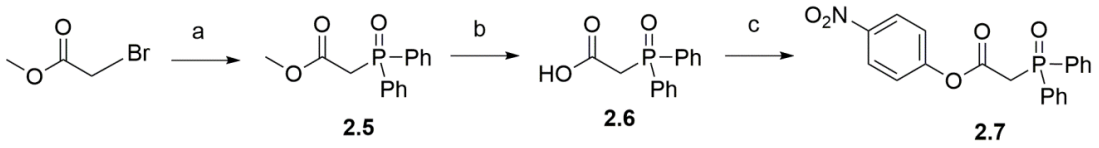

Scheme 2.2: Synthesis of CMPO starting materials, **2.5 – 2.7**.

(a) [1] chlorodiphenylphosphine, Zn, I_2, benzene, 70 °C, 18 h [2] HOOH, ethanol, RT, 1 h, 74.8% (b) NaOH, methanol/H_2O, 70 °C, 18 h, 84.4% (c) 4-nitrophenol, $CHCl_3$, 45 °C, 5 h, 77.7%.

2.5 was synthesized in a Reformatsky-type reaction between chlorodiphenylphosphine and methylbromoacetate, followed by oxidation with hydrogen peroxide, adapted from Kiełbasiński and Mikołajczyk, see Scheme 2.2.[36] The carboxylic acid, **2.6**, was synthesized by hydrolysis of **2.5**. Attempts to directly synthesize **2.6** with bromoacetic acid in place of methylbromoacetate were unsuccessful. Various unsuccessful attempts were made to couple **2.6** with **2.4**. Eventually **2.6** was functionalized with a *p*-nitrophenol leaving group to create **2.7**.

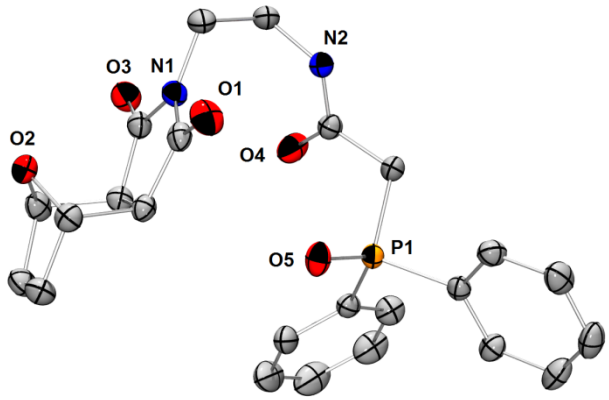

Figure 2.4: Molecular structure of **2.8**.

Selected atom labeling scheme is shown. Displacement ellipsoids are shown at the 30% probability level. The hydrogen atoms have been omitted for clarity.

The monomer, **2.8**, was then prepared in good yields through the aminolysis of **2.7** by compound **2.4**, see Scheme 2.3. The monomer, **2.8**, was characterized by ^{1}H, $^{13}C\{^{1}H\}$, and $^{31}P\{^{1}H\}$ NMR spectroscopy, IR spectroscopy, mass spectrometry, and elemental analysis by combustion. An X-ray crystal structure has been obtained of the monomer, **2.8**, see Figure 2.4. The X-ray crystal structures of **2.4** and **2.8** reveal that the *exo* isomer of the bridged bicyclic ring system is exclusively formed, yielding the monomer more active towards polymerization.[37] The material was also confirmed to be *exo* by ^{1}H NMR.

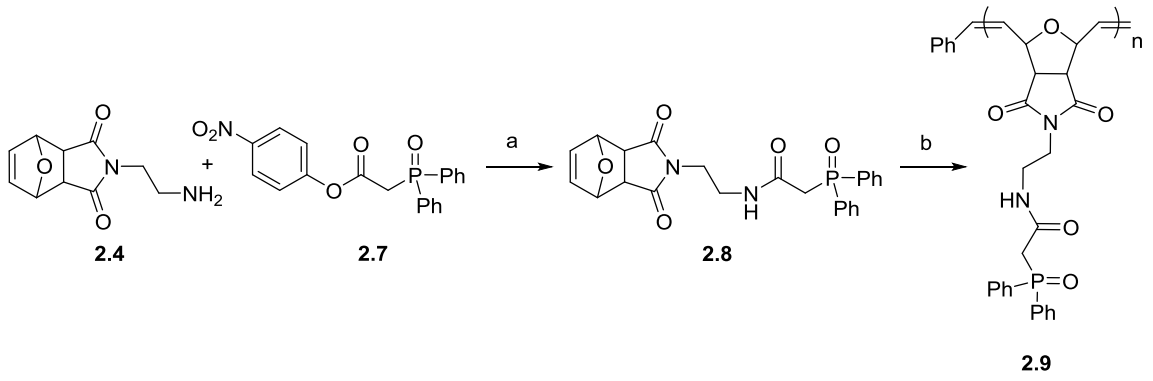

Scheme 2.3: Synthesis of monomer and polymer CMPO chelators, **2.8 – 2.9**.

(a) $CHCl_3$, 45 °C, 18 h, 67.1% (b) 2nd generation Grubbs' catalyst, $CHCl_3$, RT, 18 h, 55.7 %.

An important question we hoped to answer was whether or not the molecular weight of the polymer affects the performance of the extractant material. To investigate this, three polymers of varying molecular weights were synthesized (**2.9a-c**, Scheme 2.3). Polymerizations were first attempted with Grubbs' first generation catalyst, with no resulting polymerization. The switch to more functional group tolerant second generation catalyst yielded high molecular weight polymers.[38] The polymers were characterized by ^{1}H and $^{31}P\{^{1}H\}$ NMR spectroscopy, IR spectroscopy, and GPC analysis. We investigated

the relationship between the observed molecular weight and the molar ratio of catalyst to monomer. The relationship was found to be linear, see Figure 2.5, indicating a controlled living polymerization. The decomposition temperature of **2.9c** was investigated by thermogravimetric analysis and found to be 250 °C, see Figure 2.6.

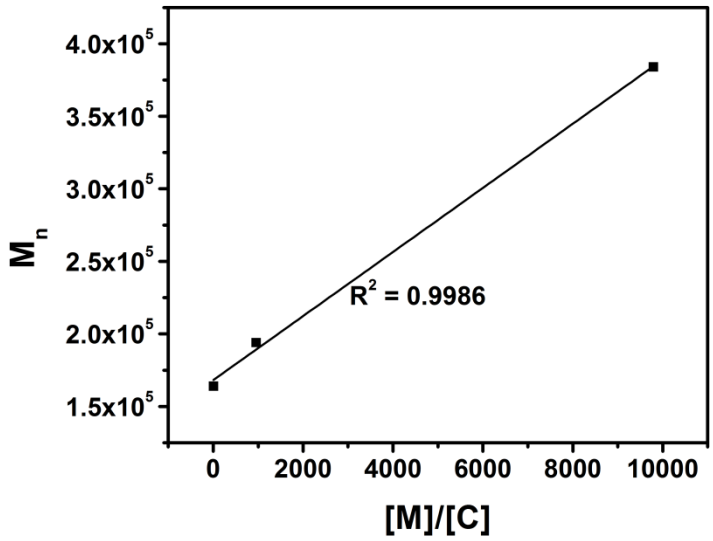

Figure 2.5: Plot of observed molecular weight (Mn) versus monomer/catalyst ratio ([M]/[C]) for polymers **2.9a-c**.

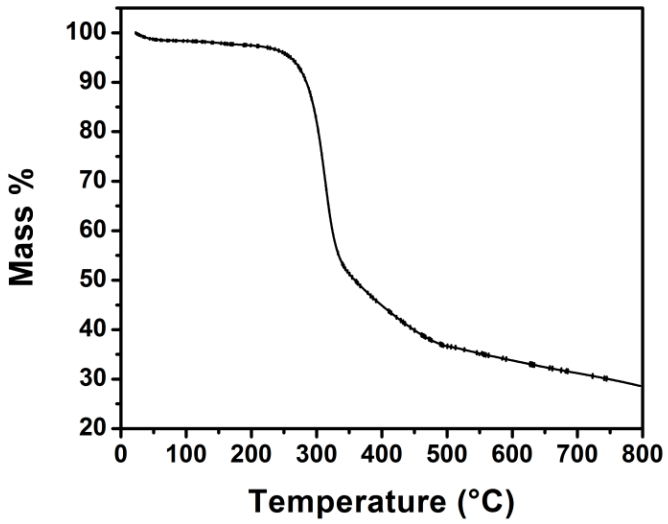

Figure 2.6: Thermogravametric analysis of **2.9c**, mass percent versus temperature (°C).

Chelation Studies

The extraction efficiencies of the monomer, **2.8**, and polymers **2.9a-c** were investigated. The efficiencies were tested by performing a liquid-liquid extraction with metal nitrates in aqueous acidic media, which were extracted into organic media by ligands in the organic phase, see Figure 2.1.

For initial testing, the aqueous phase used was 10^{-4} M Th^{4+} in 1 M HNO_3 to replicate the conditions used in the literature, to allow for simple comparison between the different materials. Choices for the organic phase were limited due to the solubility of the materials. Ultimately CH_2Cl_2 was chosen due to its popularity in CMPO extractions.

As a control, the first extraction was performed with pure CH_2Cl_2, containing no CMPO material, to ensure that the extraction ability of the system is due entirely to the

CMPO materials and not due to the solubility of the metal nitrates in CH_2Cl_2. The extraction ability of CH_2Cl_2 was found to be < 1 ± 3%.

Table 2.1: Extraction efficiencies for selected materials

[CMPO]	**2.8**	**2.9a**	**2.9b**	**2.9c**
0.05 M	82	65	>99	>99
0.01 M	7	34	>99	>99
0.005 M	4	21	>99	>99
0.001 M	< 1	16	40	93

Percent of Th^{4+} extracted from 1M HNO_3 solutions by ligands. Aqueous phase: 10^{-4} $Th(NO_3)_4 \cdot H_2O$, Organic phase: extracting materials in CH_2Cl_2.

The extraction of thorium(IV) was performed with varying concentrations of extracting material, 0.05 M – 0.001 M. The concentration of the polymeric materials was determined by using by using the same gram quantity as the monomer at each concentration, giving one mole of repeat unit per liter. The results of these tests are summarized in Table 2.1.

For the monomer **2.8**, high extraction values could be obtained with 1000 times greater CMPO to metal concentration, but sharply declined to 7% at 100 times greater concentration. All the polymeric materials outperformed the monomer, **2.8**.

Polymers **2.9b** and **2.9c** were able to achieve quantitative extractions at only 50 times greater CMPO to metal concentration. Though the performance of **2.9b** sharply declines at 10 times CMPO to metal concentration, **2.9c** still extracts over 90% of the metal ions. Quantitative extraction was not achieved with **2.9a** and at very high ligand concentrations the monomer does outperform **2.9a**, but as the concentration of the materials is decreased the polymer significantly outperforms the monomer. At 0.01 M, for

example, the polymer binds to 5 times more Th^{4+} than the monomer. It is believed that as the concentration of monomer is decreased it becomes more and more difficult for three CMPO groups to find a metal ion and complete extraction. As the concentration of the polymer is decreased the "localized concentration" remains the same; that is many CMPO groups are linked together despite the solution being somewhat dilute. Because of this the CMPO ligands can take place in cooperative binding in the case of the polymers, but not in the case of the monomers.

Looking at the differences between the three polymers, it is clear that molecular weight does play a role in the extraction efficiency of the materials. We speculate that these differences can be attributed to the differing solubilities of the three materials.

It is unclear if binding is occurring between three adjacent CMPO units or by CMPO units on adjacent chains. But it is believed that three adjacent CMPO moieties are binding because at low concentrations, where the likely hood of multiple chains coming in contact is small, high extraction efficiencies are achieved.

When comparing the ligand to other platform systems we need to decrease the ligand concentration by a factor of three to account for the three ligands on every platform system. Quantitative extractions were achieved with 0.005 M or 0.0017 M, when decreasing by three, with **2.9b** and **2.9c**. This is quite comparable to the other platform systems in which most achieve quantitative extraction with Th^{4+} at 0.001 M.[9,22]

To determine the separation efficiency of the materials, lanthanides were added to the extractions. Three lanthanides were chosen: lanthanum(III), europium(III), and cerium(III). To keep the same overall metal concentration of 10^{-4} M, the concentration of each individual metal was set at 2.5×10^{-5} M, so the final solution contained 2.5×10^{-5} M Th^{4+}, La^{3+}, Eu^{3+}, and Ce^{3+}. The percentage of each individual metal extracted was

converted to a distribution of ions in each phase using equation 2.2, given in the experimental. The separation values were determined by dividing the distribution of thorium(IV) by the distribution of a given ion, using equation 2.3, given in the experimental. A larger value indicates a higher preference to extract thorium(IV) over a given ion.

Table 2.2: Separation efficiencies for polymeric materials.

	2.9a	**2.9b**	**2.9c**
$\mathbf{S_{Th/Eu}}$	327.7	16.7	15.6
$\mathbf{S_{Th/La}}$	175.6	18.7	5.7
$\mathbf{S_{Th/Ce}}$	123.8	13.0	5.7

$S_{Th/M}$ values for extraction of Th^{4+}, Ce^{3+}, La^{3+}, and Eu^{3+} ($C_M = 2.5 \times 10^{-5}$ M) from an aqueous solution of 1 M HNO_3 into a CH_2Cl_2 solution of polymers ($C_{CMPO} = 0.01$ M) at 25 °C.

Looking at Table 2.2, it is clear that all the materials have a preference for thorium(IV) over the lanthanides. The highest molecular weight polymer **2.9a**, is the most discriminate towards thorium(IV), with much higher separation values than the other materials. The smallest molecular weight polymer has the lowest separation values for all of the ions tested, revealing a trend of better separations with higher molecular weight materials. The trend of increasing separation efficiency with increasing size has also been shown between single CMPO systems and platform CMPO systems, where multiple CMPO containing systems have shown a higher preference for actinides than homologous single CMPO containing systems.[8]

CONCLUSION

The high extraction efficiencies with the smaller polymer and the high separation efficiencies with the higher molecular weight polymer lead us to believe that there is a so called "sweet-spot" for idealized molecular weight, where both extraction and separation efficiencies can be maximized. Future efforts will focus on tuning the molecular weight to maximize extraction properties, and development of block polymer systems.

We have demonstrated an improvement in CMPO chelation by tethering the ligand to a polymeric backbone. All three polymers are better extractants than the monomer. We have also demonstrated a dependence of the polymer performance on molecular weight. While the higher molecular weight polymer, **2.9a**, has an increased separation efficiency as compared to the lower molecular weight polymers, the lowest molecular weight polymer, **2.9c**, has the highest extraction efficiency. The extraction efficiencies demonstrated by **2.9b** and **2.9c** are comparable to the performance other CMPO platform systems reported in the literature.[9,22]

EXPERIMENTAL

General Methods

All chemicals were purchased from chemical suppliers and were used without further purification. All dry reactions were performed using standard Schlenk techniques and were performed under an inert atmosphere of nitrogen. CH_2Cl_2 and $CHCl_3$ were dried using the Pure-Solv 400 solvent purification system. Anhydrous benzene was purchased from EMD. ^{1}H, $^{13}C\{^{1}H\}$, and $^{31}P\{^{1}H\}$ NMR spectra were obtained on a Varian Unity+ 300. ^{1}H, and $^{13}C\{^{1}H\}$ NMR spectra were referenced to the residual solvent peaks. $^{31}P\{^{1}H\}$ NMR spectra were referenced to a phosphoric acid external standard. Number

average molecular weights (M_n) and polydispersity indices (PDI) were measured from DMF solutions using an Agilent 1100 series GPC (Agilent Technologies) equipped with Viscotek I-series mixed bed medium molecular weight columns and refractive index detectors, and are reported relative to polystyrene standards. Melting points are not corrected. High resolution mass spectra were obtained with a Micromass Autospec Ultima. Elemental analysis was performed by QTI, Whitehouse, NJ (www.qtionline.com).

Extractions

The lanthanide and actinide salts, $Th(NO_3)_4 \cdot H_2O$ (Strem), $Ce(NO_3)_3 \cdot 6H_2O$ (Alfa Aesar), $Eu(NO_3)_3 \cdot 5H_2O$ (Strem), and $La(NO_3)_3 \cdot 6H_2O$ (Fisher), were used as received. Solutions were prepared using trace metal grade deionized water, trace metal grade HNO_3 (BDH), and twice distilled dichloromethane.

A 10^{-4} M solution of Th^{4+} in 1 M nitric acid, and a solution of 2.5 x 10^{-5} M Th^{4+}, 2.5 x 10^{-5} M Eu^{3+}, 2.5 x 10^{-5} M Ce^{3+} and 2.5 x 10^{-5} M La^{3+} in 1 M HNO_3 were prepared. Equal volumes (0.6 mL) of aqueous and organic phases were mixed in a 1 dram glass vials equipped with a polyethylene cap and PTFE coated stir bars. The vials were stirred at 1200 rpm for 20 hours. The solutions were then centrifuged and the aqueous layer pipetted off the top and transferred to a separate vial. The solution was centrifuged again and the top layer was diluted to ppb levels with 1 M HNO_3. The solutions were tested in triplicate using a GBC Optimass 8000 ICP-time-of-flight (TOF)-MS (GBC Scientific Equipment, Hampshire, IL). Solutions were introduced into the instrument using a cyclonic spray chamber (Glass Expansion; Melbourne, Australia) and concentric glass nebulizer (C type, Precision Glassblowing; Centennial, CO). The extraction efficiencies

were determined using equation 2.1, where C_1 is the average count from the sample, and C_0 is the average count of a solution stirred with no organic phase and no extracting material.

$$\%E = ((C_0 - C_1)/C_0) \times 100\% \qquad (2.1)$$

All %E values are the average of three separate trials; the standard deviations for all are under ± 5%. Extraction efficiencies were converted into distribution coefficients using equation 2.2, derived from Böhmer and coworkers.[8]

$$D = \%E/100\text{-}\%E \qquad (2.2)$$

The separation factor $S_{Th/M}$, defined by equation 2.3, is a ratio of the distribution coefficients of the respective metals.

$$S_{M1/M2} = D_{M1} / D_{M2} \qquad (2.3)$$

X-ray Crystallography

Crystals of **2.2** suitable for X-ray diffraction were obtained by slow evaporation from a saturated solution of **2.2** in dichloromethane that was layered with *n*-heptane. Crystals of **2.4** suitable for X-ray diffraction were obtained by precipitation from a CH_2Cl_2–ether (1 : 3 v/v) solution. Crystals of complex **2.8** were grown from a slowly evaporated solution of CH_2Cl_2. The single–crystal diffraction data for compound **2.2** was collected at 100 K on a on a Rigaku AFC12 with Saturn 724+ CCD using a graphite monochromator. The single–crystal diffraction data for compounds **2.4** and **2.8** were collected on a Rigaku SCX-Mini diffractometer with a Mercury CCD using a Rigaku Tec 50 low-temperature device. The complex was collected using a graphite monochromator with MoKα radiation (λ = 0.71073Å). Absorption corrections were applied using multi-scan. Data reduction was performed using the Rigaku Americas Corporation's Crystal

Clear version 1.40.[39] The structures were solved by direct methods and refined anisotropically using full-matrix least-squares methods with the SHELX-97 program package.[40] The amine and amide H atoms were located in a difference Fourier map and both positional and isotropic displacement parameters were refined. All other H atoms were positioned geometrically and refined using a riding model, with C—H = 0.93 – 0.99 Å and U_{iso}(H) = 1.2 U_{eq}(C). Neutral atom scattering factors and values used to calculate the linear absorption coefficient are from the International Tables for X-ray Crystallography (1992).[41]

Synthesis

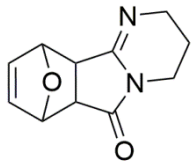

[2.2] 3,4,6a,7,10,10a-hexahydro-7,10-epoxypyrimido[2,1-*a*]isoindol-6(2*H*)-one

1,3-diaminopropane (14.9 g, 201.0 mmol) and **2.1** (4.8 g, 28.9 mmol) were refluxed at 80 °C for 2 h. The resulting solution was poured into H_2O and extracted with dichloromethane (2 x 30 mL). The combined organic layers were dried with Na_2SO_4 and concentrated. Recrystallization in toluene yielded a white solid (23.5%). m.p. 120 °C (decomp.). ^{1}H NMR ($CDCl_3$) δ: 6.44 (s, 2H), 5.20 (s, 1H), 5.16 (s, 1H), 3.52 (t, 2H, J = 6.0), 3.47 (t, 2H, J = 5.6), 2.85 (d, 1H, J = 7.2), 2.69 (d, 1H, J = 6.9), 1.81-1.73 (m, 2H), ^{13}C{^{1}H} NMR ($CDCl_3$) δ: 173.4, 155.3, 136.0 (CH), 82.4 (CH), 80.1 (CH), 46.4 (CH), 45.3 (CH), 44.3 (CH_2), 37.5 (CH_2), 18.7 (CH_2). HRMS (CI+) calcd for $C_{11}H_{12}O_2N_2$ [M + H]+ 205.0977, found 205.0977.

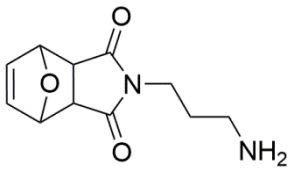

[2.3] 2-(3-aminopropyl)-3a,4,7,7a-tetrahydro-1*H*-4,7-epoxyisoindole-1,3(2*H*)-dione

1,3-diaminopropane (0.25 mL, 3.0 mmol) and **2.1** (0.20 g, 1.2 mmol), were stirred at R.T. for 18h. The resulting solution was poured into H_2O and extracted with dichloromethane (2 x 30 mL). The combined organic layers were dried with Na_2SO_4 and concentrated. Recrystallization in a mixture of dichloromethane and ether (1 : 3 *v/v*) yielded a white solid (0.03 g, 12.6%). m.p. 134 °C (decomp.). ^{1}H NMR ($CDCl_3$) δ: 6.49 (t, 2H, *J* = 0.9), 5.24 (t, 2H, *J* = 0.9), 3.55 (t, 2H, *J* = 6.9), 2.82 (s, 2H), 1.68 (br, 2H), $^{13}C\{^1H\}$ NMR (CDCl3) δ: 176.4, 136.5, 80.9, 47.4, 38.8, 36.1, 31.3.

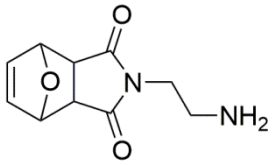

[2.4] 2-(2-aminoethyl)-3a,4,7,7a-tetrahydro-1*H*-4,7-epoxyisoindole-1,3(2*H*)-dione

Ethylenediamine (5 mL, 74.9 mmol) and **2.1** (5.0 g, 30.1 mmol) were refluxed at 80 °C for 3 h. The resulting solution was poured into H_2O and extracted with dichloromethane (2 x 30 mL). The combined organic layers were dried with Na_2SO_4 and concentrated. Recrystallization in a mixture of dichloromethane and ether (1:3 v/v) yielded a white solid (9.9%). m.p. 126 °C (decomp.). ^{1}H NMR ($CDCl_3$) δ: 6.45 (s, 2H), 5.20 (s, 2H), 3.48 (t, 2H, *J* = 6.3), 2.80 (t, 4H, *J* = 6.3), 1.01 (br, 2H), $^{13}C\{^1H\}$ NMR (CDCl3) δ: 176.4, 136.4, 80.8, 47.3, 41.9, 39.7. HRMS (CI+) calcd for $C_{10}H_{13}O_3N_2$ [M +

H]+ 209.0921, found 209.0922. Anal. calcd. for $C_{10}H_{12}O_3N_2$: C, 57.68; H, 5.81; N, 13.45. Found: C, 57.27; H, 5.51; N, 12.96.

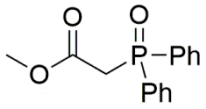

[2.5] Methyl 2-(diphenylphosphoryl)acetate

2.5 was prepared following a modified prep from Kiełbasiński and Mikołajczyk.[36] To a flame dried Schlenk flask was added dry benzene (200 mL), methyl bromoactetate (5 mL, 43.4 mmol), chlorodiphenylphosphine (12 mL, 54.4 mmol), zinc dust (3.9 g, 59.6 mmol), and a single crystal of iodine. The mixture was refluxed at 70 °C overnight. After cooling to room temperature the solution was exposed to atmosphere and a solution of 2 mL of 30% hydrogen peroxide in 8 mL EtOH was added and stirred for 1 hour. The solution was washed with brine slightly acidified with 2 M HCl, and extraced into $CHCl_3$ (40 mL x 3). The organic layer was dried with sodium sulfate and concentrated. Recrystallization in chloroform/*n*-heptane yielded a white solid (74.8%). m.p. 112 °C. ^{1}H NMR ($CDCl_3$) δ: 7.9 – 7.7 (m, 4H), 7.6 – 7.4 (m, 6H), 3.6 (s, 3H), 3.5 (d, 2H, J = 15.0), $^{13}C\{^1H\}$ NMR ($CDCl_3$) δ: 167.0, 166.9, 132.5, 131.9, 130.6, 129.0, 128.8, 58.7, 36.4, 32.0, $^{31}P\{^1H\}$ NMR ($CDCl_3$) δ: 27.8.

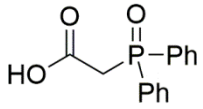

[2.6] 2-(diphenylphosphoryl)acetic acid

2.5 (7.62 g, 27.8 mmol) was dissolved in MeOH (200 mL). An equal volume of 2 M NaOH (200 mL) was added and the solution was refluxed at 70 °C overnight. The solution was extracted with $CHCl_3$ (50 mL). The aqueous layer was neutralized with 2M HCl and then extracted into CH_2Cl_2 (30 mL x 3). The organic layer was dried with sodium sulfate and concentrated to one-third the original volume. The solution was mixed with equal amounts of ether and brought to -20 °C. The resulting white solid was collected by vacuum filtration, washed with diethyl ether (84.4%). m.p. 135 °C. ^{1}H NMR ($CDCl_3$) δ: 12.10 (b, 1H), 7.75 – 7.68 (m, 4H), 7.53 – 7.38 (m, 6H), 3.484 (d, 2H, J = 13.81), ^{13}C{^{1}H} NMR ($CDCl_3$) δ: 167.0, 166.9, 132.4, 132.4, 131.4, 131.1, 131.0, 130.0, 128.8, 128.6, 38.6, 37.8, ^{31}P{^{1}H} NMR ($CDCl_3$) δ: 32.3.

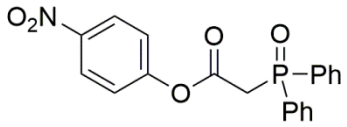

[2.7] 4-nitrophenyl 2-(diphenylphosphoryl)acetate

2.7 was prepared following a modified preparation by Böhmer and coworkers.[8] **2.6** (6.00 g, 23.0 mmol), *p*-nitrophenol (3.49 g, 25.1 mmol), and thionyl chloride (2.5 ml, 34.0 mmol) were stirred in dry chloroform for 5 hours at 45 °C and then an additional 12 hours at room temperature. The solution was washed with a 5% sodium bicarbonate solution, extracting into chloroform x 3. The organic layer was concentrated to one-third the volume and a large volume of ether was added to the solution. Upon cooling a white

crystalline solid precipitate. The solid was collected by vacuum filtration (7.05 g, 80.1 %). The ^{1}H NMR spectra matched that reported by Böhmer and coworkers.[8]

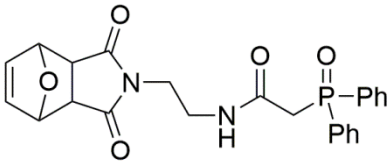

[2.8] *N*-(2-(1,3-dioxo-3a,4,7,7a-tetrahydro-1*H*-4,7-epoxyisoindol-2(3*H*)-yl)ethyl)-2-(diphenylphosphoryl)acetamide

2.4 (2.68 g, 12.9 mmol) and **2.7** (4.81 g, 12.6 mmol) were stirred at 45 °C in dry chloroform overnight under N_2. After cooling to room temperature the solution was exposed to atmosphere and 0.2 M KOH (100 mL) was added. The mixture was stirred at room temperature for another hour. The solution was washed with 5% (b.w.) sodium bicarbonate solution and extracted into $CHCl_3$ (x 3), then washed with water and extracted into $CHCl_3$ (x 3). The solution was dried with sodium sulfate and concentrated. A white solid was obtained by recrystallizing in a mixture of $CHCl_3$ and heptane (1 : 3 *v/v)* (69.1%). m.p. 223 °C. ^{1}H NMR ($CDCl_3$) δ: 7.62 – 7.72 (m, 4H), 7.38 – 7.55 (m, 6H), 6.44 (s, 2H), 5.21 (d, 2H, *J* = 0.90), 3.55 (t, 2H, *J* = 6.00), 3.37 (q, 2H, *J* = 6.30), 3.23 (d, 2H, *J* = 12.60), 2.78 (s, 2H), ^{13}C{^{1}H} NMR ($CDCl_3$) δ: 176.2, 165.3, 136.4, 132.3, 130.8, 130.6, 128.9, 128.7, 80.8, 47.4, 38.9, 38.2, 37.5. ^{31}P{^{1}H} NMR ($CDCl_3$) δ: 29.8. HRMS (CI+) calcd for $C_{24}H_{23}O_5N_2P$ [M]+ 450.1345, found 450.1343; Anal. calcd for $C_{24}H_{23}O_5N_2P$: C, 64.0; H, 5.15; N, 6.30 Found: C, 62.8; H, 4.85; N, 6.30.

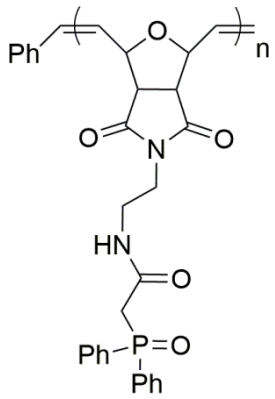

[2.9] poly *N*-(2-(1,3-dioxo-3a,4,7,7a-tetrahydro-1*H*-4,7-epoxyisoindol-2(3*H*)-yl)ethyl)-2-(diphenylphosphoryl)acetamide

In an airfree glovebox **2.8** (**2.9a**, 0.772 g, 1.714 mmol; **2.9b** 0.302 g, 0.671 mmol, **2.9c** 0.0301 g, 0.668 mmol) and Grubbs' second generation ruthenium catalyst (**2.9a**, 1.48 x 10^{-4} g, 1.75 x 10^{-4} mmol; **2.9b** 0.006 g, 0.007 mmol, 0.0576 g, 0.068 mmol) were dissolved in CH_2Cl_2. The reactions were moved outside the box and stirred under nitrogen at room temperature for 18 hours. The reactions were then exposed to the atmosphere, ethylvinyl ether was added, and the reactions were stirred for another 30 min. A gel like solid precipitated and the solvent was decanted off. The solid was re-dissolved in chloroform and precipitated out again with large amounts of MeOH. The solid was then collected by decantation and dried under reduced pressure (**2.9a** 44.0%; **2.9b** 41.2%, **2.9c** 81.9%). **2.9a** IR: ν = 1698.20 cm^{-1} (C=O, amide), 1667.22 cm^{-1} (C=O, imide), 1181.45 cm^{-1} (P=O). $^{31}P\{^1H\}$ NMR ($CDCl_3$) δ: 30.9. M_n = 3.84 x 10^5, PDI = 1.79. **2.9b**, IR: ν = 1697.92 cm^{-1} (C=O, imide), 1666.83 cm^{-1} (C=O, amide), 1180.60 cm^{-1} (P=O). ^1H NMR ($CDCl_3$) δ: 7.65 (b, 4H), 7.38 (b, 6H), 5.90 (b, 2H), 5.66 (b, 2H), 4.99 (b, 1H), 4.48 (b, 2H), 3.38 (b, 8H), 2.14 (b, 2H). $^{31}P\{^1H\}$ NMR ($CDCl_3$) δ: 31.1. **4b** M_n = 1.94 x 10^5, PDI = 1.79. **2.9c** IR: ν = 1700.65 cm^{-1} (C=O, imide), 1667.76 cm^{-1} (C=O, amide), 1183.73 cm^{-1} (P=O). ^1H NMR ($CDCl_3$) δ: 7.68 (b, 4H), 7.39 (b, 6H), 5.95 (b,

1H), 5.68 (b, 1H), 5.03 (b, 1H), 4.47 (b, 1H), 3.32 (b, 8 H). $^{31}P\{^{1}H\}$ NMR ($CDCl_3$) δ: 30.1, $M_n = 1.64 \times 10^{5,}$ PDI = 1.98.

Crystallographic Data

Table 2.3: Crystal data and structure refinement for **2.2**

CCDC # 950442

Empirical formula	$C_{11}H_{12}N_2O_2$	
Formula weight	204.23	
Temperature	100(2) K	
Wavelength	0.71069 Å	
Crystal system	Monoclinic	
Space group	$P12_1/c1$	
Unit cell dimensions	a = 4.916(5) Å	α = 90 °
	b = 8.998(5) Å	β = 94.445(5) °
	c = 21.604(5) Å	γ = 90 °
Volume	952.8(11) $Å^3$	
Z	4	
Density (calculated)	1.424 Mg/m^3	
Absorption coefficient	0.100 mm^{-1}	
F(000)	432	
Crystal size	0.38 x 0.14 x 0.09 mm^3	
θ range for data collection	3.63 to 27.48 °	
Index ranges	h = -6→6	
	k = -11→11	
	l = -27→27	
Reflections collected	21174	
Independent reflections	2193 [$R_{(int)}$ = 0.0307]	
Completeness to theta = 27.48°	99.9 %	
Refinement method	Full-matrix least-squares on F^2	
Data / restraints / parameters	2193 / 0 / 136	
Goodness-of-fit on F^2	1.051	
Final R indices [$I>2\sigma(I)$]	R_1 = 0.0372, wR_2 = 0.0980	
R indices (all data)	R_1 = 0.0398, wR_2 = 0.0996	
Largest diff. peak and hole	0.357 and -0.176 e.$Å^{-3}$	

Table 2.4: Crystal data and structure refinement for **2.4**.

CCDC # 950443

Empirical formula	C_{10} H_{12} N_2 O_3	
Formula weight	208.22	
Temperature	153(2) K	
Wavelength	0.71075 Å	
Crystal system	Monoclinic	
Space group	$P2_1/c$	
Unit cell dimensions	a = 17.840(2) Å	α = 90 °
	b = 6.8747(6) Å	β = 102.419(5) °
	c = 16.2125(17) Å	γ = 90 °
Volume	1941.9(3) Å^3	
Z	8	
Density (calculated)	1.424 Mg/m^3	
Absorption coefficient	0.107 mm^{-1}	
F(000)	880	
Crystal size	0.48 x 0.25 x 0.07 mm^3	
θ range for data collection	2.34 to 27.49 °	
Index ranges	h = -23→23	
	k = -8→8	
	l = -21→21	
Reflections collected	19826	
Independent reflections	4439 [$R_{(int)}$ = 0.0333]	
Completeness to theta = 27.49°	99.6 %	
Refinement method	Full-matrix least-squares on F^2	
Data / restraints / parameters	4439 / 0 / 287	
Goodness-of-fit on F^2	1.064	
Final R indices [I>2σ(I)]	R_1 = 0.0456, wR_2 = 0.1130	
R indices (all data)	R_1 = 0.0606, wR_2 = 0.1244	
Largest diff. peak and hole	0.221 and -0.217 e.Å^{-3}	

Table 2.5: Crystal data and structure refinement for **2.8**

Empirical formula	$C_{24}H_{23}N_2O_5P$	
Formula weight	450.41	
Temperature	153(2) K	
Wavelength	0.71069 Å	
Crystal system	Monoclinic	
Space group	$P2_1/c$	
Unit cell dimensions	a = 11.359(5) Å	α = 90 °
	b = 21.291(10) Å	β = 97.196(6) °
	c = 9.219(4) Å	γ = 90 °
Volume	2212.0(17) $Å^3$	
Z	4	
Density (calculated)	1.352 Mg/m^3	
Absorption coefficient	0.163 mm^{-1}	
F(000)	944	
Crystal size	0.37 x 0.22 x 0.12 mm^3	
θ range for data collection	1.81 to 27.46 °	
Index ranges	h = -14→14	
	k = -27→27	
	l = -11→11	
Reflections collected	23150	
Independent reflections	5039 [$R_{(int)}$ = 0.0540]	
Completeness to theta = 27.46°	99.6 %	
Max. and min. transmission	1.0000 and 0.8874	
Refinement method	Full-matrix least-squares on F^2	
Data / restraints / parameters	5039 / 0 / 293	
Goodness-of-fit on F^2	1.073	
Final R indices [$I>2\sigma(I)$]	R_1 = 0.0529, wR_2 = 0.1248	
R indices (all data)	R_1 = 0.0744, wR_2 = 0.1360	
Largest diff. peak and hole	0.421 and -0.309 e.$Å^{-3}$	

Chapter 3: Separation of *f*-Elements Using Block Copolymers

INTRODUCTION

Spent fuel from nuclear reactors contains several radioactive isotopes with long lived half lives.[32,42] With the advent of fast spectrum reactors many of these long lived products can be transmuted into shorter lived radioisotopes, creating more energy and less high level waste.[43,44] Lanthanide ions absorb neutrons quenching transmutation of the fissionable actinides, therefore it is important to be able to efficiently separate these two groups of ions. Actinide and lanthanide ions are difficult to separate, as they have similar ionic radii, are both considered hard acids, and many are trivalent in acidic media.[45] The carbamoylmethyl phosphine oxide, CMPO, ligand has shown discrimination between these two classes of materials.[5,7,30,31]

Pre-organization of several CMPO moieties, by covalently binding 2 or more CMPO groups onto a single molecule has shown improvement in extraction and separation efficiencies over single CMPO moieties.[46] Scaffolds such as calixarenes, cavitands, and tripods have been utilized for the pre-organization of CMPO.[8–10,18,20,22]

Similar to other multi-CMPO systems, our CMPO-derivatized homopolymer, **2.9c**, extracted significantly higher (> 5-25 times) amounts of thorium(IV) than analogous single CMPO systems.[10] Unlike other systems, this system can be easily synthetically modified by incorporation of additional monomers in the polymerization process, creating block polymers. The modular approach and synthetic simplicity of this system makes it a potentially valuable material for the separation of lanthanides and actinides. The impact of structural modification on these materials by incorporating new blocks has been investigated. The extraction and separations abilities of these materials have been tested utilizing both liquid-liquid and solid-liquid extractions. The introduction

of organic media into the systems creates issues of increased volume of waste, and the introduction of a volatile combustible component into the process. A solid-liquid extraction, where the ions are sequestered by passing an aqueous solution over a column of extracting material, or by mixing with a solid substrate and then filtering would eliminate the issues associated with a biphasic liquid-liquid extraction, see Figure 3.1.

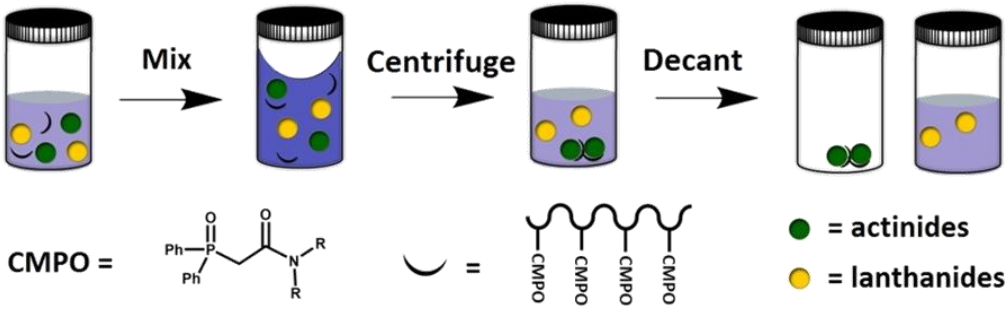

Figure 3.1: Schematic showing actinides selectively sequestered from an aqueous phase into a solid phase by a CMPO containing material.

RESULTS AND DISCUSSION

Synthesis and Characterization

The monomers **3.3** and **3.4** were synthesized as shown in Scheme 3.1. **3.1** was prepared following a modified preparation by Heath and coworkers.[34] **3.1** was converted into the mesylate **3.2** with triethylamine and methanesulfonyl chloride. 7-hydroxycoumarin was deprotonated with potassium carbonate and reacted with **3.2** to form the monomer **3.3**. The monomer was characterized by $^{13}C\{^{1}H\}$ and ^{1}H NMR spectromety, mass spectrometry, elemental analysis by combustion, and X-ray

crystallography. The X-ray structure is shown in Figure 3.2. Monomer **3.4** was prepared according to a procedure by Sleiman and coworkers.[47]

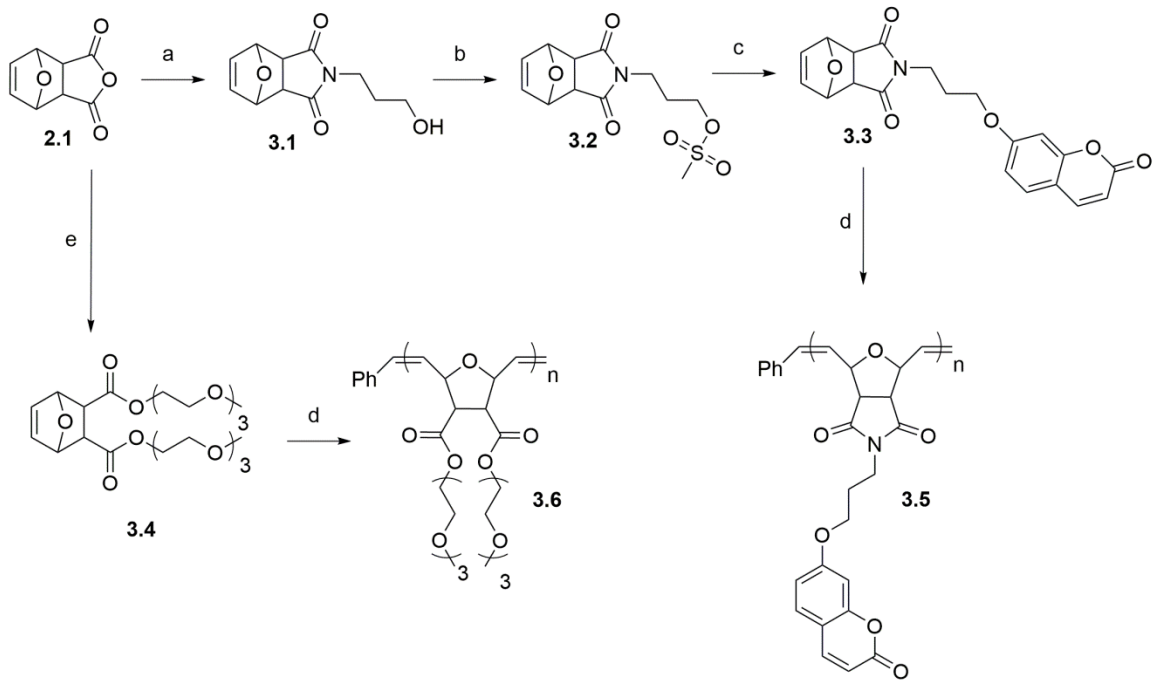

Scheme 3.1: Synthesis of homopolymers and homopolymer precursors **3.1 – 3.6**.

(a) 3-amino-1-propanol, MeOH, 66 °C, 18 h, 48.3% (b) methanesulfonyl chloride, Et_3N, CH_2Cl_2, 0 °C, 4 h, 83.7% (c) 7-hydroxycoumarin, K_2CO_3, CH_3CN, 82 °C, 18 h, 30.8% (d) Grubb's second generation catalyst, $CHCl_3$, 25 °C (e) triethylene glycol monomethyl ether, 2-chloro-1-methylpyridinium iodide, Et_3N, DMAP, CH_2Cl_2, 40 °C, 40 h, 75.85%.

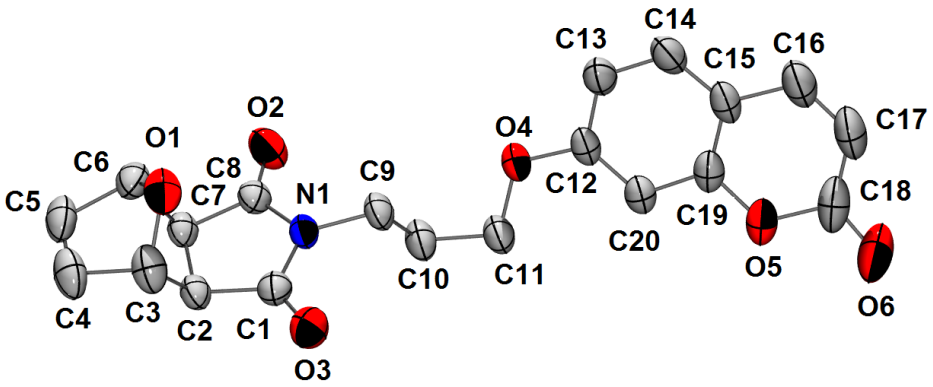

Figure 3.2: Molecular structure of **3.3**.

The atom labeling scheme is shown. Displacement ellipsoids are shown at the 50% probability level. The hydrogen atoms have been omitted for clarity.

The polymerizations were carried out using Grubbs' second generation catalyst in $CHCl_3$ for all of the polymers. To investigate the living nature of the materials, three homopolymers of **3.3** were first synthesized. The polymers were found to have a linear relationship between observed molecular weight and the ratio of monomer to catalyst used, see Figure 3.3. The homopolymers of **3.4** were studied by Sleiman and coworkers and were found to be living.[47] A homopolymer of **3.4** was synthesized to study the materials chelating properties.

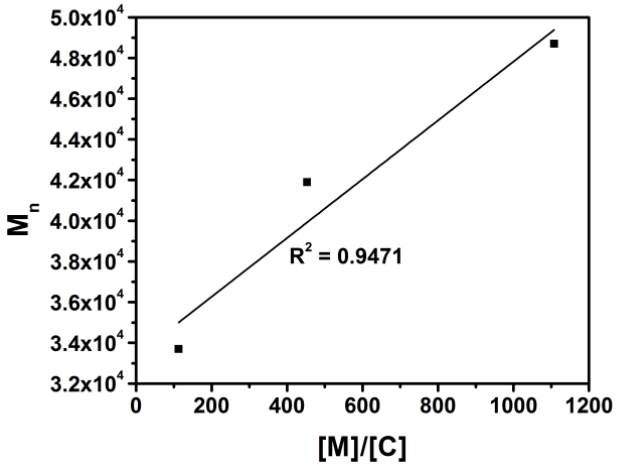

Figure 3.3: Plot of the observed molecular weight (M_n) versus monomer/catalyst ratio ([M]/[C]) for polymers **3.6a-c**.

Two diblock copolymers containing both **2.8** and **3.4** were synthesized, see Scheme 3.2. The molar ratio of **2.8** to the catalyst was kept the same in both polymerizations, but the amount of **3.4** was varied, with polymer **3.7a** having a ratio of 2 : 1 for **2.8** : **3.4** and polymer **3.7b** having a ratio of 2 : 4 for **2.8** : **3.3**. Two triblock polymers were synthesized containing **2.8**, **3.3**, and **3.4**. In these polymers the ratio of **2.8** to the catalyst and the ratio of **3.3** to the catalyst were kept constant. Polymer **3.8a** contains the blocks in the ratio 2 : 1 : 1 (**2.8** : **3.4** : **3.3**) and polymer **3.8b** has a ratio of 2 : 4 : 1 (**2.8** : **3.4** : **3.3**). All of the block copolymers were found to have high molecular weights and were characterized by GPC, ^{1}H, $^{31}P\{^{1}H\}$ NMR and IR spectroscopy.

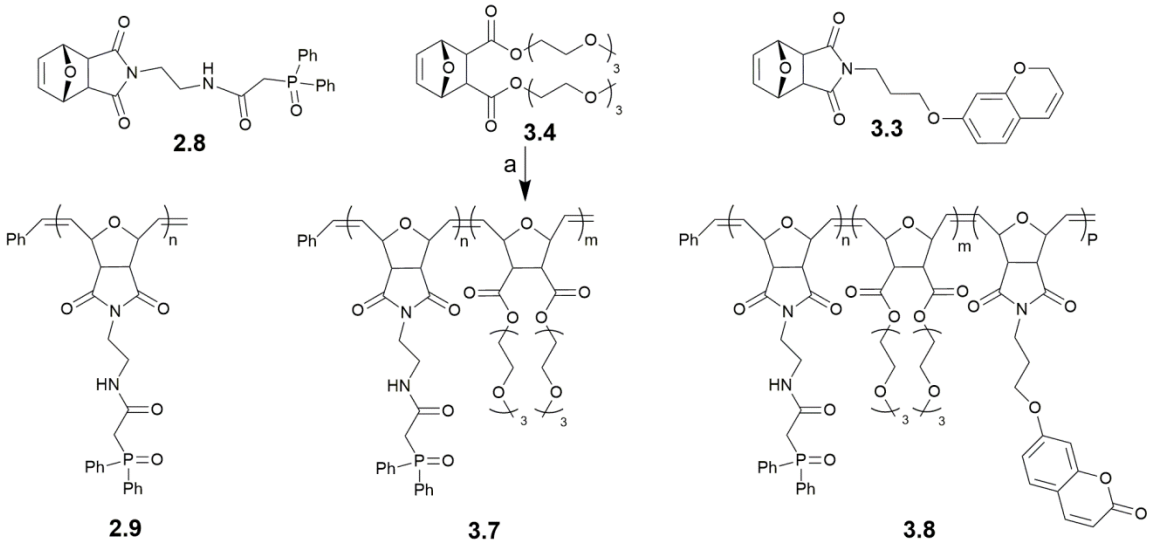

Scheme 3.2: Synthesis of homo and block polymers **2.9**, **3.7 - 3.8**.

(a) Grubb's second generation catalyst, $CHCl_3$, 25 °C.

The coumarin moiety was incorporated into the monomer **3.3** because of its ability to cross-link. The material is known to undergo a [2+2] cyclization of the double bond on the ester functionalized 6-membered ring when exposed to light with wavelengths greater than 300 nm.[48,49] The coumarin moiety is known to have a λ_{max} absorption at 320 nm.[50,51] As the material photo-cross-links, the level of unsaturation

$$D = [(A_0 - A_t) / A_0] \times 100\% \qquad (3.1)$$

decreases resulting in a decrease in the absorption at 320 nm. Due to this, the peak at 320 nm can be monitored to determine the degree of cross-linking following equation 3.1, where *D* is the degree of cross-linking, A_0 is the absorbance at 320 nm before irradiation, and A_t is the absorbance at 320 nm after irradiation. The triblock polymers **3.8a** and **3.8b** were dissolved in CH_2Cl_2 and irradiated with 365 nm light to induce cross-linking, see Figure 3.4, until increased exposure did not result in additional decrease in absorption at 320 nm. Using equation 3.1 the degree of cross-linking was determined to be 64.8% for

polymer **3.8a** and 51.8% for **3.8b**, to form the cross-linked materials **3.9a** and **3.9b** respectively.

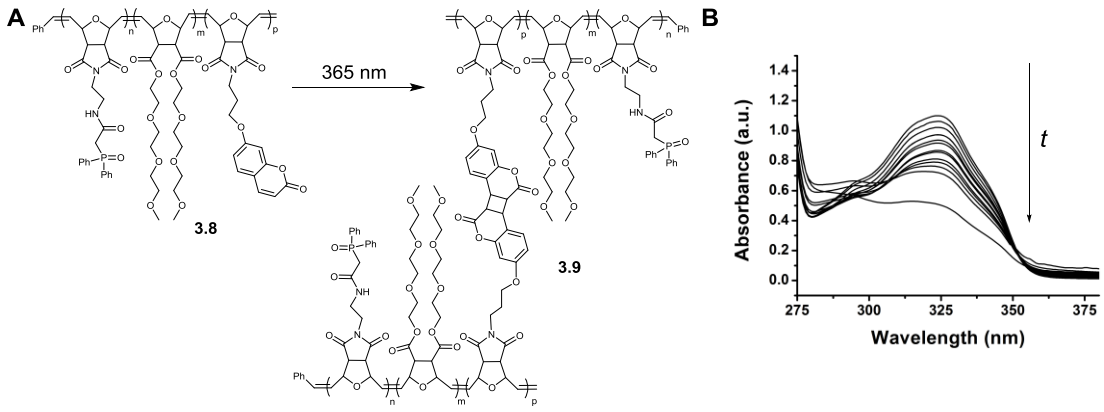

Figure 3.4: (A) Scheme showing the crosslinking of triblock copolymers 3.8 (B) UV-Vis spectra of **3.8b** in CH_2Cl_2 against irradiation time *t* with a 365 nm UV lamp.

Chelation Studies

Initial testing focused on the extraction efficiencies for a liquid-liquid extraction. This was accomplished by mixing a solution of 10^{-4} M Th^{4+} in 1 M HNO_3 with equal volumes of an immiscible organic solution of polymer. Once bound to the polymer, the metal nitrates are pulled into the organic phase.

The solubility of the homopolymer **2.9c** in *n*-dodecane was investigated due to its use in the TRUEX process. It was determined that the polymer was not sufficiently soluble in *n*-dodecane and ultimately dichloromethane was chosen as the organic media for the extractions.

The extraction of thorium(IV) was performed with varying concentrations of extracting material, 0.05 M – 0.001 M. The results of these tests are summarized in Table

3.1. At CMPO : Th^{4+} ratios of 10 : 1 all three polymers, **2.9c**, **3.7a** and **3.7b** extract over 90% of the present thorium(IV).

Table 3.1: Extraction efficiencies for selected materials in liquid-liquid extractions.

[CMPO]	**2.9c**	**3.7a**	**3.7b**
0.05	99.8 ± 0.2	99.93 ± 0.03	99.97 ± 0.03
0.01	99.947 ± 0.005	99.96 ± 0.01	98.3 ± 0.5
0.005	99.95 ± 0.01	99.962 ± 0.002	97 ± 3
0.001	93 ± 8	99 ± 1	99.2 ± 0.4

Percent of Th^{4+} extracted from 1M HNO_3 solutions by ligands. Aqueous phase: 10^{-4} $Th(NO_3)_4 \cdot H_2O$, Organic phase: extracting materials in CH_2Cl_2.

Solid-liquid extractions were performed to decrease the volume of organic waste and to eliminate a volatile/flammable component in the extractions, see Figure 3.1. The results are summarized in Table 3.2. The molarities given represent the moles of CMPO per the volume of the aqueous layer. To ensure that complexation was due to the presence of the CMPO moieties and not due to functional groups present in the other blocks, extraction tests were performed with homopolymers **3.5c** and **3.6**. It was found that homopolymers **3.5c** and **3.6** at a concentration of 0.0029 g polymer per 6 mL of 10^{-4} M Th^{4+} in 1 M HNO_3 that less than 1% of the present thorium(IV) was extracted.

Beginning with the homopolymer, **2.9c**, in a thorium(IV) only extraction, it was seen that at 100 : 1 (CMPO : Th^{4+}) and at 50 : 1 (CMPO : Th^{4+}) over 90% of the thorium(IV) was uptaken from the aqueous layer into the solid polymer. In contrast to what was observed in the liquid-liquid extractions where the extraction value remains high at 10:1 (CMPO : Th^{4+}), this value decreases to only 67% for the solid-liquid

Table 3.2: Extraction efficiencies for selected materials in solid-liquid extractions.

C_{CMPO}	**2.9c**	**3.7a**	**3.7b**	**3.9a**	**3.9b**
0.01	99.80 ± 0.04	99.86 ± 0.04	86 ± 3	93 ± 2	95 ± 1
0.005	99.2 ± 0.6	99.7 ± 0.2	88 ± 5	74 ± 4	89.7 ± 0.8
0.001	67 ± 7	99 ± 1	70 ± 3	7.7 ± 0.4	19 ± 6

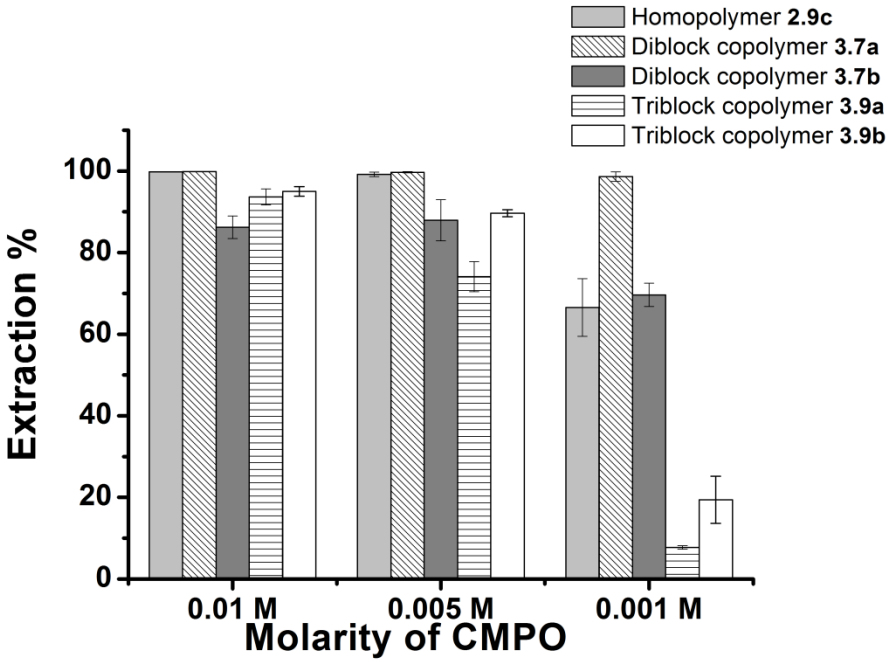

Percent of Th^{4+} extracted from 1M HNO_3 solutions by ligands. Aqueous phase: 10^{-4} $Th(NO_3)_4 \cdot H_2O$.

extraction. Similar results were observed for diblock copolymer **3.7b**. In both the liquid-liquid and solid-liquid extractions, **3.7b** uptakes over 86% of the thorium(IV) at 100 : 1 and 50 : 1 (CMPO : Th^{4+}). At 10 : 1 (CMPO : Th^{4+}) the extraction of thorium(IV) remains high (> 99%) for the liquid-liquid extraction, but the amount of thorium(IV) extracted declines to 68% for the solid-liquid extraction. Diblock copolymer **3.7a** unlike **3.7b** uptakes over 98% of the thorium(IV) present in all three tested ratios. Our theory was that the presence of the long glycol chains would be beneficial in encouraging the interaction of the polymer with the aqueous media, increasing the contact of the CMPO

units with the metal ions. It is possible that this is occurring and is causing the increase in performance seen by the diblock copolymer **3.7a**, which has half the number of repeat units of the glycol chains as it does the number of repeat units of CMPO. **3.7b** might also be experiencing a strong interaction with the aqueous media, but not incurring the same extraction values due to the fact that the larger ratio of glycol chains are blocking access to the CMPO units.

To hinder the ability of the glycol units to encapsulate the CMPO moieties and to examine this theory, triblock copolymers incorporating a cross-linkable pendant group were synthesized. To mimic the two triblock polymers, these polymers also contain the CMPO and glycol chains in ratios of 2 : 1 and 2 : 4. The cross-linking groups were incorporated for both materials in a ratio of 2 : 1 with the CMPO units. These materials were also tested for their ability to extract thorium(IV) from an aqueous acidic medium into a solid polymer. The incorporation of the cross-linking groups negatively affected the extraction ability of the materials. While the two triblock copolymers extract over 74% of the thorium(IV) for 100 : 1 and 50 : 1 (CMPO : Th), the performance at 10 : 1 (CMPO : Th) is quiet low, only 4% and 8% of the thorium(IV) was uptaken by the polymers **3.9a** and **3.9b** respectively. What is interesting is when we compare the performance of the two triblock polymers to that of the two diblock polymers. In the case of the diblock polymers more glycol chains hindered the performace of the material. When comparing **3.9a** to **3.9b**, it was seen that the material with more glycol chains, **3.9b**, outperformed the material with fewer glycol chains, **3.9a**. This evidence may support the theory that the cross-linked material does not allow the glycol chains to encapsulating the CMPO units, and thus more glycol chain units have the effect of only increasing the interactions with the aqueous media.

Table 3.3: Extraction efficiencies for selected materials in solid-liquid extractions at varying acid concentrations.

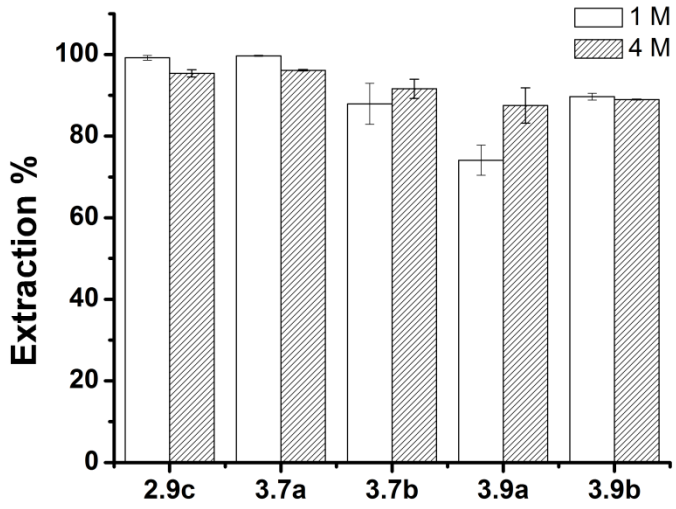

	1 M	4 M
2.9c	99.2 ± 0.6	95.4 ± 0.9
3.7a	99.6 ± 0.2	96.1 ± 0.2
3.7b	87 ± 5	92 ± 2
3.9a	74 ± 4	87 ± 4
3.9b	89.7 ± 0.8	88.97 ± 0.09

Percent of Th^{4+} extracted from 1 M and 4 M HNO_3 solutions by ligands, $C_{CMPO} = 5 \times 10^{-3}$ M . Aqueous phase: 10^{-4} $Th(NO_3)_4 \cdot H_2O$.

The extraction abilities of the materials were also tested in 4 M nitric acid, see Table 3.3. It was observed that for all five polymers the amount of thorium(IV) extracted does not change significantly (< 4%) between 1 M HNO_3 and 4 M HNO_3, except for polymer **3.9a**, which actually extracts more thorium(IV) at the higher acid concentration.

Table 3.4: Extraction efficiencies for **2.9c** in solid-liquid extractions with varying contact times.

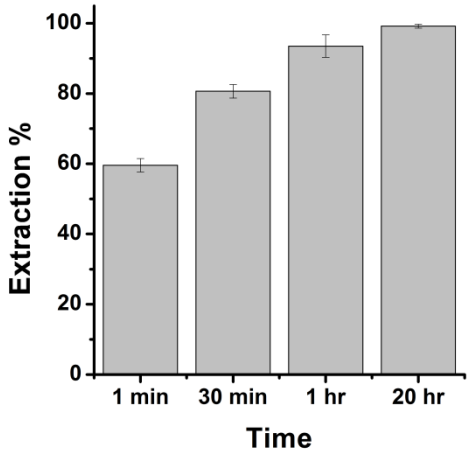

Time	% Th
1 min	60 ± 2
30 min	81 ± 2
1 hr	93 ± 3
20 hr	99.2 ± 0.6

Percent of Th^{4+} extracted from 1 M HNO_3 solutions by ligands, $C_L = 5 \times 10^{-3}$ M . Aqueous phase: 10^{-4} $Th(NO_3)_4 \cdot H_2O$.

The timescale on which extractions occur was investigated using homopolymer **2.9c**. The extraction of thorium(IV) was performed with contact times of 1 minute, 30 minutes, 1 hour, and 20 hours, see Table 3.4. After only 1 minute over 50% of the thorium(IV) was extracted, but it takes between 30 minutes and 1 hour for over 90% of the thorium(IV) to be extracted.

The selectivity for thorium(IV) over the lanthanides europium(III), lanthanum(III) and cerium(III) was investigated see Table 3.5. It was found that the homopolymer **2.9c**, the diblock copolymer **3.7b**, and the triblock copolymers **3.9a** and **3.9b** were selective for thorium(IV). The diblock copolymer **3.7a** was found to be indiscriminate for thorium(IV) over the lanthanides(III). The two diblocks were the lowest performing materials from the set and did not outperform the homopolymer. The triblock copolymers **3.9a** and **3.9b**

were over 2 times more selective than the homopolymer **2.9c**, with **3.9a** being more selective than **3.9b**.

Table 3.5: Extraction and separation efficiencies for selected materials in solid-liquid extractions.

	2.9c	**3.7a**	**3.7b**	**3.8a**	**3.8b**
%Th	97.8 ± 0.5	64 ± 8	89 ± 5	81 ± 6	96.2 ± 0.7
%Eu	49 ± 3	80 ± 3	80 ± 4	9 ± 3	21 ± 3
$\mathbf{X_{Th/Eu}}$	2.0	0.8	1.1	8.9	4.6
%La	65 ± 4	90 ± 1	77 ± 2	12 ± 4	20 ± 4
$\mathbf{X_{Th/La}}$	1.5	0.7	1.2	6.9	4.9
%Ce	67 ± 4	87 ± 5	84 ± 4	13 ± 4	14 ± 4
$\mathbf{X_{Th/Ce}}$	1.5	0.7	1.1	6.3	6.7

Percentage of Th^{4+},Eu^{3+}, La^{3+}, and Ce^{3+} (C_M = 2.5 x 10^{-4} M) extracted by polymeric materials (C_{CMPO} = 5 x 10^{-3} M) and separation ratios $X_{Th/M}$.

CONCLUSION

A series of block polymers containing CMPO pendent groups have been synthesized, characterized and the ability of the materials to efficiently and selectively extract thorium(IV) has been evaluated. Liquid-liquid extractions revealed that polymers **2.9c**, **3.7a**, and **3.7b** have high affinities (>99 %) for Th^{4+} even at low concentrations of ligand (ligand : Th^{4+} 10 : 1). Solid-liquid extractions revealed that all of the materials had high affinities (> 85%) at sufficiently high ligand concentrations (CMPO : Th^{4+} 100 : 1). The incorporation of blocks of long glycol chains has caused improvements in extraction of thorium(IV) as compared to the homopolymer. At lower ligand concentrations, only diblock copolymer **3.7a** had high affinities. At 4 M HNO_3 each material extracted comparable amounts of thorium(IV) as compared to extractions with 1 M HNO_3. A time

dependence study revealed that within 30 min, over of 80% of the thorium(IV) is removed.

The selectivity for thorium(IV) over lanthanum(III), europium(III), and cerium(III) was also tested. The triblock copolymers had the highest selectivies, followed by the homopolymers, then the diblock copolymers. The incorporation of both long glycol chains and cross-linking groups has caused improvements in the selectivity of the materials as compared to the homopolymer.

EXPERIMENTAL

General Methods

All chemicals were purchased from chemical suppliers and were used without further purification. All dry reactions were performed using standard Schlenk techniques and were performed under an inert atmosphere of nitrogen. CH_2Cl_2 and $CHCl_3$ were dried using the Pure-Solv 400 solvent purification system. ^{1}H $^{13}C\{^{1}H\}$, and $^{31}P\{^{1}H\}$ NMR spectra were obtained on a Varian 300 MHz, or 400 MHz spectrometer. ^{1}H, and $^{13}C\{^{1}H\}$ NMR spectra were referenced to the residual solvent peaks. $^{31}P\{^{1}H\}$ NMR spectra were referenced to a phosphoric acid external standard. High resolution mass spectra were obtained with an Agilent Technologies 6530 Accurate Mass QTofLC/MS. Elemental analysis was performed by QTI, Whitehouse, NJ (www.qtionline.com). IR spectra were recorded on a Nicolet iS50 ATR spectrometer with a deuterated triglycine sulfate (DTGS) detector from Thermo Scientific. Number average molecular weights (M_n) and polydispersity indices (PDI) were measured from DMF solutions using an Agilent 1100 series GPC (Agilent Technologies) equipped with Viscotek I-series mixed bed medium molecular weight columns and refractive index detectors, and are reported relative to

polystyrene standards. Absorption spectra were recorded in CH_2Cl_2 on a Varian Cary 6000i UV-Vis-NIR spectrophotometer with Starna Quartz fluorometer cells with a path length of 1 cm. Compound **3.6** were prepared according to literature procedures.[47]

Extractions

The lanthanide and actinide salts, $Th(NO_3)_4 \cdot H_2O$ (Strem), $Ce(NO_3)_3 \cdot 6H_2O$ (Alfa Aesar), $Eu(NO_3)_3 \cdot 5H_2O$ (Strem), and $La(NO_3)_3 \cdot 6H_2O$ (Fisher), were used as received. Solutions were prepared using trace metal grade deionized water, trace metal grade HNO_3 (BDH), and twice distilled dichloromethane.

Three aqueous solutions were prepared: a solution of 10^{-4} M Th^{4+} in 1 M HNO_3, a solution of 10^{-4} M Th^{4+} in 4 M HNO_3, and a solution of 2.5 x 10^{-5} M Th^{4+}, 2.5 x 10^{-5} M Eu^{4+}, 2.5 x 10^{-5} M Ce^{4+} and 2.5 x 10^{-5} M La^{4+} in 1 M HNO_3.

For the liquid-liquid extractions 0.6 mL of aqueous and organic phases (ligands dissolved in CH_2Cl_2) were mixed in a 1 dram glass vials equipped with a polyethylene cap and PTFE coated stir bars. The vials were stirred at 1200 rpm for 20 hours. The solutions were then centrifuged and the aqueous layer pipetted off the top and transferred to a 1 mL centrifuge tube. The solution was centrifuged again and the top layer was diluted to ppb levels with 2% HNO_3.

The solid-liquid extractions were performed by weighing solid ligands into 1 dram glass vials and adding 0.6 mL of a metal nitrates in nitric acid. The molarities reported represent the moles of each CMPO repeat unit per 0.6 mL. Due to the varying ratio of blocks in each polymer, different masses of each polymer were required to reach the same concentration of CMPO in solution, see Table 3.6 for masses of each polymer used. The solution was mixed at 1200 rpm for 20 hours, unless otherwise noted. The

solution was centrifuged and the aqueous layer decanted off the solid material and transferred to a 1 mL centrifuge tube. The solution was centrifuged again to remove any remaining solid materials and the top later was diluted to ppb levels with 2% HNO_3. For both the liquid-liquid and solid-liquid extractions the diluted solutions were counted in triplicate using a GBC Optimass 8000 ICP-time-of-flight (TOF)-MS (GBC Scientific Equipment, Hampshire, IL) or a PerkinElmer NexION 300D ICP-MS. The extraction efficiencies were determined using equation 3.2, where C_1 is the average count from the sample, and C_0 is the average count of a solution stirred with no organic phase and no extracting material. All % E values are the average of three separate trials.

$$\% E = ((C_0 - C_1)/C_0) \times 100\% \qquad (3.2)$$

Separation factors, X, were determined using equation 3.3, where % M is the extraction percentage for a given cation.

$$X_{M1/M2} = \% M1 / \% M2 \qquad (3.3)$$

X-ray Crystallography

Crystals of **3.3** suitable for X-ray diffraction were obtained by layering a solution of **3.3** in CH_2Cl_2 with MeOH. The single–crystal diffraction data was collected on a Rigaku SCX-Mini diffractometer with a Mercury CCD using a Rigaku Tec 50 low-temperature device. The complex was collected using a graphite monochromator with MoKα radiation (λ = 0.71073Å). Absorption corrections were applied using multi-scan. Data reduction was performed using the Rigaku Americas Corporation's Crystal Clear version 1.40.[39] The structures were solved by direct methods using SIR92 and refined anisotropically using full-matrix least-squares methods with the SHELX-97 program package.[40,52] Structure analysis was aided by the use of the programs PLATON98 and

WINGX.[53,54] The coordinates of the non-hydrogen atoms were refined anisotropically. All H atoms were positioned geometrically and refined using a riding model, with C—H = 0.93 – 0.98 Å and U_{iso}(H) = 1.2 U_{eq}(C). Neutral atom scattering factors and values used to calculate the linear absorption coefficient are from the International Tables for X-ray Crystallography (1992).[41]

Synthesis

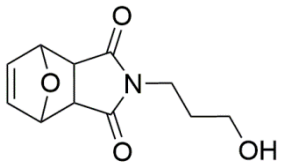

[3.1] 2-(3-hydroxypropyl)-3a,4,7,7a-tetrahydro-1*H*-4,7-epoxyisoindole-1,3(2*H*)-dione

3.1 was prepared according to a modified procedure of Heath and coworkers.[34] 3-amino-1-propanol (27.05 g, 162.92 mmol), and **2.1** (12.40 g, 165.09 mmol) were refluxed in MeOH (500 mL) at 66 °C for 18 hours. The resulting solution was concentrated to half its volume and cooled to 0 °C. A colorless solid precipitated out after 24 hours and was collected by vacuum filtration to yield **3.1** (17.67g, 48.3%). (m.p. 119 °C). ^{1}H NMR (300 MHz, $CDCl_3$) δ: 6.49 (s, 2H), 5.23 (s, 2H), 3.61 (t, 2H, J = 6.3), 3.48 (t, 2H, J = 5.7), 2.84 (s, 2H), 2.52 (b, 1H), 1.73 (5, 2H, J = 5.4). ^{13}C{^{1}H} NMR (75 MHz, $CDCl_3$) δ: 177.2, 136.8, 81.2, 58.9, 47.7, 35.4, 30.6.

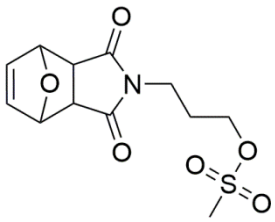

[3.2] 3-(1,3-dioxo-1,3,3a,4,7,7a-hexahydro-2*H*-4,7-epoxyisoindol-2-yl)propyl methanesulfonate

To a flame dried Schlenk tube was added dry CH_2Cl_2 (30 mL), **3.1** (2.07 g, 9.28 mmol), and triethylamine (2.21 g, 21.84 mmol). The mixture was cooled to 0 °C and methanesulfonyl chloride (2.59 g, 22.61 mmol) in dry CH_2Cl_2 (30 mL) was added dropwise. The mixture was stirred overnight; under argon, letting it slowly warm to room temperature. A 2M HCl solution (30 mL) was added and the mixture was then extracted with CH_2Cl_2 (3 x 15 mL). To the combined organic layers, a saturated $NaHCO_3$ solution was added (30 mL) and the mixture was extracted with CH_2Cl_2 (3 x 15 mL). The combined organic layers were dried with sodium sulfate and concentrated. The resulting oil was added to diethyl ether and cooled to 0 °C. A yellow solid was collected by vacuum filtration to yield **3.2** (2.34g, 83.7 %). (m.p. 94 °C). ^{1}H NMR (300MHz, $CDCl_3$) δ: 6.48 (d, 2H, *J* = 0.9), 5.23 (t, 2H, *J* = 0.9), 4.14 (t, 2H, *J* = 6.0), 3.60 (t, 2H, *J* = 6.6), 3.00 (s, 3H), 2.84 (s, 2H), 2.01 (5, 2H, *J* = 6.30). ^{13}C{^{1}H} NMR (75 MHz, $CDCl_3$) δ: 176.5, 136.8, 81.2, 67.2, 47.7, 37.5, 35.5, 27.3.

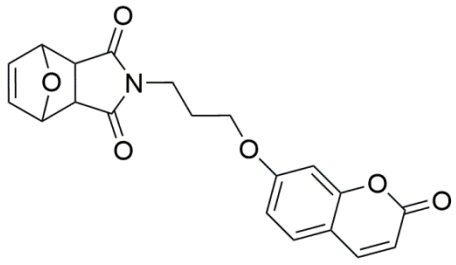

[3.3] 2-(3-((2-oxo-2*H*-chromen-7-yl)oxy)propyl)-3a,4,7,7a-tetrahydro-1*H*-4,7-epoxyisoindole-1,3(2*H*)-dione

To a flame dried schlenk flask was added **3.2** (2.87 g, 9.54 mmol), 7-hydroxycoumarin (1.57 g, 9.70 mmol), and K_2CO_3 (1.49 g, 10.75 mmol) in acetonitrile. The solution was refluxed for 18 hrs. The solution was cooled to room temperature and the product was collected by vacuum filtration. The product was purified by dissolving in dichloromethane and precipitating with methanol to yield a pale pink solid (yield 1.08g, 30.8 %). m.p. 149 °C. ^{1}H NMR (300MHz, $CDCl_3$) δ: 7.56 (d, 1H, J = 9.3), 7.29 (d, 1H, J = 8.7), 6.75 (d,t, 1H, J = 8.4, 1.2), 6.68 (s, 1H), 6.45 (t, 2H, J = 0.9), 6.16 (d, 1H, J = 9.6), 5.17 (t, 2H, J = 0.9), 3.92 (t, 2H, J = 6.0), 3.63 (t, 2H, J = 6.9), 2.79 (d, 2H, J = 0.9), 2.03 (5, 1H, J = 6.3), ^{13}C{^{1}H} NMR (75MHz, $CDCl_3$) δ: 176.1, 161.8, 161.0, 155.6, 143.3, 136.4, 128.7, 112.9, 112.6, 112.4, 101.2, 80.8, 65.6, 47.3, 35.8, 26.9. HRMS (ESI+), calculated for $C_{20}H_{17}NO_6$: $[M + H]^+$ 368.11290; found 368.11310. Anal. calcd for $C_{20}H_{17}NO_6$: C, 65.39; H, 4.66; N, 3.81 Found: C, 65.26; H, 4.72; N, 3.81.

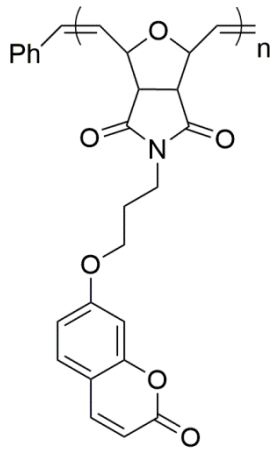

[3.5] poly 2-(3-((2-oxo-2*H*-chromen-7-yl)oxy)propyl)-3a,4,7,7a-tetrahydro-1*H*-4,7-epoxyisoindole-1,3(2*H*)-dione

In an airfree glovebox **3.3** (**3.5a**, 0.04 g, 0.11 mmol; **3.5b** 0.04 g, 0.11 mmol; **3.5c** 0.040 g, 0.11 mmol) and (**3.5a**, 2 mL, 9.9 x 10^{-4} mmol; **3.5b** 0.5 mL, 2.5 x 10^{-4} mmol; **3.5c** 0.2 mL, 9.9 x 10^{-5} mmol) of a 4.9 x 10^{4} M Grubbs' second generation ruthenium catalyst were dissolved in CH_2Cl_2. The reactions were moved outside the box and stirred under nitrogen at room temperature for 18 hours. The reactions were then exposed to the atmosphere, ethylvinyl ether was added, and the reactions were stirred for another 30 min. A gel like solid precipitated and the solvent was decanted off. The solid was re-dissolved in chloroform and precipitated out again with large amounts of MeOH. The solid was then collected by decantation and dried under reduced pressure (yield **3.5a** 37.90%; **3.5b** 94.40 %; **3.5c** 80.10%). **3.5a** IR: ν = 1696.29 cm^{-1} (C=O, imide), M_n = 3.37 x 10^{4}, PDI = 2.81. **3.5b** IR: ν = 1694.21 cm^{-1} (C=O, imide), M_n = 4.19 x 10^{4}, PDI = 2.67. ^{1}H NMR (400 MHz, $CDCl_3$): δ 7.58 (b), 7.31 (b), 6.88 – 6.51 (m), 6.10 (b), 5.98 (b), 5.74 (b) 5.02 (b), 4.43 (b), 3.87 (b), 3.80 – 3.13 (m) 2.06 (b), 1.39 (b). **3.5c** IR: ν = 1693.62 cm^{-1} (C=O, imide), M_n = 4.87 x 10^{4}, PDI = 2.87.

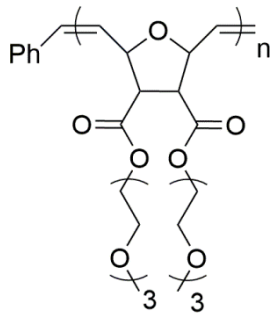

[3.6] poly 2-(3-((2-oxo-2*H*-chromen-7-yl)oxy)propyl)-3a,4,7,7a-tetrahydro-1*H*-4,7-epoxyisoindole-1,3(2*H*)-dione

Following the procedure described for the synthesis of **3.5**, **3.4** (0.33 g, 0.69 mmol) and Grubbs' second generation ruthenium catalyst (0.006g, 0.007 mmol) gave a 70.2% yield of product. M_n = 1.19 x 10^4, PDI = 1.82.

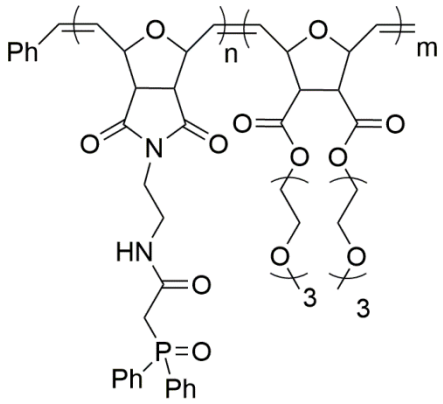

[3.7] Diblock Coploymer

In an airfree glovebox **2.8** (**3.7a**, 0.30 g, 0.67 mmol; **3.7b** 0.30 g, 0.67 mmol) and was dissolved in dry CH_2Cl_2. A 1.2 x 10^{-2} M solution of Grubbs' second generation ruthenium catalyst (**3.7a**, 0.63 mL, 7.32 x 10^{-3} mmol; **3.7b** 0.63 mL, 7.32 x 10^{-3} mmol) was added. The solution was stirred in the box for 1 hr. The consumption of the monomer was confirmed by TLC and a 1.64 M solution of **3.4** (**3.7a**, 0.20 mL, 0.33 mmol; **3.7b**, 0.81 mL, 1.33 mmol) was added. The solution was stirred for an additional hour. The

consumption of the monomer was confirmed by TLC, and reactions were then exposed to the atmosphere. Ethyl vinyl ether was added, and the reactions were stirred for another 30 min. A gel like solid precipitated and the solvent was decanted off. The solid was re-dissolved in chloroform and precipitated out again with large amounts of MeOH. The solid was then collected by decantation and dried under reduced pressure. (yield **3.7a** 23.4%; **3.7b** 23.6%). **3.7a** IR: ν = 1699.13 cm^{-1} (C=O, imide), 1662.14 cm^{-1} (C=O, amide), 1181.67 cm^{-1} (P=O). ^{1}H NMR (300 MHz, $CDCl_3$): δ 7.67 (b), 7.39 (b), 6.01 – 5.80 (m), 5.58 (b), 5.07 (b), 4.69 (b), 4.22 (b, 8H), 3.78 – 3.02 (m), 2.53 (b). $^{31}P\{^{1}H\}$ NMR ($CDCl_3$) δ: 29.7. GPC: M_n = 5.78 x 10^4 g mol^{-1}, PDI = 1.89. **3.7b** IR: ν = 1700.92.13 cm^{-1} (C=O, imide), 1662.12 cm^{-1} (C=O, amide), 1177.32 cm^{-1} (P=O). ^{1}H NMR (300 MHz, $CDCl_3$): δ 7.69 (b), 7.41 (b), 6.01 – 5.80 (m), 5.58 (b), 5.07 (b), 4.69 (b), 4.22 (b, 8H), 3.78 – 3.02 (m), 2.53 (b). $^{31}P\{^{1}H\}$ NMR ($CDCl_3$) δ: 32.9. GPC: M_n = 6.40 x 10^4 g mol^{-1}, PDI = 1.76.

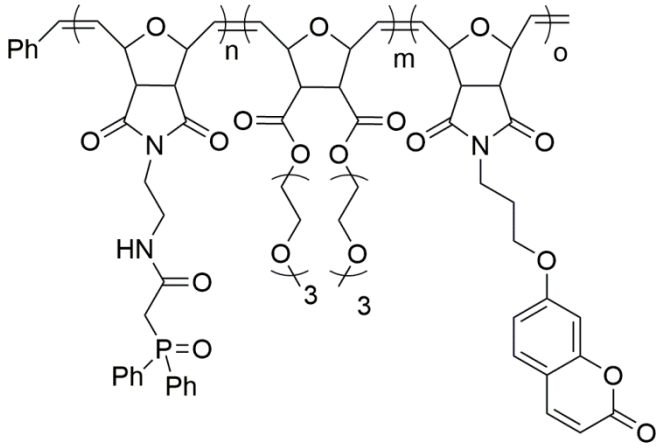

[3.8] Triblock Coplymer

In an air-free glovebox **2.8** (**3.8a**, 0.30 g, 0.664 mmol; **3.8b** 0.30 g, 0.668 mmol) was dissolved in 10mL of dry CH_2Cl_2. A 0.011 M solution of Grubbs' second generation ruthenium catalyst in CH_2Cl_2 was added (**3.8a**, 0.64 mL, 6.99 x 10^{-3} mmol; **3.8b** 0.64 mL, 6.99 x 10^{-3} mmol). The solution was stirred in the box for 1 hr. The consumption of the monomer was confirmed by TLC. Next **3.4** (**3.8a**, 0.161 g, 0.34 mmol; **3.8b**, 0.630 g, 1.32 mmol) was added and allowed to stir for an additional hour. The consumption of the monomer was confirmed by TLC, next **3.3** (**3.8a**, 0.123 g, 0.33 mmol; **3.8b**, 0.122 g, 0.33 mmol) was added and allowed to stir for an additional hour. The consumption of the monomer was confirmed by TLC, and reactions were then exposed to the atmosphere. Ethylvinyl ether was added, and the reactions were stirred for another 30 min. A gel like solid precipitated and the solvent was decanted off. The solid was re-dissolved in chloroform and precipitated out again with large amounts of MeOH. The solid was then collected by decantation and dried under reduced pressure (**3.8a** 39.8% yield; **3.8b** 27.4% yield). **3.8a** IR: ν = 1697.97 cm^{-1} (C=O, imide), 1697.97 cm^{-1} (C=O, amide), 1178.42 cm^{-1} (P=O). ^{1}H NMR (400 MHz, $CDCl_3$): δ 7.62 (b), 7.36 (b), 6.69 (b), 6.37 – 6.46 (m), 6.14 (b), 5.89 (b), 5.64 (b), 5.20 (t, J = 11), 4.85 (b), 4.39 (b), 3.93 (b), 3.74 – 2.94 (m), 2.77 (t,

J = 8), 2.10 – 1.03 (m). $^{31}P\{^{1}H\}$ NMR ($CDCl_3$) δ: 29.5. GPC: M_n = 2.31 x 10^5 g mol^{-1}, PDI = 2.73. **3.8b** IR: *v* = 1695.23 cm^{-1} (C=O, imide), 1658.01 cm^{-1} (C=O, amide), 1181.09 cm^{-1} (P=O). ^{1}H NMR (300 MHz, $CDCl_3$): *δ* 7.61 (b), 7.42 (b), 6.75 (b), 6.46 (b), 6.24 – 5.55 (m), 4.95 (b), 4.43 (b), 4.17 (b), 3.98 (b), 3.76 – 3.06 (m), 2.80 (t, *J* = 5), 2.14 (b), 1.63 (b), 1.22 (b). $^{31}P\{^{1}H\}$ NMR ($CDCl_3$) δ: 29.2. GPC: M_n = 8.63 x 10^5 g mol^{-1}, PDI = 1.86.

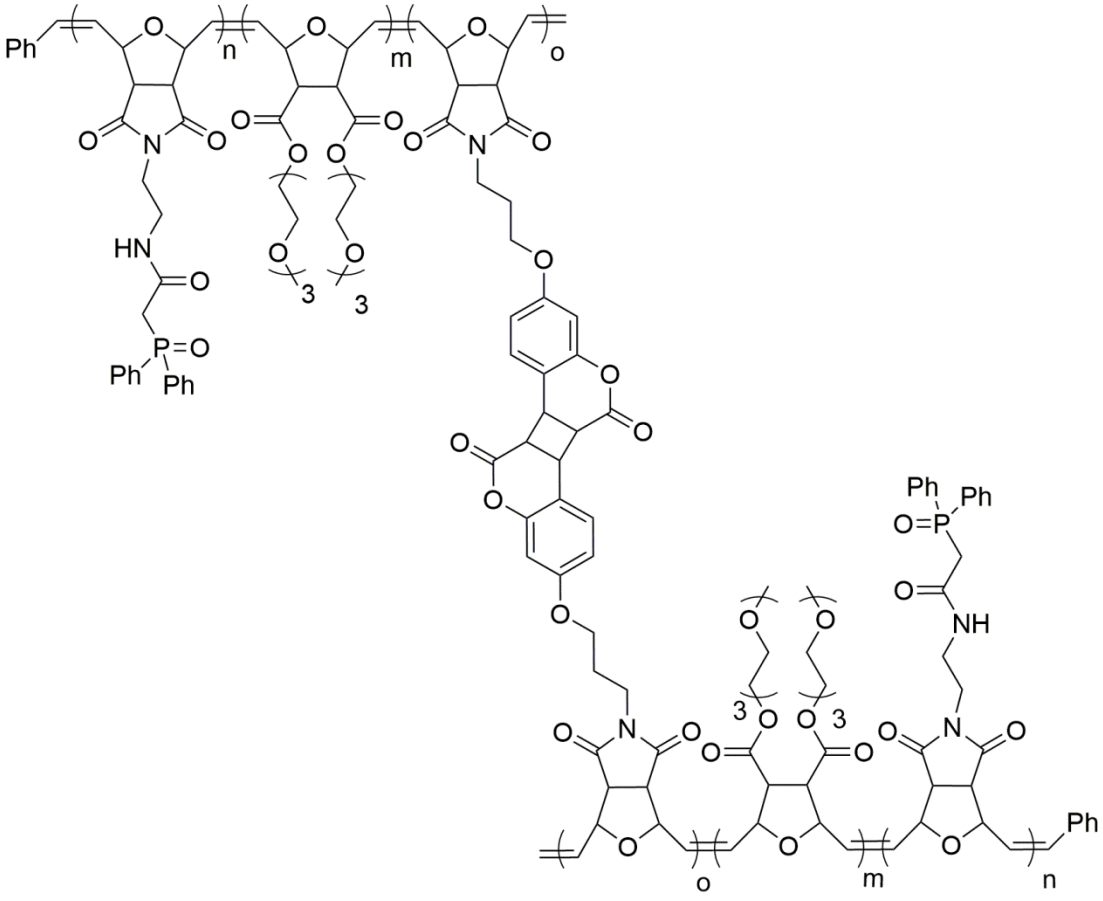

[3.9] Crosslinked Triblock Polymers

Photocrosslinking was achieved by irradiating a dilute solution (absorbance at 320 nm < 1.3 au) with a 365 nm 8 W handheld lamp while stirring. The process was

monitored by UV-Vis spectroscopy using the λ_{max} = 320nm. The absorbance decreased with increasing exposure to the lamp. The cross linking was continued until no further decrease in the absorption was observed with increasing exposure to the lamp (about 72 hours). (**3.9a** *D* = 64.8%; **3.9b** *D* = 51.8%). **3.9a** IR: *v* = 1698.15 cm^{-1} (C=O, imide), 1668.15 cm^{-1} (C=O, amide), 1181.52 cm^{-1} (P=O). **3.9b** IR: *v* = 1694.85 cm^{-1} (C=O, imide), 1659.53 cm^{-1} (C=O, amide), 1179.42 cm^{-1} (P=O).

Table 3.6: Quantities of polymeric materials used in 0.6 mL extractions.

	0.01 M (g)	0.005 M (g)	0.001 M (g)
HomoPolmyer 2.9c	0.0027	0.0014	0.0003
Diblock Copolymer 3.7a	0.0041	0.0021	0.0004
Diblock Copolymer 3.7b	0.0029	0.0015	0.0003
Triblock Copolymer 3.9a	0.0053	0.0026	0.0005
Triblock Copolymer 3.9b	0.0095	0.0047	0.0009

Crystallographic Data

Table 3.7: Crystal data and structure refinement for **3.3**

Empirical formula	$C_{20}H_{17}NO_6$	
Formula weight	367.35	
Temperature	223(2) K	
Wavelength	0.71069 Å	
Crystal system	Monoclinic	
Space group	$P12_1/n1$	
Unit cell dimensions	a = 11.240(5) Å	α = 90 °
	b = 5.388(5) Å	β = 100.469(5) °
	c = 29.028(5) Å	γ = 90 °
Volume	1728.7(18) $Å^3$	
Z	4	
Density (calculated)	1.411 Mg/m^3	
Absorption coefficient	0.105 mm^{-1}	
F(000)	768	
Crystal size	0.48 x 0.17 x 0.08 mm^3	
θ range for data collection	1.43 to 27.48 °	
Index ranges	h = -14→14	
	k = -6→6	
	l = -37→37	
Reflections collected	28771	
Independent reflections	3831 [$R_{(int)}$ = 0.0724]	
Completeness to theta = 27.46°	99.7 %	
Max. and min. transmission	1.0000 and 0.7244	
Refinement method	Full-matrix least-squares on F^2	
Data / restraints / parameters	3931 / 0 / 244	
Goodness-of-fit on F^2	1.073	
Final R indices [$I>2\sigma(I)$]	R_1 = 0.0529, wR_2 = 0.1248	
R indices (all data)	R_1 = 0.0744, wR_2 = 0.1360	
Largest diff. peak and hole	0.421 and -0.309 e.$Å^{-3}$	

LUMINESCENT MATERIALS

Chapter 4: A Review of Tetradentate Platinum(II) Complexes

INTRODUCTION

Light emitting compounds have become highly desirable materials for their potential in light-emitting diodes,[55,56] sensors,[57,58] and biological labeling.[59,60] In organic light-emitting diodes (OLEDs) exciton formation occurs so that 25% of the excitons created have singlet character, while 75% have triplet character.[61,62] While fluorescent emitters are only able to utilize the singlet excitons, the presence of a heavy metal can facilitate intersystem crossing to utilize both the singlet and triplet excitons. Platinum, in particular, has a high spin-orbital coupling constant, which promotes intersystem crossing.[63]

Four coordinate, square planar, platinum(II) complexes have long been known to be highly emissive over a wide range of wavelengths.[64–66] These complexes have typically been either bidentate or tridentate, with the only tetradentate examples being that of porphyrin based ligands. Platinum(II) porphyrin compounds have been in the literature for over 45 years.[67–72] It was not until 2003, with the appearance of platinum(II) salen complexes, that a new type of tetradentate platinum complex was developed.[73] Since then, tetradentate platinum(II) complexes with wide ranging ligand sets have been developed.[73–80] These complexes have high luminescent quantum yields and thermal stabilities, and emit over a wide range of wavelengths. Herein is a review of the photophysical properties and thermal stabilities of the non-porphyrin-based tetradentate platinum(II) complexes in the current literature. The known complexes have been divided into 5 different classes: N^N^N^N, O^N^C^N, O^N^N^O, carbenes, and C^N^N^C.

N^N^N^N Tetradentate Platinum(II) Complexes

Only one study, by Lai *et al.*, reported non-porphyrin tetradentate platinum(II) complexes of the type N^N^N^N.[75] The three complexes are shown in Figure 4.1. These complexes are *bis*(pyrrolidene) Schiff bases. *Bis*(pyrrolidene) compounds have been employed in the polymerization of lactide[76,81] and in developing lanthanide sensors.[82,83]

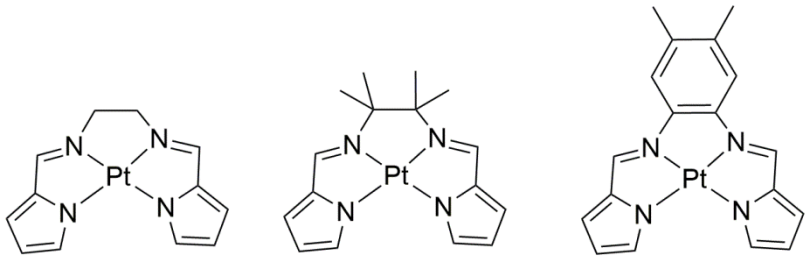

Figure 4.1: N^N^N^N tetradentate platinum(II) complexes.[75]

All three complexes were found to be highly absorbing with molar absorptivities of approximately 0.5 – 2.5 x 10^4 M^{-1} cm^{-1}. Complexes **4.1a** and **4.1b** absorbed between 250 – 500 nm and complex **4.1c** absorbed between 250 – 570 nm. **4.1a** and **4.1b** were both found to have emission maxima around 560 nm and 610 nm, while complex **4.1c** was found to have emission energy around 700 nm and 750 nm for solution-state (CH_3CN) room temperature emission studies. The emission wavelength and low quantum efficiency (0.01%) of **4.1c** made it unsuitable for OLED applications and thus Lai and coworkers did not study the complex further. Complexes **4.1a** and **4.1b** were found however to have higher quantum efficiencies of 0.97% and 1.05%, respectively. The emission of **4.1a** was found to have a maximum at 566 nm with a shoulder at 613 nm for the room temperature emission. Upon cooling the solution to 77 K, an emission shift was observed at 560 nm and 611 nm with a shoulder at 650 nm. As the concentration of the

solution was increased, a red shift in the emission was observed, which was attributed to the formation of excimers or oligomers at high concentrations. Excimer formation is common in Pt(II) compounds.[84,85] Complex **4.1b** however, does not exhibit the same behavior, possibly due to the methylethylene moiety hindering close intermolecular interactions. The photoluminescent lifetimes for **4.1a** and **4.1b** were reported as 4.2 μs and 3.6 μs, respectively. These lifetimes are somewhat short when compared with Pt(II) porphyrin compounds, which are also of the type N^N^N^N.[75]

The thermal stabilities of complexes **4.1a** and **4.1b** were investigated by thermogravimateric analysis (TGA). It was found that complex **4.1a** and **4.1b** had decomposition temperatures of 288 °C and 320 °C, respectively.

O^N^C^N Tetradentate Platinum(II) Complexes

Two studies, both by Che and coworkers, report tetradentate platinum(II) complexes of the type O^N^C^N.[56,78] These studies report eight different complexes, which are shown in Figure 4.2. All of the ligand sets are asymmetric, which is less prevalent in the literature than symmetric ligands.

The absorption profiles of all eight complexes were reported.[56,78] The complexes were found to be have high molar absorptivities on the order of 10^4 M^{-1} cm^{-1}, see Table 4.1. All 8 complexes were found to be highly absorbing at wavelengths below 300 nm, moderately absorbing at 400 – 438 nm, and weakly absorbing with absorption tails at > 460 nm. The high intensity absorptions (< 300 nm) were assigned to intraligand $^1\pi$-π^* transitions by Che and coworkers. Solvatochromism was not discussed for complexes **4.2a – 4.2e**. The solvatochromic effect was observed in the absorption profile for

complexes **4.3a – 4.3c**. Complexes **4.3a – 4.3c** display a blue shift in the absorption moving from less to more polar solvents.

The solution state emission maxima range from 482 – 522 nm for all eight complexes. Complexes **4.2a** – **4.2e** all show vibronic structured emission bands, while complexes **4.3a** – **4.3c** exhibit structureless emission. A concentration dependence study was performed for complexes **4.2a** – **4.2e**. When the concentration of the solutions was increased, a low energy absorption was observed for complexes **4.2b**, **4.2d**, and **4.2e**.

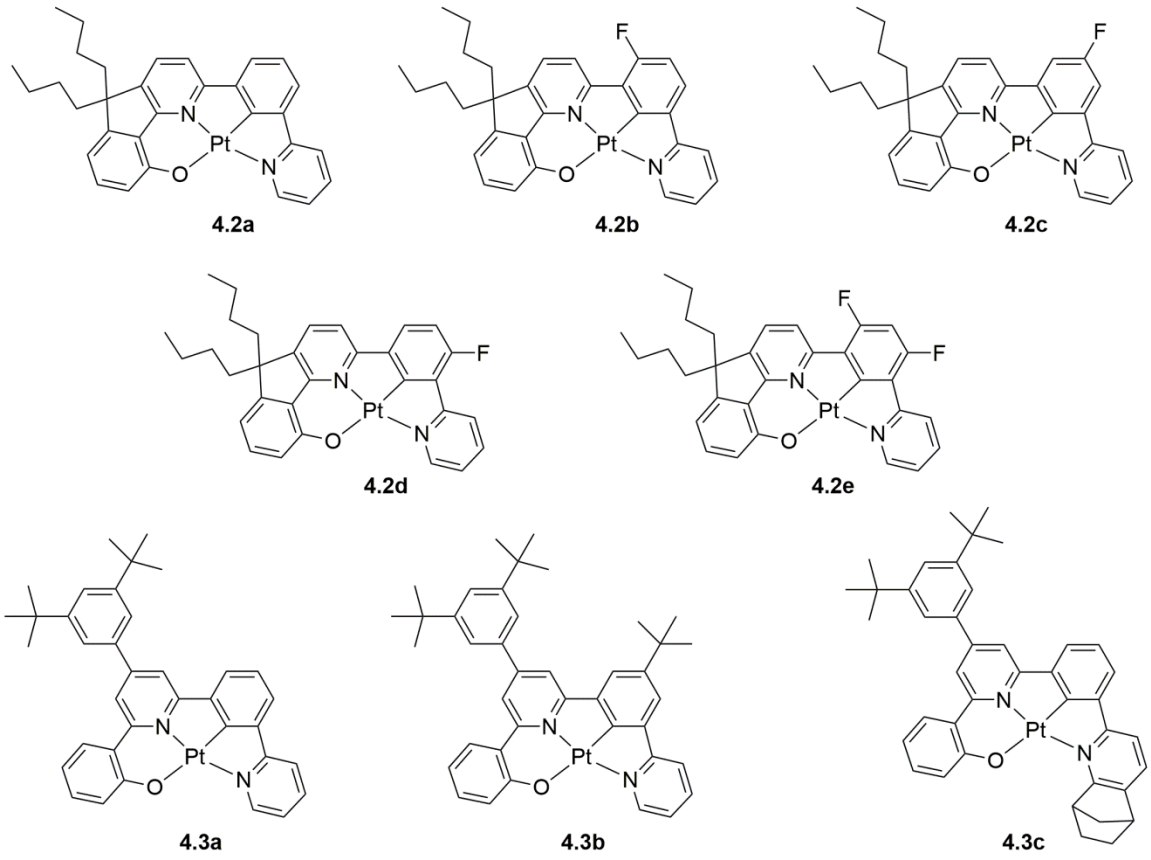

Figure 4.2: O^N^C^N tetradentate platinum(II) complexes.[56,78]

This has been attributed to excimer formation by Che and coworkers. The solvent emission dependence was studied for complexes **4.3a** – **4.3c**. As in the absorption profiles, these complexes display a blue shift in the emission moving from less to more polar solvents. The emission quantum yields ranged from 72% to 93%. Complex **4.2d** with an emission quantum yield of 93% is the highest solution state quantum yield among all the discussed tetradenate platinum(II) complexes. The emission lifetimes for all eight complexes are in the microsecond range, with the shortest being 3.7 μs and the longest being 28.0 μs. Complexes **4.2a** – **4.2e** have longer lifetimes (11.0 – 28.0 μs) than the complexes **4.3a** – **4.3c** (3.7 – 4.9 μs).

Table 4.1: Physical, spectroscopic, and photophysical data for **4.2a -4.3c**

	λ_{Abs} [nm] (ε [x 10^{-4} M^{-1} cm^{-1}])	λ_{Em} [nm]	Φ_{Em}	τ [μs]	T_d [°C]
4.2a[56]	254 (4.59), 280 (3.16), 354 (1.77), 390 (1.46), 426 (0.91)	485, 517, 557	0.72	12.0	414
4.2b[56]	254 (4.24), 261 (4.18), 290 (2.51), 352 (1.71), 388 (1.42), 429 (.057)	488, 522	0.8	28.0	418
4.2c[56]	247 (3.72), 261 (3.43), 279 (2.67), 356 (1.52), 395 (1.15), 439 (0.7)	508, 543, 594	0.89	11.0	411
4.2d[56]	251 (4.82), 261 (4.55), 294 (2.07), 350 (1.83), 381 (1.4),424 (0.86)	488, 518	0.93	13.2	406
4.2e[56]	245 (4.58), 259 (4.45), 289 (2.65), 301 (1.86), 349 (1.78), 376 (1.35), 424 (0.66)	482, 512	0.75	17.7	432
4.3a[78]	284 (3.81), 371 (1.32), 426 (6.58)	503	0.73	4.7	518
4.3b[78]	285 (4.25), 374 (1.57), 404 (1.01), 438 (0.72)	518	0.82	3.7	430
4.3c[78]	284 (4.47), 371 (2.10), 421 (0.94)	522	0.90	4.9	405

Absorption, emission, quantum yield, and lifetimes determined in degassed CH_2Cl_2 (2 x 10^{-5} M).

The thermal stabilities of all eight complexes were investigated by TGA. It was found that all of the complexes had decomposition temperatures greater than 400 °C. Complex **4.3a** had the highest decomposition temperature at 518 °C.

O^N^N^O Tetradentate Platinum(II) Complexes

The most widely studied non-porphyrin tetradenate platinum complexes are of the type O^N^N^O, with twenty-one structures, as shown in Figure 4.3.[73,86–88] These complexes are all Schiff bases. Schiff bases are thermally stable and easily synthesized and structurally modified.[74] For these reasons Schiff bases have been employed in the development catalysts,[89] sensors,[88] electronic materials,[90] and light-emitting diodes.[91]

The absorption profiles for all twenty-one structures have been reported, and are summarized in Table 4.2. The complexes with alkane linkers between nitrogens (**4.6** – **4.8d**) were found to be highly absorbing between 242 – 352 nm (ε = 1.09 – 5.09 x 10^4 M^{-1} cm^{-1}), moderately absorbing between 394 – 485 nm (ε = 0.45 – 0.66 x 10^4 M^{-1} cm^{-1}), and weakly absorbing between 465 – 535 nm (ε = 0.005 – 0.008 x 10^4 M^{-1} cm^{-1}). The complexes with aromatic linkers between nitrogens (**4.4**, **4.5**, and **4.9a** – **4.9f**) were found to be highly absorbing between 244 – 379 nm (ε = 1.43 – 4.45 x 10^4 M^{-1} cm^{-1}) and moderately absorbing between 390 – 546 nm (ε = 0.31 – 0.80 x 10^4 M^{-1} cm^{-1}), with no weak absorption tails. The complexes with alkene linkers and cyano groups between nitrogens (**4.10a** – **b**) had very different absorption profiles than the other O^N^N^O-type Pt(II) complexes. While the complexes with aromatic and alkane linkers between the nitrogens showed a decrease in absorptivities moving from blue to red wavelengths, the alkene-linked complexes displayed an increase in absorptivities moving from blue to red wavelengths.

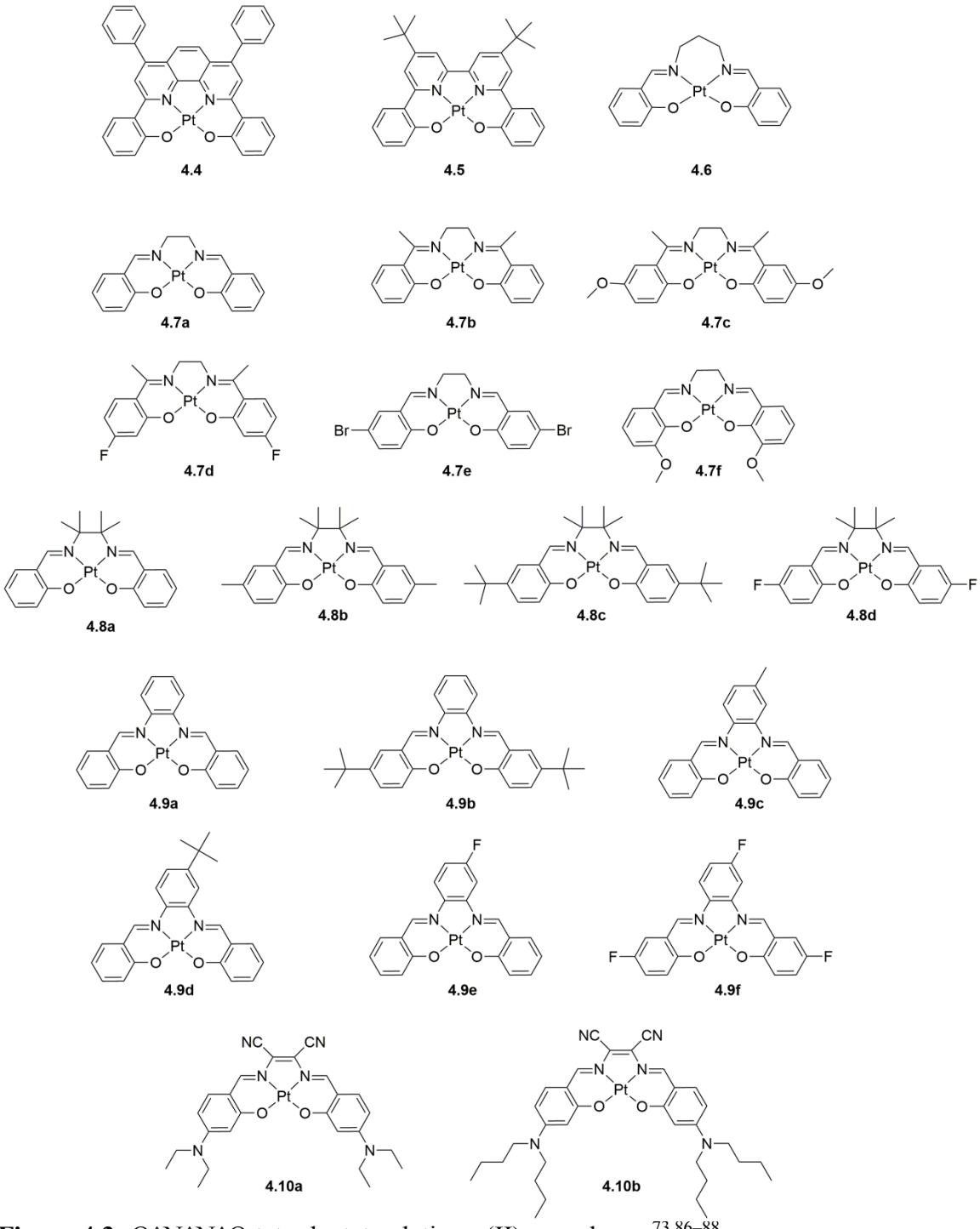

Figure 4.3: O^N^N^O tetradentate platinum(II) complexes.[73,86–88]

Table 4.2: Spectroscopic and photophysical data for **4.4 -4.10b**

	λ_{Abs} [nm] (ε [x 10^{-4} M^{-1} cm^{-1}])	λ_{Em} [nm]	Φ_{Em}	τ [μs]
4.4 [73, a]	292 (3.45), 317 (3.64), 326 (sh, 3.54), 353 (2.84), 376 (2.69), 420 (0.64), 478 (sh, 0.73), 502 (0.78)	589	0.45	3.2
4.5 [73, b]	250 (4.45), 315 (1.85), 390 (0.85), 465 (0.31)	596	0.06	1.3
4.6 [87, c]	250 (4.08), 320 (sh, 0.96), 340 (1.12), 420 (0.51), 500 (sh, 0.006)	592	0.09	0.46
4.7a [87, c]	250 (4.62), 314 (1.30), 336 (1.53), 417 (0.59), 503 (sh, 0.008)	550, 580(sh)	0.19	3.5
4.7b [87, c]	252 (3.23), 319 (1.05), 337 (1.24), 409 (0.47), 426 (0.14), 493 (0.006)	548	0.08	1.68
4.7c [87, c]	242 (3.77), 316 (1.09), 352 (1.11), 439 (0.55), 458 (sh, 0.49), 535 (0.005)	588	0.08	2.31
4.7d [87, c]	249 (4.00), 306 (1.40), 324 (1.40), 394 (0.66), 465 (0.008)	552	0.07	1.57
4.7e [87, d]	319 (1.24), 345 (1.35), 424 (0.56)	560	0.14	2.4
4.7f [86, b]	348 (1.30), 423 (0.45)	559, 605	0.10	0.12
4.8a [87, c]	246 (4.60), 316 (1.16), 339 (1.42), 413 (0.53), 432 (sh, 0.48), 501 (sh, 0.006)	541, 580(sh)	0.18	3.4
4.8b [87, c]	252 (5.01), 317 (1.37), 346 (1.57), 427 (0.60), 446 (sh, 0.56), 520 (0.007)	556	0.23	2.88
4.8c [87, c]	251 (5.09), 316 (1.35), 345 (1.59), 423 (0.57), 440 (sh, 0.53), 514 (0.007)	551	0.26	3.81
4.8d [87, c]	245 (3.78), 320 (1.16), 346 (1.21), 429 (0.52), 448 (sh, 0.50), 529 (0.007)	568	0.13	2.32
4.9a [87, c]	250 (3.49), 312 (1.82), 358 (2.99), 376 (3.07), 451 (0.65), 504 (sh, 0.65), 523 (0.71)	611	0.23	3.43
4.9b [87, c]	255 (4.17), 316 (1.88), 361 (3.31), 379 (3.57), 460 (0.71), 532 (0.72)	625	0.27	4.62
4.9c [87, c]	250 (3.72), 315 (1.94), 357 (3.09), 375 (3.22), 453 (0.73), 521 (0.73)	611	0.18	3.2
4.9d [87, c]	250 (4.05), 315 (2.16), 357 (3.29), 375 (3.43), 453 (0.76), 520 (0.80)	610	0.23	4.54
4.9e [87, c]	248 (3.25), 311 (1.51), 360 (2.71), 378 (2.73), 455 (0.58), 523 (0.60)	615	0.21	4.43
4.9f [87, c]	244 (2.77), 314 (1.43), 361 (2.45), 377 (2.64), 467 (0.58), 516 (sh, 0.59), 546 (0.65)	649	0.07	2.87
4.10a [88,e]	389 (3.1), 443 (2.4), 552 (3.5), 596 (11.2)	764	0.10	11
4.10b [88,e]	390 (3.6), 447 (2.8), 555 (4.0), 599 (12.6)	763	0.11	13

Absorption, emission, quantum yield and lifetimes determined in (a) DMF, (b) CH_3CN (c) degassed CH_3CN (d) degassed DMF or (e) degassed toluene.

The complexes with cyano groups between the nitrogens were also more highly absorbing overall, with maximum absorptivities of 11.2 – 12.6 x 10^4 M^{-1} cm^{-1}, while the other complexes displayed maximum absorptivities of only 1.3 – 5.09 x 10^4 M^{-1} cm^{-1}.

Solvatochromic studies of **4.4**, **4.5**, **4.7c**, **4.8a**, **4.9a**, **4.10a**, and **4.10b** were performed. For complexes **4.4** and **4.5**, the absorption bands at $\lambda \leq 315$ nm remained unchanged, but the lower energy absorption bands blue shifted in solvents of greater polarity. A blue shift in the emission was observed for complex **4.7c**, **4.8a**, and **4.9a** with increasing polarity. Complexes **4.10a** and **4.10b** displayed a change in the absorption λ_{max} for all of the absorption bands, but the shift did not follow a trend relative to the polarity of the solvent.

The solution-state emission ranges from 548 – 764 nm, which is similar to other Schiff-based tetradenate complexes **4.1a** and **4.1b**. The choice of linker between the nitrogens seems to have a large effect on the emission wavelength. It was observed that the complexes with alkane linkers between nitrogens (**4.6** – **4.8d**) had emission maxima ranging from 548 – 592 nm. The complexes with aromatic linkers between nitrogens (**4.4**, **4.5**, and **4.9a** – **4.9f**) had emission maxima ranging from 596 – 649 nm. The complexes with alkene linkers and cyano groups between nitrogens, complexes **4.10a** and **4.10b** had emission maxima of 764 nm and 763 nm, respectively.

The solvatochromic effects on the emission of complexes **4.4**, **4.5**, **4.7c**, **4.8a**, **4.9a**, **4.10a**, and **4.10b** were examined in addition to the absorption. Unlike the absorption, there was a distinct bathochromic shift in the emission for complexes **4.10a** and **4.10b** with increasing polarity. Complexes **4.4**, **4.5**, **4.7c, 4.8a**, and **4.9a** displayed hypsochromic shifts with increasing polarity. Compared with the solvent effects observed

for **4.7c**, **4.8a**, and **4.9a** in the absorption profiles, the shifts are much smaller in the emission profiles.

Table 4.3: Decomposition temperatures for **4.4**-**4.9f**

Complex	T_d [°C]	Complex	T_d [°C]
4.4[73]	440	**4.8b**[87]	474
4.5[73]	530	**4.8c**[87]	495
4.6[87]	369	**4.8d**[87]	484
4.7a[87]	406	**4.9a**[87]	415
4.7b[87]	345	**4.9b**[87]	339
4.7c[87]	455	**4.9c**[87]	411
4.7d[87]	379	**4.9d**[87]	396
4.7e[87]	315	**4.9e**[87]	414
4.8a[87]	382	**4.9f**[87]	408

T_d values determined under N_2 atmosphere.

The lifetimes range from 0.12 – 13 μs. The complexes with alkane linkers between nitrogens (**4.6** – **4.8d**) have the shortest lifetimes, 0.12 – 3.81 μs. The complexes with aromatic linkers between nitrogens (**4.4**, **4.5**, and **4.9a** – **4.9f**) have some overlapping, but generally somewhat longer lifetimes, 1.3 – 4.62 μs, than the alkane-bridged complexes. The complexes with alkene linkers and cyano groups between nitrogens had much longer lifetimes than any of the other complexes with lifetimes of 11 μs and 13 μs for complexes **4.10a** and **4.10b**, respectively. The emission quantum yields range from 10 – 45%. No trends were observed for the emission quantum yields of the complexes.

The thermal stabilities of complexes **4.4** – **4.7e** and **4.8b** – **4.9f** were studied by TGA under nitrogen. It was found that the decomposition temperatures ranged from 315 – 530 °C, see Table 4.3. Complex **4.5** had the highest decomposition temperature of 530 °C. This is the highest temperature reported among the discussed tetradenate compounds.

The decomposition temperature decreases significantly in air, from 530 °C under nitrogen to 380 °C in air.

It was observed that a significant increase in the decomposition temperature occurred for the **4.8a** – **4.8d** class of compounds when a substituent was placed in the position *para* to the oxygen. Complex **4.8a** had a decomposition temperature of 382 °C which increased to 474 °C with the addition of methyl groups in the positions *para* to the oxygen, and to 495 °C with the addition of *tert*-butyl groups in the positions *para* to the oxygen, and to 484 °C with the addition of fluorines in the positions *para* to the oxygen. Other significant changes in the decomposition temperature occurred when the position *para* to the oxygen was changed from H (345 °C) to OCH_3 (455 °C) in complexes **4.7b** and **4.7c** This trend does not continue in all cases, the decomposition temperature decreased from complex **4.7a** (406 °C) with a hydrogen *para* to the oxygen to complex **4.7e** (315 °C) with a bromine *para* to the oxygen.

Carbene Tetradentate Platinum(II) Complexes

Six tetradentate platinum(II) complexes have been reported that employ an *N*-heterocyclic carbene in one or more binding sites, as shown in Figure 4.4.[80,92] Several iridium complexes have been reported with deep blue emission at room temperature that are cyclcometallated with *N*-heterocyclic carbenes.[93–95]

Complexes **4.12a** and **4.12b** exhibit strong absorption bands below 300 nm, which have been attributed to $^1\pi$-π^* transitions localized on the cyclometalating ligands by Hang and coworkers.[92] More moderate absorption bands in the 300 – 420 nm region have been assigned to metal-to-ligand charge transfer (MLCT) transitions. Weaker absorption bands between 420 – 450 nm were assigned as triplet absorption. The absorptions in all regions

was observed to be stronger for **4.12b** than for **4.12a**. Complexes **4.11a** – **4.11d** exhibit strong absorption bands (ε = 7.1 – 12.7 x 10^4 M^{-1} cm^{-1}) between 277 – 365 nm, with no moderate or weak absorbing tails.

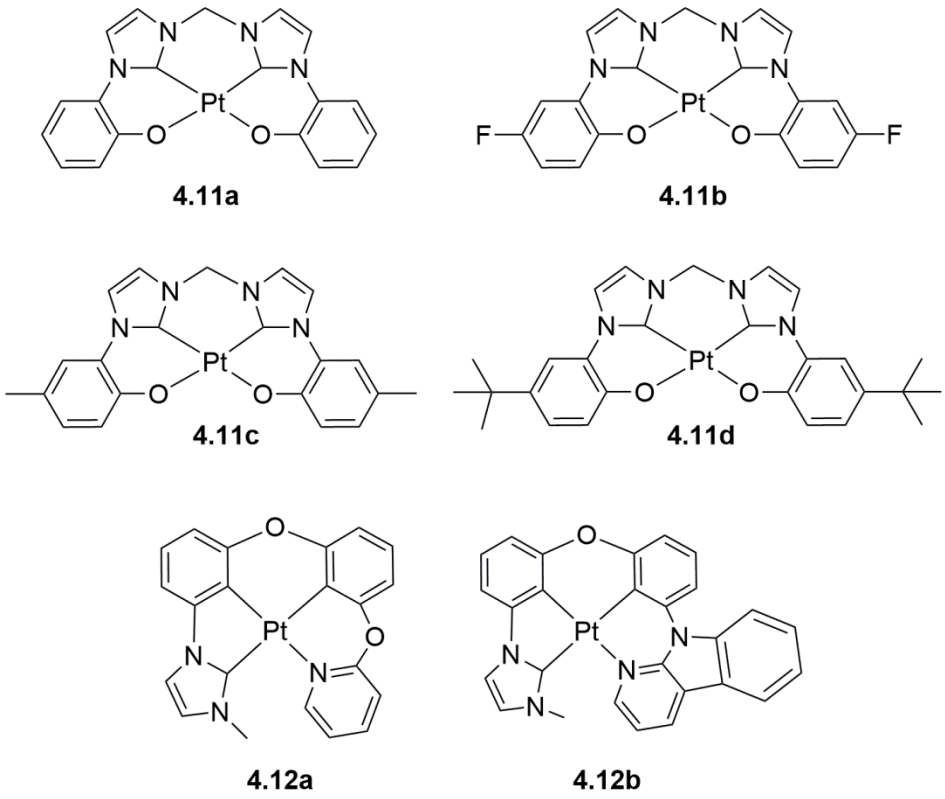

Figure 4.4: Carbene tetradentate platinum(II) complexes.[80,92]

The emission maxima for complexes **4.11a** - **4.12b** ranged from 442 – 461 nm, see Table 4.4. The emission quantum yields ranged widely from 0.03 to 0.78. The lifetimes were in the microsecond range (0.4 μs – 4.2 μs). The emission maxima of complex **4.11a** was blue shifted by 14 nm, the emission quantum yield increased from 3 to 18%, and the lifetime increased from 0.5 μs to 3.5 μs when fluoride groups were added to the *para* position of the phenolate group (**4.11b**). The emission maxima remained

nearly unchanged with the addition of methyl (**4.11c**) and *t*-butyl (**4.11d**) groups at the *para* position of the phenolate. The addition of these two groups does increase the emission quantum yield and the lifetime, although not as significantly as the fluoride. A red-shift of 5 nm was observed for complexes **4.11a** – **4.11c** when the solvent was changed from a mixture of THF/DMF to the more polar CH_2Cl_2/DMF (19:1, v/v). Only a 10 nm difference was observed in the emission maxima for complexes **4.12a** and **4.12b**. However, the quantum yield increased from 7% for complex **4.12a** to 78% for complex **4.12b** by moving from a phenoxyl pyridine to a carbazoyl pyridine.

Table 4.4: Physical, spectroscopic, and photophysical data for **4.11a - 4.12b**.

	λ_{Abs} [nm] (ε [x 10^{-4} M^{-1} cm^{-1}])	λ_{Em} [nm]	Φ_{Em}	τ [μs]	T_d [°C]
4.11a[80, a]	277 (sh, 8.4), 302 (7.3), 342 (7.1), 353 (7.1)	457	0.03	0.5	250
4.11b[80, a]	286 (8.5), 310 (9.7), 353 (10.4), 365 (10.5)	443, 459	0.18	3.5	410
4.11c[80, a]	284 (sh, 10.0), 308 (9.4), 351 (9.7), 362 (9.7)	460	0.07	1.8	390
4.11d[80, a]	282 (sh, 11.5), 308 (10.5), 352 (12.3), 363 (12.7)	461	0.08	1.8	400
4.12a[92, b]	N/A	442	0.07	0.4	N/A
4.12b[92, b]	N/A	452	0.78	4.2	N/A

Absorption, emission, quantum yield, and lifetimes determined in degassed (a) DMF/THF (19:1, *v/v*) (b) CH_2Cl_2. T_d values determined under N_2 atmosphere.

The thermal stabilities of complexes **4.11a** – **4.11d** were studied by TGA under nitrogen. It was found that the decomposition temperatures ranged from 250 – 410 °C. Though high, these values are in the lower range for tetradentate platinum(II) complexes. The decomposition temperatures of **4.12a** and **4.12b** were not studied.

C^N^N^C Tetradentate Platinum(II) Complexes

The second most widely studied non-porphyrin tetradenate platinum(II) complexes are of the type C^N^N^C, with fourteen reported structures, as shown in Figure 4.5.[66,76,79,92] Cyclometalated platinum(II) complexes have been the focus of research for a wide range of applications including oxygen sensors,[58] pH sensing,[96] catalysis,[97] anti-cancer agents,[98] and in light-emtting diodes.[66]

The absorption profiles of all but complex **4.14d** were reported. Complexes **4.13a – f**, **4.14a – c**, and **4.15a – 4.16b** exhibit intense (ε = 1.00 to > 3 x 10^4 M^{-1} cm^{-1}) vibronic-structured absorption bands below 360 nm, which have been attributed to $^1\pi$-π^* transitions. Additional more moderate absorption bands were observed for complexes **4.14a – c**, **4.15a – 4.16b** between 368 – 394 nm, with weaker tails at > 400 nm. Complexes **4.13a – 4.13f** displayed moderate absorption bands (ε = 0.14 – 0.96 x 10^4 M^{-1} cm^{-1}) between 365 – 507 nm, and displayed no weak tails. The absorption profile of the very similar complexes **4.15a** and **4.16a** are nearly identical, as are the absorption profiles of the similar complexes **4.15b** and **4.16b**. Complex **4.16a** was found to follow Beer's law up to 5 x 10^{-4} M. This suggests there is no significant aggregation occurring. Solvent effects on the absorption specta for complexes **4.13a**, **4.13c – 4.13f** were studied. Complex **4.13b** was not studied due to its poor solubility. For all the complexes a blue shift was observed in the absorption maximum when moving from less polar to more polar solvents. The effect is moderate in complexes **4.13a**, **4.13d**, **4.13e**, and **4.13f**, with shifts of 7 – 9 nm from toluene to CH_3CN. The effect was much more pronounced in complex **4.13c**, with a shift of 16 nm.

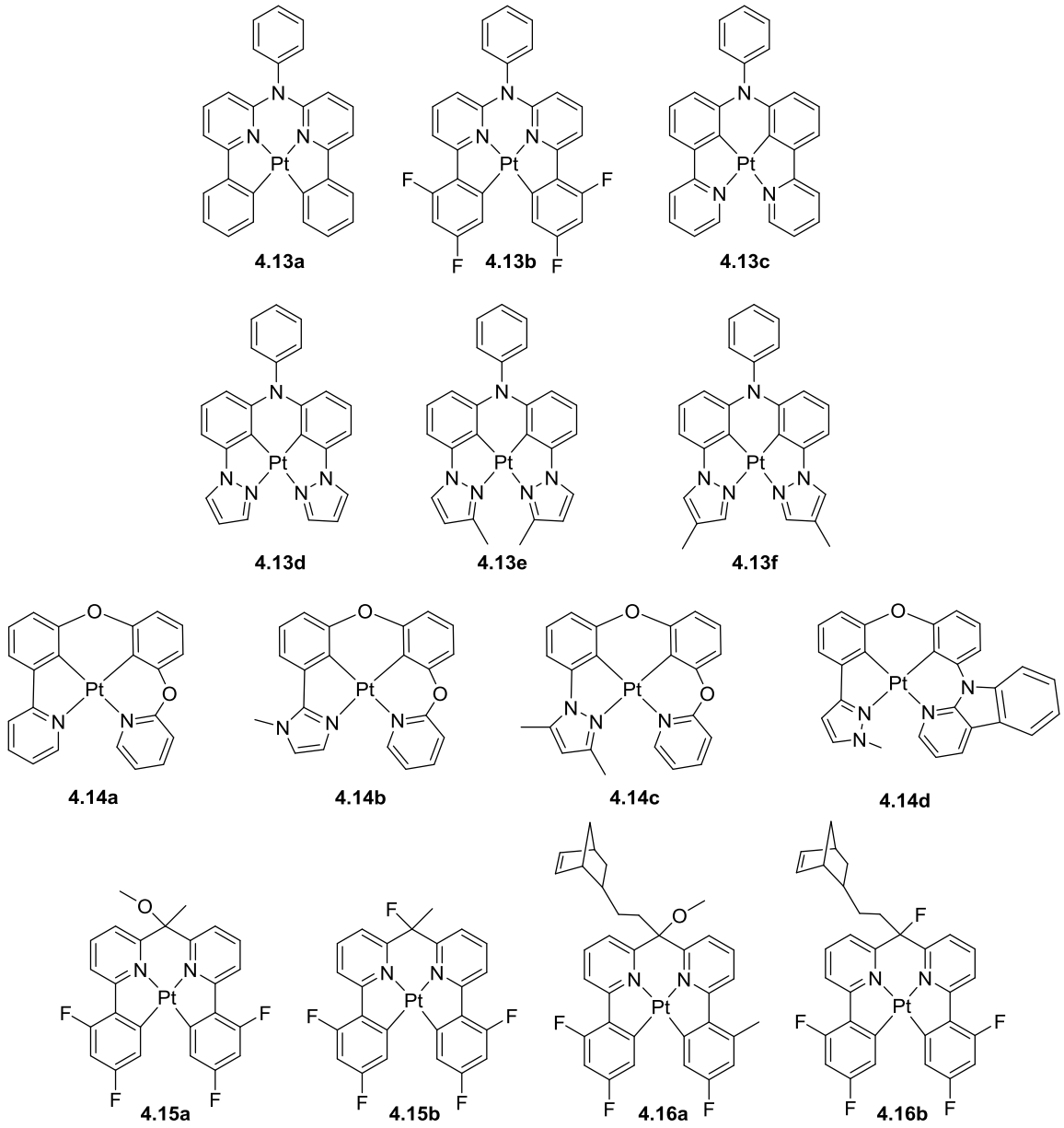

Figure 4.5: C^N^N^C tetradentate platinum(II) complexes.[66, 76, 79, 92]

The emission maxima range from 430 – 613 nm, see Table 4.5, making this the second most wide ranging class of tetradentate platinum(II) complexes discussed. The complexes which employ one or more pyrazole ligands have emission wavelengths

which are bluer (430 – 516 nm) than the complexes which do not have a pyrazole (488 – 613 nm).

Table 4.5: Physical, spectroscopic, and photophysical data for **4.13a -4.16b**

	λ_{Abs} [nm] (ε [x 10^{-4} M^{-1} cm^{-1}])	λ_{Em} [nm]	Φ_{Em}	τ [μs]
4.13a[66, a]	324 (2.52), 342 (2.62), 384 (0.49), 407 (.60)	512, 548	0.74	7.6
4.13b[66, a]	268 (2.92), 329 (1.90), 387 (0.39)	488, 523	0.75	11.4
4.13c[66, a]	274 (2.85), 324 (1.74), 338 (1.74), 409 (0.97), 507 (0.14)	613	0.14	7.6
4.13d[66, a]	302 (3.44), 335 (1.62), 351 (2.85), 370 (0.85), 421 (0.34), 442 (0.29)	484, 512	0.56	4.9
4.13e[66, a]	304 (2.14), 334 (1.03), 348 (1.33), 365 (0.50), 408 (0.17), 428 (0.14)	474	0.37	3.4
4.13f[66, a]	307 (2.81), 342 (1.03), 357 (1.82), 376 (0.47), 428 (0.18), 451 (0.16)	486, 516	0.63	5.7
4.14a[79, b]	N/A	512	0.63	2.0
4.14b[79, b]	N/A	468	0.64	9.0
4.14c[79, b]	N/A	430, 456	0.39	3.0
4.14d[92, b]	N/A	454 (sh), 478	0.71	3.3
4.15a[76, a]	257 (3.32), 284 (3.23), 319 (1.90), 339 (1.05), 368 (0.49), 390 (0.94), 478 (0.09)	493, 525, 560 (sh)	0.54	0.38
4.15b[76, a]	255 (3.38), 284 (3.24), 320 (1.84), 340 (1.03), 369 (0.44), 394 (0.93), 478 (0.08)	492, 520, 564 (sh)	0.58	0.32
4.16a[76, a]	258 (3.33), 285 (3.16), 318 (1.93), 339 (1.08), 369 (0.52), 390 (0.95), 477 (0.08)	492, 520, 560 (sh)	0.56	0.39
4.16b[76, a]	255 (3.36), 285 (3.34), 321 (1.82), 341 (1.00), 370 (0.43), 394 (0.88), 478 (0.08)	492, 522, 564 (sh)	0.55	0.38

Absorption, emission, quantum yield and lifetimes determined in degassed (a) 2-methyltetrahydrofuran (b) CH_2Cl_2.

Solvent effects on the emission of complexes **4.13a**, **4.13c** – **4.13f** were also studied. As in the absorption, complexes **4.13a** and **4.13c** exhibited moderate hypsochromic shifts from less to more polar solvents. The emission of complexes **4.13d** – **4.13f** shifted minimally (< 5 nm) in varying solvents, and displayed no clear trend in relation to solvent polarity.

Concentration dependence studies were performed for complexes **4.13a** and **4.14a – 4.14c**. No excimer based emission was observed for complexes **4.14a** – **4.14c**. Li and coworkers attribute this for complexes to the distortion from planarity induced by the oxygen linking atoms, which prevent the intermolecular interactions needed for excimer formation. Complex **4.13a** exhibits a long wavelength band that appears at high concentrations, which Huo and coworkers have attributed to excimer formation.

The lifetimes for the fourteen C^N^N^C type tetradentate platinum(II) complexes range from 0.32 – 11.4 μs. The complexes with carbon bridges (**4.15a** – **4.16b**) have much shorter lifetimes (0.32 – 0.39 μs) than the complexes with oxygen (**4.14a** – **d**) or nitrogen (**4.13a** – **4.13f**) bridges (2.0 – 11.4 μs). The emission quantum yields range from 14 – 75 %, with the average being 56%. The thermal stabilities were not investigated for any of the C^N^N^C type compounds.

Conclusions

All of the non-porphyrin tetradentate platinum(II) complexes are highly absorbing, with molar absorptivities > 10^4 M^{-1} cm^{-1}. The most highly absorbing group of complexes are that of the carbenes (ε_{max} = 8.4 to 12.7 x 10^4 M^{-1} cm^{-1}). The rest of the complexes have maximum molar absorptivities < 5 x 10^4 M^{-1} cm^{-1} with the exception of two of the O^N^N^O Schiff base complexes (**4.10a** and **4.10b**). These complexes have absorptivities comparable to the carbenes (ε_{max} = 11.2 to 12.6 x 10^4 M^{-1} cm^{-1}). The solvatochromic effects were discussed for the absorption for fifteen complexes. All of these complexes displayed a blue shift in the absorption moving from less polar to more polar solvents, except for complexes **4.10a** and **4.10b** which displayed no clear trend.

The non-porphryin tetradentate platinum(II) complexes were found to have emission maxima over a wide range of wavelengths from 430 – 764 nm. The complexes of the type O^N^N^O were found to have the largest coverage of wavelengths, from 548 – 764 nm. This extensive range may be due to the fact that this ligand set is the most widely studied. The complexes of the type C^N^N^C and N^N^N^N were also found to span a large range of wavelengths. The emission λ_{max} for C^N^N^C type complexes ranges from 430 – 613 nm. The emission peaks for N^N^N^N type complexes ranges from 560 nm to 750 nm. The other classes were found to cover less than a 40 nm range. The carbenes were found to generally emit in the blue region, and the O^N^C^N complexes were found to emit generally in the green region.

Many of the complexes were found to have high emission quantum yields. The complexes with the highest quantum yields were of the type O^N^C^N. These eight compounds all had quantum yields over 0.72. This class included the complex with the highest quantum yield of the series, complex **4.2d** (93 %). Complexes of the type C^N^N^C were also found to have high emission quantum yields, with an average of 56%. The carbene complexes were generally found to have low emission quantum yields (3 – 18%), with the exception of complex **4.12b** (78%). The Schiff base complexes of the type N^N^N^N and O^N^N^O had lower quantum yields, with all less than 45%.

The lifetimes for all fifty-two complexes were found to be in the microsecond range, ranging from 0.12 – 28 μs. No trends in the lifetimes of the varying groups of complexes were observed.

The thermally stabilities of all the compounds reporting thermogravametric analysis (thirty-two complexes) were found to be high (> 250 °C). Over 65% of the complexes have decomposition temperatures above 400 °C.

Tetradentate platinum(II) complexes have been shown to be emissive over a wide range of wavelengths from blue to the near-infrared. These complexes have displayed high thermal stabilities. Additionally many of the complexes have shown high emission quantum yields. These attributes make tetradentate platinum(II) complexes promising class of materials for a range of applications.

Chapter 5: Conducting Metallopolymers Incorporating Luminescent Cyclometallated Platinum(II) Complexes

INTRODUCTION

LED, light emitting diode, devices are typically composed of a cathode, an electron transport layer, an emitting layer containing small molecule phosphores such as platinum or iridium containing complexes, a hole transport layer, and then finally a transparent anode.[62,99] Many devices also contain additional buffering layers and injection layers to improve device performance.[55,100,101] Often these systems suffer from aggregation of the emitters, non-uniform films, and the need for a composite material.[102] To combat these issues polymeric systems based upon a conducting polymer backbone with covalently bound luminescent centers has been synthesized, to prevent emitter aggregation and the need for a composite material. Additionally electropolymerization was specifically chosen because the polymerization process creates a thin film directly on an electrode, eliminating the need for the processing of bulk material into films.[103–105] To create a device that emits white light, materials need to be synthesized that emit red, green, and blue.[106]

Previous research into electropolymerized iridium and platinum complexes has shown significant red shifts in the emission wavelength from that of similar complexes which do not contain electropolymerizable substituents.[107,108] [2,6-*Bis*(2-pyridyl)phenyl-*C*,*N*,*N*′]chloroplatinum(II) for example has an emission maxima at 491 nm; with the appendage of 3,4-dibutyl-2,2’:5,2’’-terthiophene groups at the 5-position on the pyridine rings the emission maxima shifts to 560 nm.[108,109] Upon polymerization the emission is even farther red shifted to 590 nm. This is believed to be due to the increased conjugation that the electropolymerizable substituents provide lowering the energy level of lowest unoccupied molecular orbital. Due to this effect, electropolymerizable complexes that

emit in the blue and green region have been difficult to achieve. To combat this, an approach has been taken to design a system in which the electropolymerizable groups are not in direct contact with the luminescent center. This approach could be achieved by placing non-conjugated linkers between the polymerizable handle and the emitter. This however would likely decrease the conductivity of the material. Complex **4.12a** synthesized by Hou *et al*. is shown in Figure 5.1.[66] Hou and coworkers found through single crystal X-ray diffraction and density functional theory (DFT) calculations that there is a nearly 90 ° torsion angle between the aniline and portion of the molecule where the HOMO and LUMOs lie. This twist could allow substitutions on the aniline that do not influence the photophysical properties of the metal complex and do not introduce insulating materials into the system. Our approach involves synthesizing a platinum(II) complex based on the complex by Hou *et al.*, with electropolymerizable groups on the aniline in an attempt to create a material that is conductive, yet does not alter the photophysical properties of the original materials.

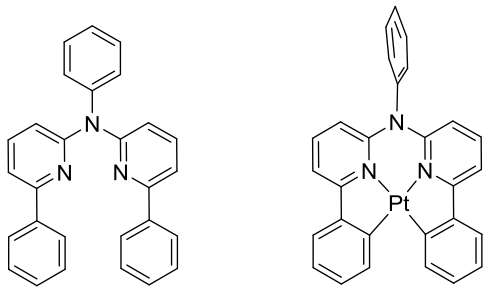

5.1 **4.12a**

Figure 5.1: Structure of ligand **5.1** and platinum complex **4.12a** shown with torsion.[66]

RESULTS AND DISCUSSION

Synthesis and Characterization

Scheme 5.1 shows the synthesis of the ligand **5.6** and the platinum complex **5.7**. 1,3-dibromo-5-nitrobenzene was prepared using a modified procedure from Bérubé *et al.*[110] A Stille coupling was employed between tributyl(2,3-dihydrothieno[3,4-*b*][1,4]dioxin-5-yl)stannane and 1,3-dibromo-5-nitrobenzene to form **5.3**. The nitro functionality was then reduced with sodium borohydride and stannous chloride to form the aniline **5.4**. Product **5.5** was synthesized through a Buchwald-Hartwig amination between **5.4** and 2,6–dibromopyridine. Both the monosubstituted and disubstitued products were recovered and were separated by column chromatography. Crystals suitable for single crystal X-ray diffraction of **5.4** were achieved by layering a saturated solution of **5.4** in CH_2Cl_2 with hexanes. The structure is shown in Figure 5.2. Detailed information on the structure is given in Table 5.2.

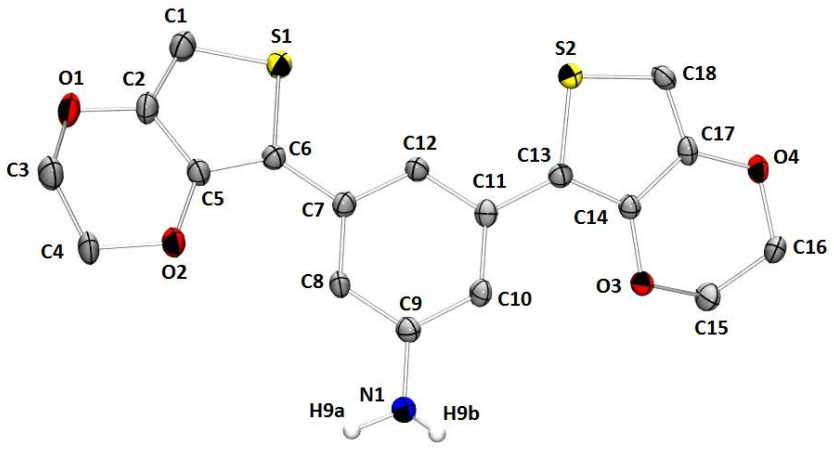

Figure 5.2: Molecular structure of **5.4.**

The atom labeling scheme is shown. Displacement ellipsoids are shown at the 50% probability level. The hydrogens, with the exception of the amine hydrogens, have been omitted for clarity.

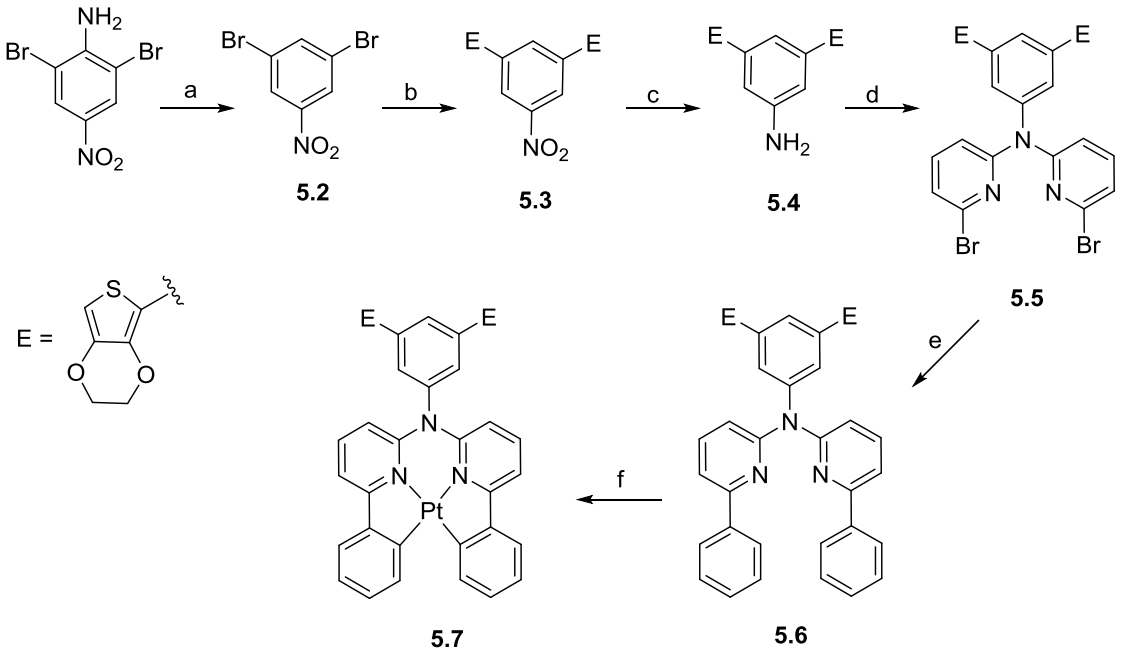

Scheme 5.1: Synthesis of platinum complex and precursors, **5.2 – 5.7**.

(a) [1] H_2SO_4, $NaNO_2$, 0 °C, 1 h [2] $CuSO_4 \cdot 5H_2O$, EtOH, 60 °C, 1h, 82.8% (b) $EDOTSnBu_3$, $PdCl_2(PPh_3)_2$, CuI, Toluene, 110 °C, 18 h, 53.5% (c) $NaBH_4$, $SnCl_2$, EtOH, H_2O, 66 °C, 18h, 35.0% (d) 2,6-dibromopyridine, $Pd_2(dba)_3$, DPPF, NaO*t*Bu, Toluene, 110 °C, 18 h, 13.0% (e) Phenylboronic acid, $Pd(OAc)_2$, PPh_3, K_2CO_3, DME, 85 °C, 4 h, 31.6% (f) K_2PtCl_4, Bu_4NCl, AcOH, 118 °C, 45 h, 11.6%.

The ligand **5.6** was obtained by the Suzuki cross coupling of the ligand precursor with benzeneboronic acid. Potassium tetrachloroplatinate was reacted with the ligand to give the desired cyclometallated complex, **5.7**. All the compounds were found to be soluble in common organic solvents. All novel compounds were characterized by ^1H and $^{13}C\{^1H\}$ NMR spectroscopy, mass spectrometry, and elemental analysis by combustion. The photophysical properties of **5.1** were not reported by Hou and coworkers, so compound **5.1** was synthesized following Hou and coworker's procedure.[66]

Spectroscopic Properties of Small Molecules

The photophysical properties of the model ligand, **5.1**, the ligand **5.6** and the platinum complex **5.7** were studied and the results are summarized in Table 5.1. Both the model ligand, **5.1**, the ligand, **5.6,** and the platinum complex, **5.7,** exhibit intense ($\varepsilon \approx 1.69 - 4.23 \times 10^4\ M^{-1}\ cm^{-1}$) vibronic-structured absorption bands below 360 nm, which have been attributed to π-π^* transitions. No weaker bands were observed, see Figure 5.3.

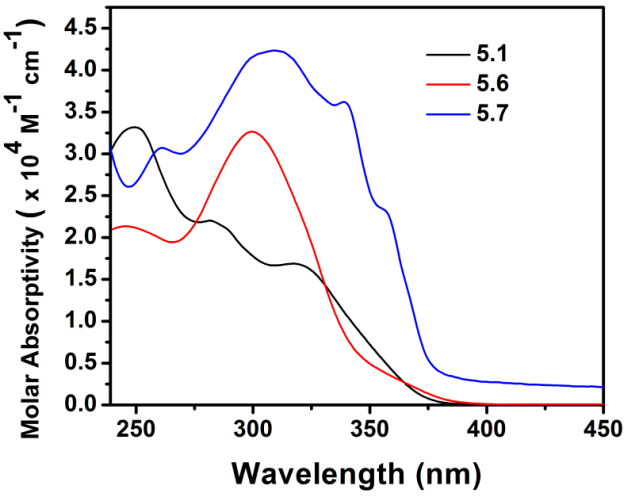

Figure 5.3: Absorption, spectra of **5.1**, **5.6** and **5.7** in CH_2Cl_2 at room temperature.

The emission and excitation profiles of all three compounds are shown in Figures 5.4 and 5.5. The emission profiles of the ligands **5.1** and **5.6** closely match, both with broad peaks at ~405 nm. For the platinum complex excitation into the ligand singlet state enhances ligand fluorescence, but higher excitation wavelengths results in predominately phosphorescence at 510 and 544 nm. This matches closely with the model platinum complex, **4.12a**, studied by Hou and coworkers, which displays peaks at 512 and 548 nm.[66] In previous work the addition of electropolymerizable groups onto a substrate has

altered the emission, but for this system, neither the ligand nor the platinum complex displays a significant change in emission from similar compounds without ethylenedioxythiophene appendages.

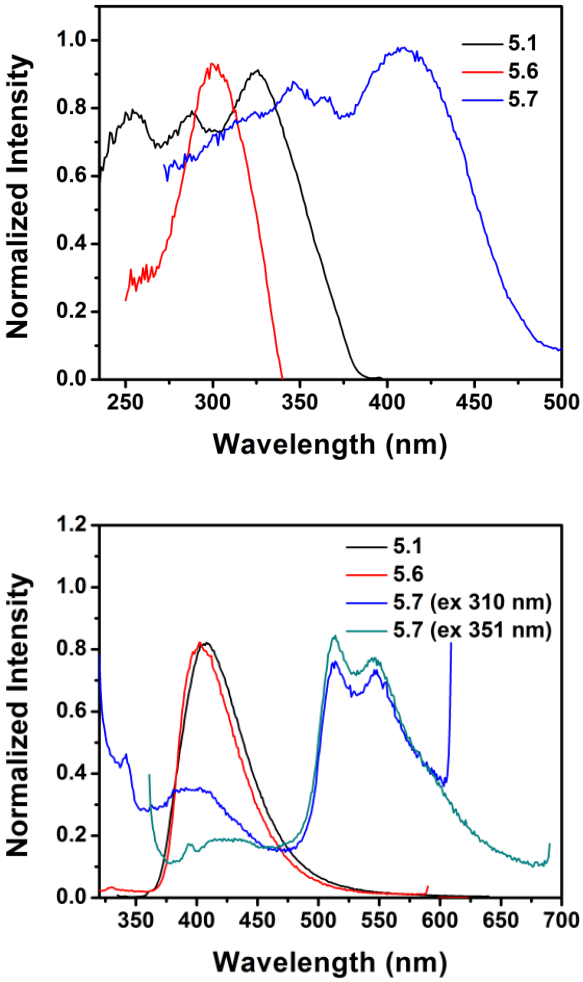

Figure 5.4: Top: Excitation spectra of **5.1**, **5.6** and **5.7**, in CH_2Cl_2 at room temperature
Bottom: Emission spectra of **5.1**, **5.5** and **5.6** in CH_2Cl_2 at room temperature.

The solvent effect on the emission of **5.6** and **5.7** was studied. Compound **5.6** did not show any solvent dependence, but complex **5.7** displayed a shift of 10 nm from

toluene to acetonitrile, see Figure 5.5. This is comparable to the change in emission observed for complex **4.12a**, by Hou and coworkers, which shifted 14 nm from toluene to acetonitirile.[66] The hypsochromic shift with increasing solvent polarity indicates ^{3}LC emission.

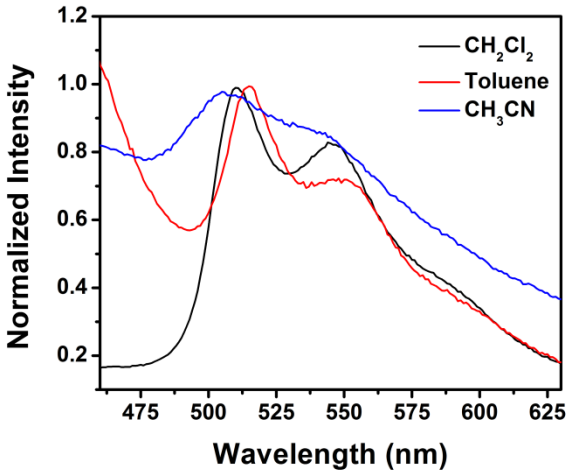

Figure 5.5: Emission profile of **5.7** in various solvents at room temperature.

Table 5.1: UV-vis absorption and photoluminescence data for **5.1**, **5.6**, **5.7**, and **poly5.7**.

	λ_{Abs}, nm, (ε, M^{-1} cm^{-1})	λ_{Ex} (nm)	λ_{Em} (nm)	Φ_{Em} (%)	τ (μs)
5.1	249 (33157), 282 (22060), 319 (16853)	325	407	-	0.31 ± 0.03
5.6	245 (21334), 299 (32646)	300	403	4.51	0.43 ± 0.02
5.7	261 (29794), 309 (42326), 339 (36069), 354 (23002)	408	510 544	0.29	6.2 ± 0.8
poly5.7[a]	336, 409, 485	311	454	-	0.11 ± 0.1

Recorded in degassed CH_2Cl_2 at room temperature, (b) recorded on ITO-coated glass.

Electrochemistry

As shown in Figures 5.6 and 5.7, monomers **5.6** and **5.7** were electropolymerized to form **poly5.6** and **poly5.7** respectively. The polymers were grown as electrode confined thin films on a platinum button for scan rate dependence studies and ITO-coated glass for emission studies. The cyclic voltammetry was performed in a window from -0.3 to 1.7 (vs Fc/Fc^+) in CH_2Cl_2 containing 0.1 M $TBAPF_6$.

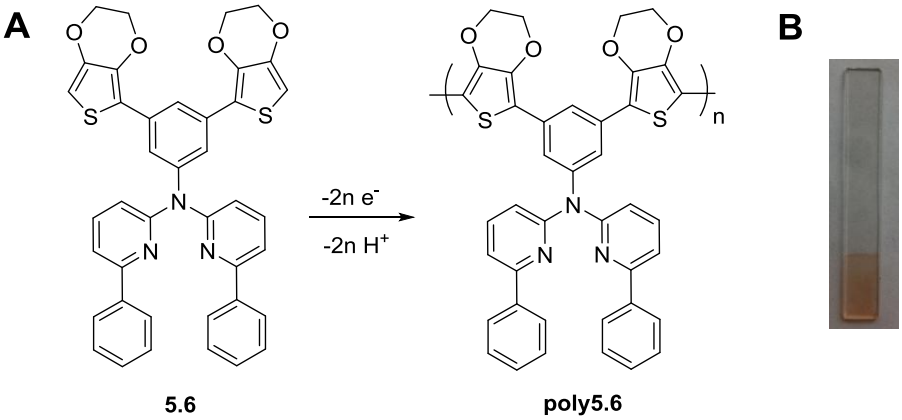

Figure 5.6: (A) Electropolymerization of **5.6**, (B) **poly5.6** on ITO coated glass.

Figure 5.8(top right) shows a linear relationship between the oxidative/reductive peaks and the number of scans during polymerization indicating uniform growth of the polymer, **poly5.6**, for 2 - 3 scans. It is expected that film growth would continue to be linear with further scans if a higher potential could be achieved, but the electrochemical window of the solvent would be exceeded with higher potentials. Attempts to find a solvent in which **5.5** was soluble and the electrochemical window allows oxidative potentials higher than 1.7 (vs Fc/Fc^+) was unsatisfactory. Figure 5.9(top right) shows the shows a linear relationship between the oxidative/reductive peaks and the number of

scans during polymerization for **poly5.7**. For this complex the linear relationship continues for about six scans before the solvent window is reached. Scan rate dependence studies were conducted for both **poly5.6** and **poly5.7**, the cyclic voltammograms are shown in Figure 5.8C and 5.9C respectively. Both polymers show a linear relationship between the oxidative/reductive peaks and the scan rate up to 250 mV/s. This indicates that the films are conductive, have good ionic porosity by allowing the quick influx of counterions, and that the films are strongly absorbed. The relationship between the oxidative/reductive peaks and the scan rate for **poly5.7** deviates from linearity at 500 mV/s, indicating a "less facile ion transport" than **poly5.6**, which does have a linear relationship out to 500 mV/s. It is likely that **poly5.7** is a thicker film than **poly5.6** since a larger number of film growth scans was achieved before reaching the electrochemical solvent window. A difference in film thickness might be the cause the differences in the scan rate study; a thinner film of **poly5.7** might result in a linear relationship out to 500 mV/s.

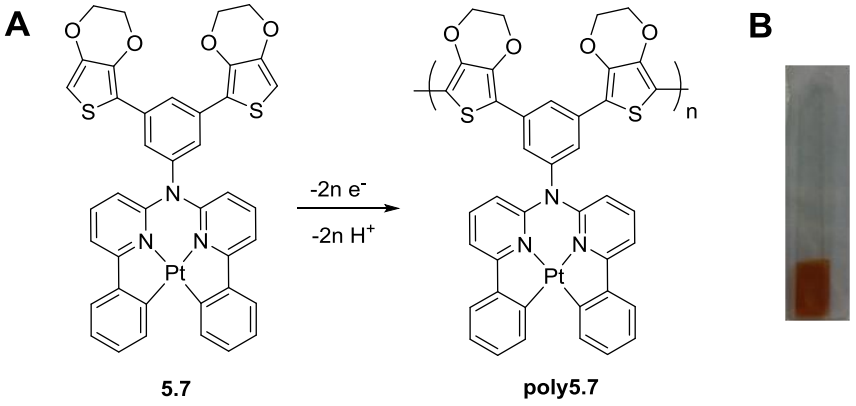

Figure 5.7: (A) Electropolymerization of **5.7**, (B) **poly5.7** on ITO coated glass.

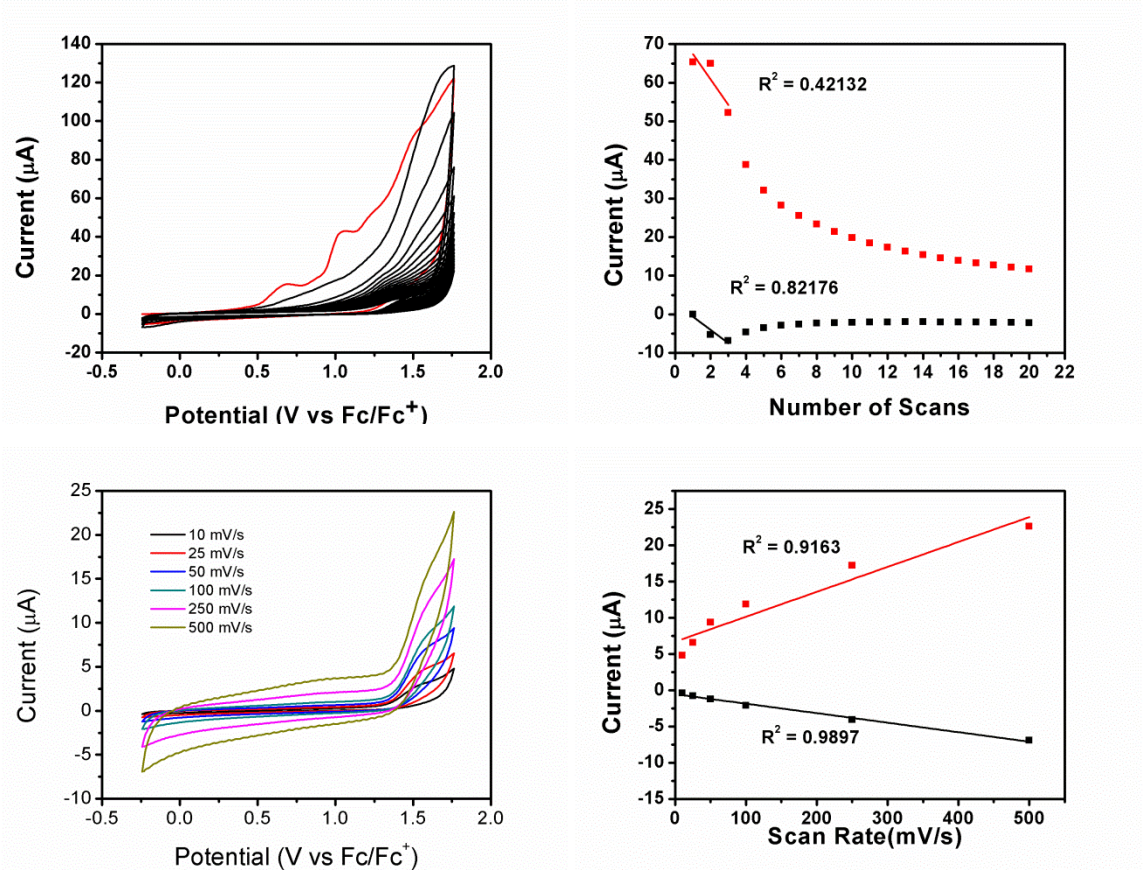

Figure 5.8: Electrochemistry of compound **5.6**.

(Top left) Cyclic voltammogram of **5.6** in 0.1 M $TBAPF_6$ in CH_2Cl_2 at a scan rate of 0.1 V/s. (Top right) Plot of oxidative and reductive peak currents versus number of scans. (Bottom left) Scan rate dependence study of **poly5.6** in 0.1 M $TBAPF_6$ in CH_2Cl_2. (Bottom right) Plot of oxidative and reductive peak currents versus scan rate.

Spectroscopic Properties of Polymers Films

The absorbance profile of **poly5.7** is shown in Figure 5.10. The broad absorption bands are typical of ethylenedioxythiophene metallopolymers and are likely due to the extended conjugation of the system.

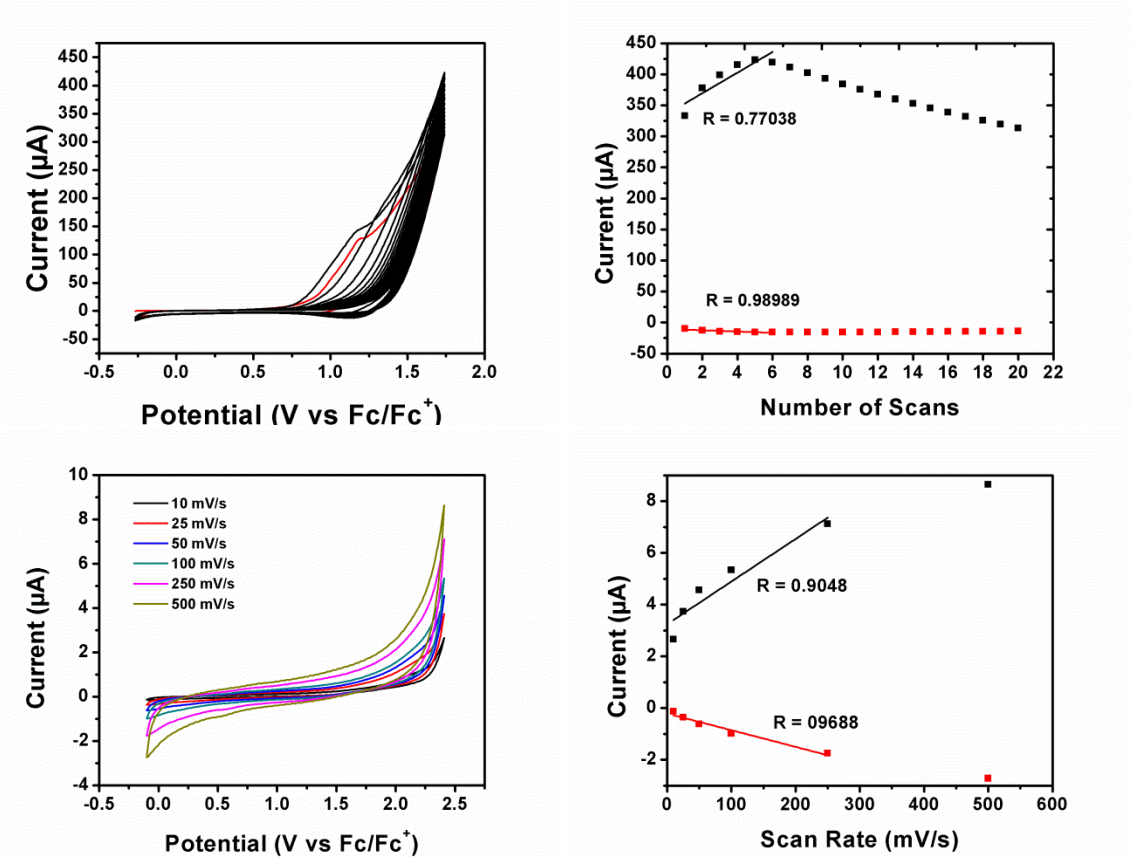

Figure 5.9: Electrochemistry of complex **5.7**.

(A) Cyclic voltammogram of **5.7** in 0.1 M $TBAPF_6$ in CH_2Cl_2 at a scan rate of 0.1 V/s. (B) Plot of oxidative and reductive peak currents versus number of scans. (C) Scan rate dependence study of **poly5.7** in 0.1 M $TBAPF_6$ in CH_2Cl_2. (D) Plot of oxidative and reductive peak currents versus scan rate.

The emission for the platinum metallopolymer, **poly5.7**, was observed to be blue shifted from that of the platinum monomer **5.7**, shown in Figure 5.11. Additionally the emission for the metallopolymer, **poly5.7**, was observed to be structureless, unlike the monomer, **5.7**. It is expected that the increase of the conjugation near the LUMO, would lower the LUMO energy level, creating a sFmaller energy gap between the ground and excited states and thus red shift the emission.

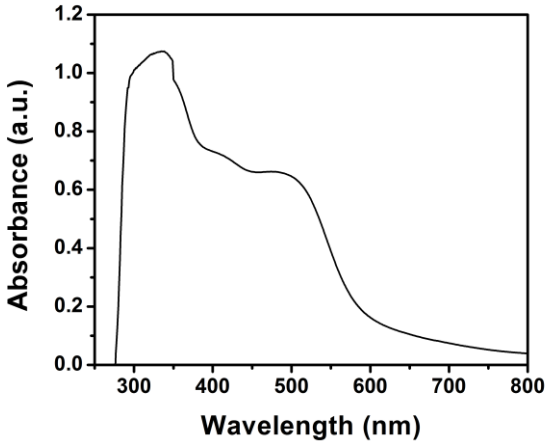

Figure 5.10: Absorption profile of **poly5.7** as a thin film on ITO coated glass.

We anticipated that the polymerization would either cause no change in emission or would cause a red shift in the emission. It has been seen in other systems that the increase in conjugation, caused by the polymerization on or near the LUMO of the material, lowers the energy level of the LUMO and thus causes a red shift in the emission. When comparing the excitation profiles of the platinum monomer, **5.7**, to the metallopolymer, **poly5.7**, it was observed that they differ by ~ 100 nm. The excitation maximum for the ligand, **5.6**, differs by only ~ 10 nm from that of **poly5.7**. The emission of the ligand **5.6** and **poly5.7** are both broad and featureless. It is likely the metallopolymer emission is ligand centered emission, with no contribution from the metal. This means the emission is red shifted from that of the ligand, and not blue shifted from that of the platinum monomer. No emission was observed from the ligand based polymer, **poly5.6**.

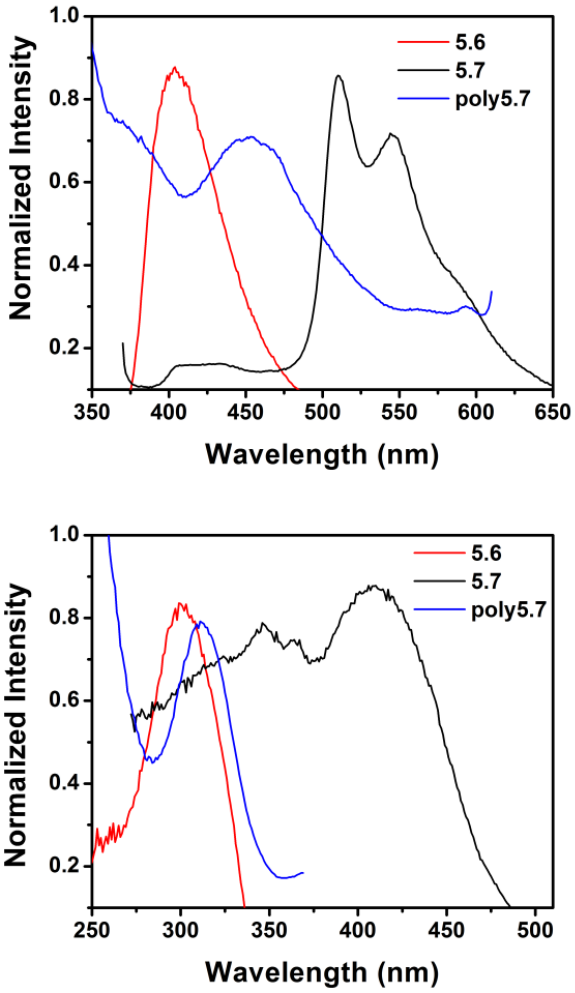

Figure 5.11: Top: Excitation spectra of **5.6**, **5.7** and **poly5.7**, in CH_2Cl_2 at room temperature. Bottom: Emission spectra of **5.6**, **5.7** and **poly5.7** in CH_2Cl_2 at room temperature.

CONCLUSION

A novel ethylenedioxythiophene-derivatized tetradentate platinum(II) complex has been designed, synthesized, and characterized. The appendage of the ethylenedioxythiophene groups did not alter the wavelength of emission. The monomer

was electropolymerized onto ITO-coated glass to form a thin film that was found through a scan rate dependence study to be electrically conductive. The emission of the metallopolymer was determined to be ligand centered. The emission was red-shifted from the ligand, but the shift was minimal as compared to the shift from monomer to polymer seen in other systems with ethylenedioxythiophene appendages.[107]

EXPERIMENTAL

General Methods

All chemicals were purchased from chemical suppliers and were used without further purification. All dry reactions were performed using standard Schlenk techniques and were performed under an inert atmosphere of nitrogen. Tetrahydrofuran and toluene were dried by allowing the solvent to sit over freshly activated 3Å molecular sieves for 24 hrs, followed by sparging with N_2 for 1 hr, as described by Williams and coworkers.[111] ^{1}H and $^{13}C\{^{1}H\}$ NMR spectra were obtained on a Varian Unity+ 300 or 400 MHz instrument. ^{1}H, and $^{13}C\{^{1}H\}$ NMR spectra were referenced to the residual solvent peaks. High resolution mass spectra were obtained with an Agilent Technologies 6530 Accurate Mass QTofLC/MS (ESI) or a Micromass Autospec Ultima (CI+). Elemental analysis was performed by QTI, Whitehouse, NJ (www.qtionline.com). Melting points are not corrected. Tributyl(2,3-dihydrothieno[3,4-*b*][1,4]dioxin-5-yl)stannane was prepared according to Swager and coworkers.[112]

Electrochemistry

All electrochemical syntheses and studies were performed in a dry-box under a nitrogen atmosphere using a GPES system from Eco. Chemie B.V and an autolab

potentiostat. All the electrochemical experiments were carried out in a three-electrode cell with $Ag/AgNO_3$ reference electrode (silver wire suspended in a 0.01 M silver nitrate solution with 0.1 M $[(n\text{-}Bu)_4N][PF_6]$ in dry CH_3CN), and a Pt wire coil counter electrode, either a platinum working electrode, Delta Technologies ITO-coated glass (70-100 Ω/□), or stainless steel. Potentials were measured relative to the $Ag/AgNO_3$ reference electrode. Ferrocene was purified by sublimation at 95 °C and used as an external reference to calibrate the reference electrode before and after experiments were performed and that value was used to correct the measured potentials. All electrochemistry was performed in either CH_2Cl_2 or CH_3CN solutions using 0.1 M $[(n\text{-}Bu)_4N][PF_6]$ as the supporting electrolyte. $[(n\text{-}Bu)_4N][PF_6]$ was purified by recrystallization three times from hot ethanol before being dried for 3 days at 100 °C under reduced pressure prior to use. Electrosyntheses of the polymer films were performed from a dilute monomer solutions by continuous cycling between -0.3 V and 1.7 V (vs Fc/Fc^+) at 100 mVs^{-1}. The films obtained were then washed with fresh CH_2Cl_2 before performing further experiments.

Spectroscopy

Absorption spectra were recorded on a Varian Cary 6000i UV-Vis-NIR spectrophotometer with starna quartz fluorometer cells with a pathlength of 10 mm. Luminescent measurements were recorded on a Photon Technology International QM 4 spectrophotometer equipped with a 6-inch diameter K Sphere-B integrating sphere. Quantum yields were determined using an aqueous solution of quinine sulfate in 5 M H_2SO_4 according to equation 5.1, where Φ_s is the quantum yield of the sample, Φ_q is the quantum yield of quinine sulfate, A_q is the absorbance of the quinine solution at the excitation wavelength, A_q is the absorbance of the sample at the excitation wavelength, I_q

is the area of the quinine emission peak, I_s is the area of the sample emission peak, and η_q is the refractive index of 0.5 M H_2SO_4, η_s is the refractive index of the solvent used for the sample.

$$\Phi_s = \Phi_q \left(\frac{A_q}{A_s}\right)\left(\frac{I_s}{I_q}\right)\left(\frac{\eta_q}{\eta_s}\right)^2 \qquad (5.1)$$

X-ray Crystallography

Crystals of **5.4** suitable for X-ray diffraction were obtained by layering a saturated solution of **5.4** in CH_2Cl_2 with hexanes and allowing the solutions to slowly diffuse. The single–crystal diffraction data was collected on a on a Rigaku SCX-Mini diffractometer with a Mercury CCD using a Rigaku Tec 50 low-temperature device. The complex was collected using a graphite monochromator with MoKα radiation (λ = 0.71073Å). Absorption corrections were applied using multi-scan. Data reduction was performed using the Rigaku Americas Corporation's Crystal Clear version 1.40.[39] The structures were solved by direct methods and refined anisotropically using full-matrix least-squares methods with the SHELX-97 program package.[40] The amine H atoms were located in a difference Fourier map and both positional and isotropic displacement parameters were refined. All other H atoms were positioned geometrically and refined using a riding model, with C—H = 0.93 – 0.97 Å and U_{iso}(H) = 1.2 U_{eq}(C). Neutral atom scattering factors and values used to calculate the linear absorption coefficient are from the International Tables for X-ray Crystallography (1992).[41]

Synthesis

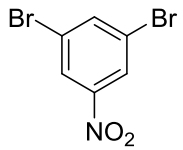

[5.1] 1,3-dibromo-5-nitrobenzene

The preparation of **5.1** was prepared according to a modified procedure of Bérubé *et al.* for 1,3-diiodo-5-nitrobenzene.[110] To a solution of conc. H_2SO_4 (45 mL) in a 0 °C ice bath was added 2,6-dibromo-4-nitroaniline (11.7g, 39.6 mmol). Complete dissolution took 1 hr, after which time sodium nitrate (4.9 g, 70.5 mmol) was added and stirred for an additional 1.5 hrs. A beaker was filled with approx 300 g of ice and the solution was poured into the ice, rinsing with cold water. The ice solution was filtered over a coarse frit. The filtrate was added to a refluxing solution of copper sulfate (0.5 g, 0.2 mmol) in ethanol (400 mL), and stirred for 2 hours. An orange solid precipitated. The solid was collected by vacuum filtration and was washed with H_2O until neutral, yielding a tan solid (82.8%). The ^1H NMR spectra matched that reported by Kubiczak and coworkers.[113]

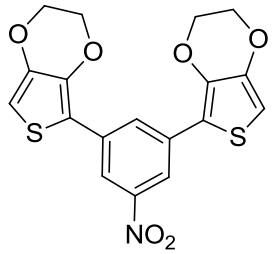

[5.2] 5,5'-(5-nitro-1,3-phenylene)bis(2,3-dihydrothieno[3,4-*b*][1,4]dioxine)

To a solution of dry toluene under N_2 was added tributyl(2,3-dihydrothieno[3,4-*b*][1,4]dioxin-5-yl)stannane (25.3 g, 58.7 mmol), **5.1** (7.0 g, 25.0 mmol), *trans*-dichloro*bis*triphenylphosphine palladium (II) (1.1 g, 1.6 mmol), and copper (I) chloride (0.1 g, 0.5 mmol). The solution was refluxed at 110 °C overnight. The black solution exposed to atmosphere and conc. under reduced pressure. The solid was dissolved in dichloromethane and filtered over a bed of silica. The filtrate was conc and recycrystalized in a dichloromethane/hexanes mixture to yield a bright yellow solid (53.5 %) m.p. 247-250 °C ^{1}H NMR (300 MHz, $CDCl_3$) δ 8.42 (d, 2H, J = 1.5), 8.18 (t, 1H, J = 1.5), 6.38 (s, 2H), 4.35-4.38 (m, 4H), 4.25 – 4.28 (m, 4H). ^{13}C{^{1}H} NMR (75 MHz, $CDCl_3$) δ: 149.0, 142.3, 139.7, 134.9, 127.8, 118.1, 114.9, 99.3, 65.0, 64.4. HRMS (CI+) calcd for $C_{40}H_{29}N_3O_4S_2$ $[M + Na]^+$ 426.00748, found 426.00765.

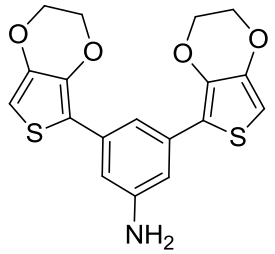

[5.3] 3,5-*bis*(2,3-dihydrothieno[3,4-*b*][1,4]dioxin-5-yl)aniline

5.2 (3.33 g, 8.25 mmol) was dissolved in 200 mL of THF. Sodium borohydride (0.85 g, 22.47 mmol) was dissolved in 66 mL of EtOH, to the EtOH solution was added stannous chloride (2.11 g, 9.35 mmol). The THF and EtOH mixtures were combined and refluxed at 60 °C overnight. The solution was cooled to R.T. and concentrated under reduced pressure. The mixture was dissolved in CH_2Cl_2, and vacuum filtered. The filtrate was washed with water, extracting into CH_2Cl_2 (50 mL x 3), dried with magnesium sulfate, and concentrated. The residue was purified on a silica gel column with CH_2Cl_2 as the eluent to afford a tan solid (35.0 %). m.p. 175 °C (decomp.). ^{1}H NMR (300 MHz, $CDCl_3$) δ 7.41 (t, 1H, *J* = 1.2), 6.95 (d, 2H, *J* = 1.5), 6.26 (s, 2H), 4.21 – 4.28 (m, 8H), 3.71 (br, 2H). $^{13}C\{^1H\}$ NMR (75 MHz, $CDCl_3$) δ: 146.7, 142.1, 138.2, 134.2, 117.5, 114.6, 111.3, 97.5, 64.7, 64.4. HRMS (ESI) calcd for $C_{40}H_{29}N_3O_4S_2$ $[M + H]^+$ 374.05169, found 374.05153. Anal Calcd for $C_{18}H_{15}NO_4S_2$: C, 57.89; H, 4.05; N, 3.75. Found: C, 57.53; H, 3.77; N, 3.73. Anal Calcd for $C_{18}H_{15}NO_4S_2$: C, 57.89; H, 4.05; N, 3.75. Found: C, 57.53; H, 3.77; N, 3.73.

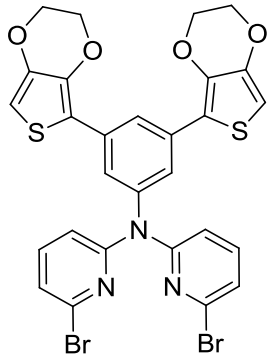

[5.4] *N*-(3,5-*bis*(2,3-dihydrothieno[3,4-*b*][1,4]dioxin-5-yl)phenyl)-6-bromo-*N*-(6-bromopyridin-2-yl)pyridin-2-amine

In an air-free glovebox *tris*(dibenzylideneacetone)dipalladium(0) (0.221 g, 0.241 mmol) was added to a dry schlenk. The schlenk was pumped out, dry toluene was transferred into the flask by cannula and **5.3** (2.000 g, 5.355 mmol), 2,6-dibromopyridine (2.998 g, 12.656 mmol), DPPF (0.333 g, 0.601 mmol), and sodium *tert*-butoxide (1.111 g, 11.561 mmol) were added to the solution. The solution was refluxed at 120 °C for 20 hours. The solution was cooled to room temperature and the toluene was removed by rotoevaporation. The product was extracted into CH_2Cl_2 (x3) washing with H_2O. Purified by silica gel column chromatography with 75% CH_2Cl_2: 25% hexanes by volume (R_f = 0.34) to yield a bright yellow solid (0.478 g, 13.033 %). m.p. 157 °C. ^{1}H NMR (400 MHz, $CDCl_3$) δ 7.86 (s, 1H), 7.42 (d, 2H, *J* =1.2), 7.37 (t, 2H, *J* = 7.8), 7.09 (d, *J* = 7.6), 6.95 (d, 2H, *J* = 8.0), 6.29 (s, 2H), 4.25 – 4.20 (m, 8H). $^{13}C\{^1H\}$ NMR (101 MHz, $CDCl_3$) δ: 157.0, 143.8, 142.2, 139.5, 139.4, 138.7, 135.1, 123.6, 122.0, 118.5, 116.3, 115.0, 98.2, 64.7, 64.4. HRMS (CI+) calcd for $C_{28}H_{19}Br_2N_3O_4S_2$ [M]+ 682.9184, found 682.9187. Anal Calcd for $C_{28}H_{19}Br_2N_3O_4S_2$: C, 49.07; H, 2.79; N, 6.13. Found: C, 48.86; H, 2.99; N, 5.87.

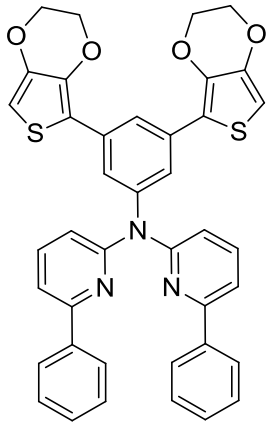

[5.5] *N*-(3,5-*bis*(2,3-dihydrothieno[3,4-*b*][1,4]dioxin-5-yl)phenyl)-6-phenyl-*N*-(6-phenylpyridin-2-yl)pyridin-2-amine

5.4 (0.305 g, 0.44mmol) and benzenboronic acid (0.162 g, 1.33 mmol) were dissolved in 15 mL of 2-methoxyethanol. 2.2 mL of 2M aq K_2CO_3 were added. The solution was purged with N_2 for 45 min. Palladium acetate (0.009 g, 0.04 mmol) was added and the solution was refluxed at 120 °C for 4 hrs. The reaction was transferred to a separatory funnel and washed with H_2O extracting into ethyl acetate (15 mL x 2). The combined organic layers were dried with magnesium sulfate and concentrated. The residue was purified on a silica gel column with CH_2Cl_2 as the eluent to afford an orange solid (31.6 %). ^{1}H NMR (400 MHz, $CDCl_3$) δ 7.91(d, 4H, *J* = 8.4), 7.88 (s, 1H), 7.64 (t, 2H, *J* = 7.8), 7.58 (s, 2H), 7.41 (d, 2H, *J* = 7.6), 7.32 (m, 6H), 7.08 (d, 2H, *J* = 8.0), 6.26 (s, 2H), 4.17 (s, 4H). ^{13}C{^{1}H} NMR (101 MHz, $CDCl_3$) δ: 157.3, 155.2, 145.1, 142.1, 139.1, 138.4, 137.9, 134.5, 128.6, 128.5, 126.7, 123.9, 120.8, 116.8, 115.2, 114.0, 97.98 64.6, 64.3. HRMS (ESI) calcd for $C_{40}H_{29}N_3O_4S_2$ $[M + H]^+$ 680.16722, found 680.16656; Anal Calcd for $C_{40}H_{29}N_3O_4S_2$: C, 70.67; H, 4.30; N, 6.18. Found: C, 69.87; H,4.85; N, 5.37.

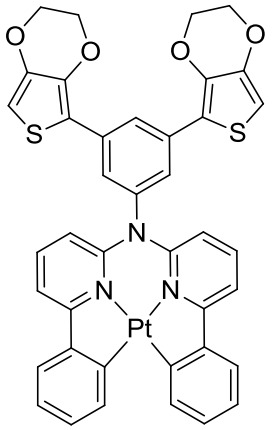

[5.6] *N*-(3,5-*bis*(2,3-dihydrothieno[3,4-*b*][1,4]dioxin-5-yl)phenyl)-6-phenyl-*N*-(6-phenylpyridin-2-yl)pyridin-2-amine platinum (II)

5.5 (0.111 g, 0.163 mmol) and potassium tetrachloroplatinate (0.123 g, 0.296 mmol) were dissolved acetic acid (15 mL) and degassed with N_2. The solution was refluxed at 118 °C for 4 days. The solvent was removed under reduced pressure, and the residue dissolved in CH_2Cl_2, filtered through a silca gel plug and the filtrate reduced. The solid was dissolved in a minimal amount of CH_2Cl_2 and then precipitated with hexanes. The solid was collected by filtration and washed with hexanes then methanol to yield a yellow solid (11.56 %). mp 158 – 160 °C (decomp). ^{1}H NMR (400 MHz, $CDCl_3$) δ 8.21 (d, *J* = 8.0, 2H), 8.07 (s, 1H), 7.80 (d, *J* = 7.2, 2H), 7.79 – 7.70 (m, 6H), 7.53 (t, *J* = 9.6, 2H), 7.30 (t, *J* = 7.2, 2H), 6.84 (d, *J* = 8.0, 2H), 6.38 (s, 2H), 4.27 – 4.21 (m, 8H). HRMS (CI+) calcd for $C_{40}H_{27}N_3O_4S_2Pt$ $[M]^+$ 872.1074, found 872.1091.

Crystallographic Data

Table 5.2: Crystal data and structure refinement for **5.4**

Empirical formula	$C_{18}H_{15}NO_4S_2$	
Formula weight	373.43	
Temperature	153(2) K	
Wavelength	0.71075 Å	
Crystal system	Monoclinic	
Space group	$P2_1/c$	
Unit cell dimensions	a = 15.625(2) Å	α = 90 °
	b = 13.4740(15) Å	β = 99.798(5) °
	c = 7.7266(10) Å	γ = 90 °
Volume	1602.9(3) $Å^3$	
Z	4	
Density (calculated)	1.547 Mg/m^3	
Absorption coefficient	0.357 mm^{-1}	
F(000)	776	
Crystal size	0.154 x 0.085 x 0.078 mm^3	
θ range for data collection	1.32 to 25.00 °	
Index ranges	h = -18→18	
	k = -16→16	
	l = -9→9	
Reflections collected	13882	
Independent reflections	2817 [$R_{(int)}$ = 0.1176]	
Completeness to theta = 25.00°	99.8 %	
Max. and min. transmission	1.0000 and 0.7457	
Refinement method	Full-matrix least-squares on F^2	
Data / restraints / parameters	2817 / 0 / 234	
Goodness-of-fit on F^2	1.074	
Reflections with [$I>2\sigma(I)$]	R_1 = 0.0565, wR_2 = 0.1412	
R indices (all data)	R_1 = 0.0718, wR_2 = 0.1608	
Largest diff. peak and hole	0.532 and -0.347 e.$Å^{-3}$	

Appendix A: Luminescent Aluminum Salophen Complexes Incorporated into Conducting Metallopolymers

INTRODUCTION

Sarah F. Swingle developed an electropolymerizable aluminum salophen complex with bithiophene ester-R groups, see complex **A.2**.[114] Sarah electropolymerized both the ligand and the aluminum complex to form thin films, see Scheme A.1. Both the aluminum complex and the corresponding metallopolymer exhibit blue-green emission. After Sarah's graduation I continued work with these complexes. This is a summary of my contribution to the project.

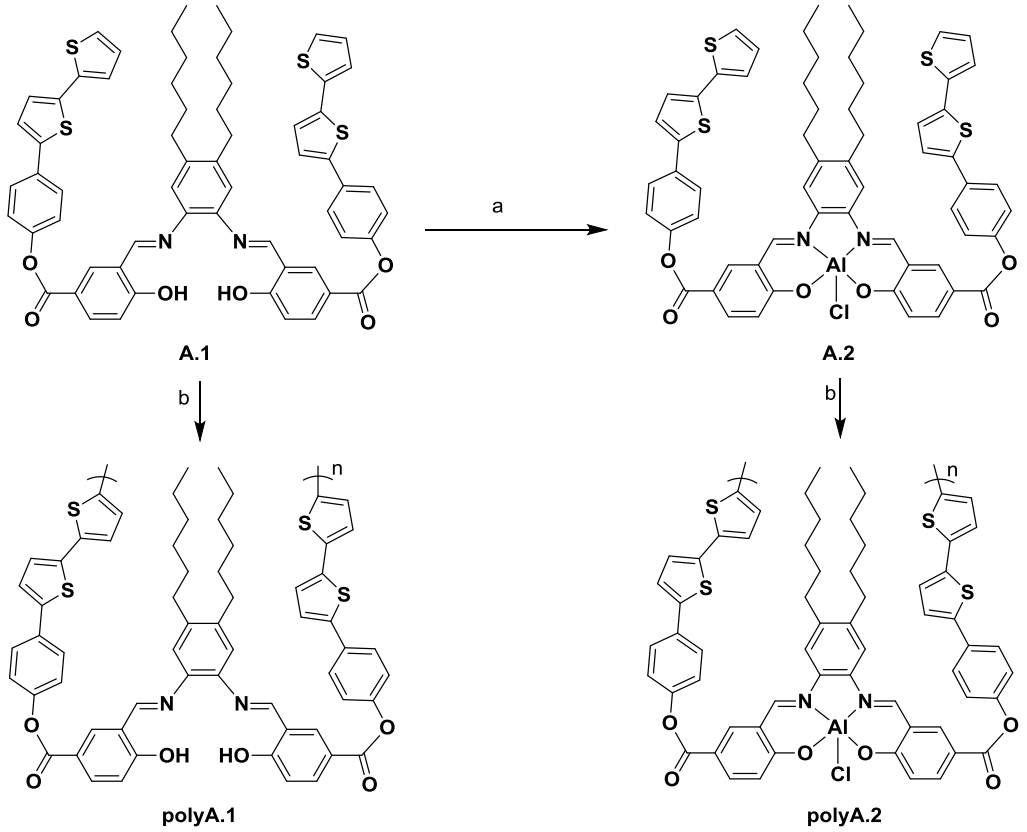

Scheme A.1: Synthesis of aluminum complex **A.2** and polymers **polyA.1** and **polyA.2**.
(a) Me_2AlCl, toluene, 65 °C, 18 h (b) -2n e^-, -2n H^+.

SPECTROELECTOCHEMISTRY

Sutter and coworkers developed a series of ester functionalized aluminum salophen complexes in 2012.[115] The series investigated the influence of varying the ester-R group on C5 of the salicylidene rings. It was observed that the emission quantum yield increased when more electron withdrawing ester-R groups were utilized. These systems were the basis for the complex developed by Sarah Swingle. Our system can be chemically or electrically doped to create a polaron or bipolaron, see Figure A.1. The formation of these cationionic species at the ester is anticipated to have the effect of increasing the emission efficiency for the system, as was seen when electron-withdrawing substituents were placed on the ester in the systems developed by Sutter and coworkers.

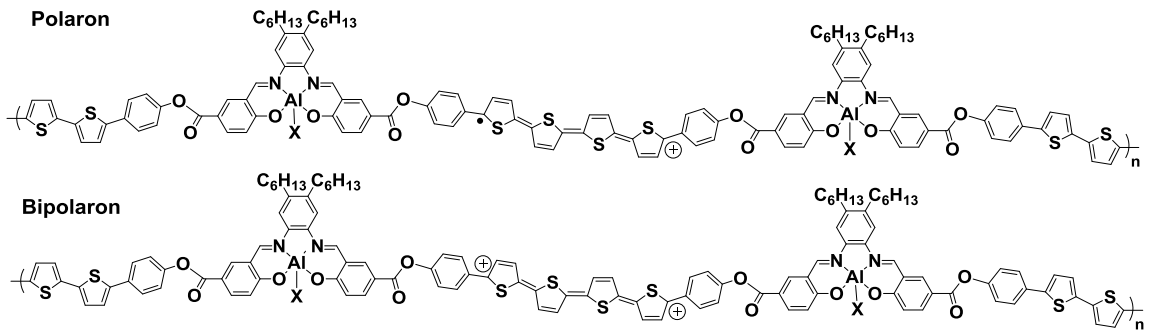

Figure A.1: Proposed structures of polaron and bipolaron formation in **polyA.2**.

To investigate the formation of the cationic species, UV-vis-NIR spectroelectochemical experiments were performed on films of **polyA.2** grown by Sarah Swingle. Low energy transitions at 650 nm and 950 nm were observed upon oxidation at 0.5 V (vs Fc/Fc^{+}), see Figure A.2. As higher potentials were applied, an increase in the absorbance of the peak at 950 nm and a decrease in the peak at 650 nm were observed.

These transitions are consistent with the formation of polaron and bipolaron states that are frequently observed in thiophene based polymer systems.[107,116,117]

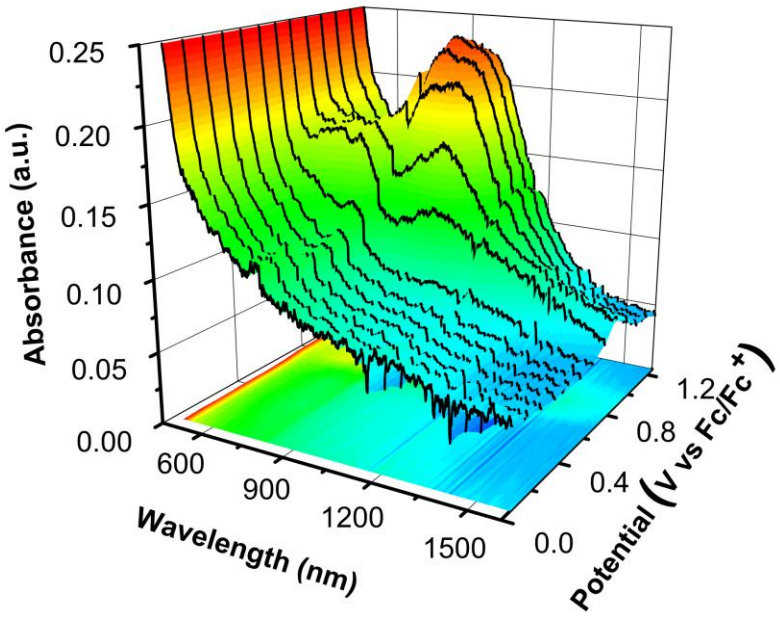

Figure A.2: UV-vis-NIR spectroelectrochemistry of **polyA.2**.

ELECTROCHEMISTRY

Attempts were made to make more electropolymerized films of **polyA.2**, but the **A.2** provided by Sarah Swingle did not yield any films. **A.2** was re-synthesized and characterized, see Experimental. The freshly synthesized monomer, **A.2**, was electropolymerized as an electrode confined film onto a platinum button working electrode, see Figure A.3(top left). The first electrochemical cycle is shown in red and subsequent cycles are shown in black. With each additional scan, additional layers of polymer are deposited onto the electrode. Figure A.3(top right) shows the relationship

between the oxidative peak and number of scans (red) and the reductive peak and the number of scans (black). The relationship is linear for about six scans indicating a

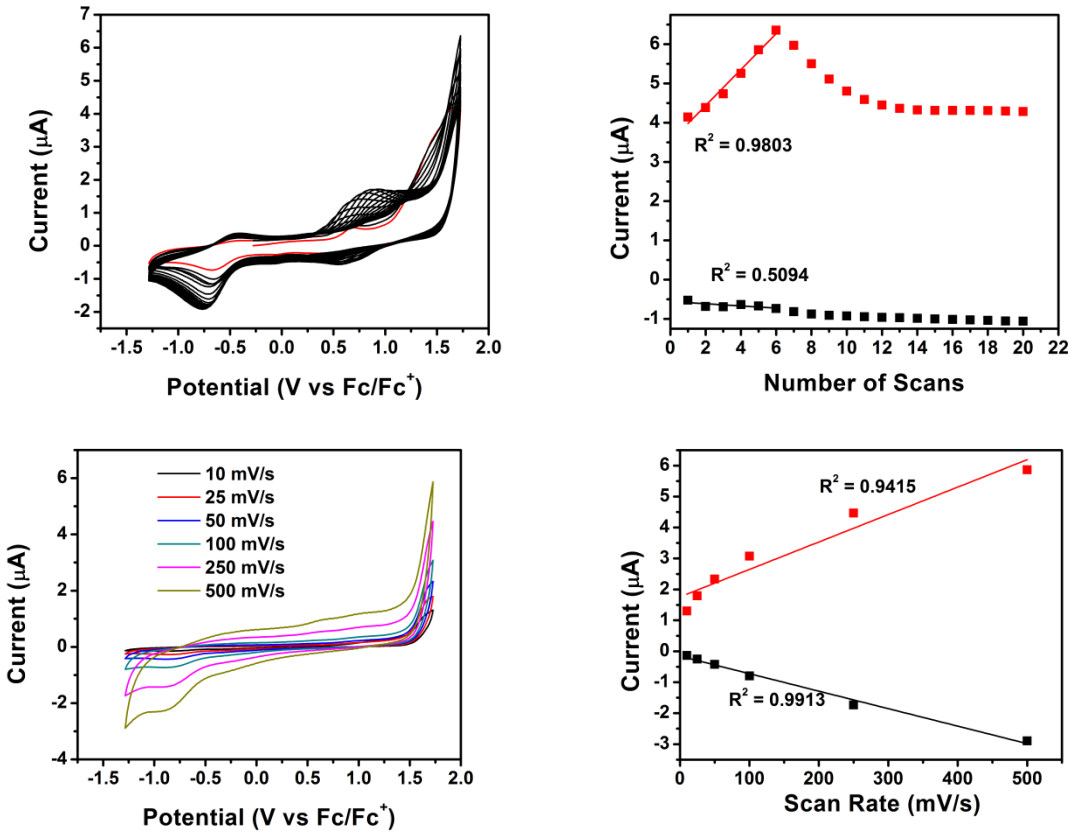

Figure A.3: Electrochemistry of complex **A.2**.

(Top Left) Cyclic voltammogram of polymer growth **A.2** in 0.1 M $TBAPF_6$ in CH_2Cl_2 at a scan rate of 0.1 V/s. (Top Right) Plot of oxidative and reductive peak currents versus number of scans. (Bottom Left) Scan rate dependence study of **polyA.2** in 0.1 M $TBAPF_6$ in CH_2Cl_2. (Bottom Right) Plot of oxidative and reductive peak currents versus scan rate.

uniform growth of the polymer. After the sixth scan it is likely that the electrode has been passivated by the film and no additional polymer can be grown. The electrode was transferred to a fresh solution of electrolyte and the potential was cycled at varying scan

rates, see Figure A.3(bottom left). The oxidative peak verses the scan rate (red) and the reductive peak verses the scan rate (black) were plotted, see Figure A.3(bottom right). A linear relationship was observed between the peaks and the scan rate, indicating an ionically porous, conductive film.

Similar experiments were performed by Swingle with **A.2** using a stainless steel working electrode. X-ray photoelectron spectroscopy (XPS) was conducted to determine the elemental composition of the polymer. Theoretically **polyA.2** is anticipated to have a aluminum:sulfur:nitrogen ratio of 1:4:2, quantitative XPS of a thin film of **polyA.2** on a stainless steel substrate revealed a ratio of aluminum (2*p*):sulfur (2*p*):nitrogen (1*s*) of 1:3.6:1.9. These small deviations from the theoretical value have been previously reported in other polymers and are within the accuracy tolerance of the XPS measurement.[107]

SPECTROSCOPY

The room temperature emission for **A.1**, **A.2** and **polyA.2**, and the 77 K data for **A.2** are given in Sarah Swingle's thesis.[114] The emission of **A.1** in 2-methyltetrahydrofuran at room temperature and at 77 K was recorded, see Figure A.4. Upon cooling, the emission displays increased vibronic structure and the peak at ~550 nm blue shifts. The lifetimes of all the peaks were determined, see Table A.1. All of the lifetimes were in the microsecond range, which agrees with the assignment of phosphorescence made by Sarah Swingle.[114]

Table A.1: Photoluminescence data for **A.1** at 77 K.

λ_{Em} (nm)	546	515	448	415	399
τ (μs)	5.0 ± 0.7	5.1 ± 0.9	10.9 ±0.3	7 ± 1	8 ± 3

Recorded in 2MeTHF at 77K.

The polymer films of **polyA.1** were delaminated from the electrode by sonicating in DMF and studied as a suspension in DMF. The absorption spectrum of **polyA.1** is shown in Figure A.5A. The polymer displays red shifted and broadened absorption as compared to the monomer **A.1**. **PolyA.2** also displayed a broadened and red-shifted absorption profile as compared to the monomer, **A.2**, which has been attributed to the increased delocalization caused by the the polymerization.[114]

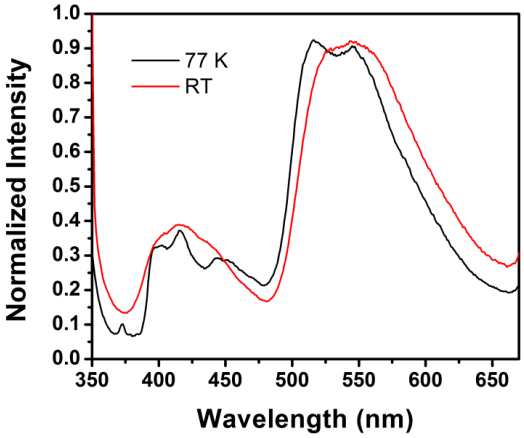

Figure A.4: Emission of **A.1** in 2MeTHF at ambient temperature and 77 K

The emission spectrum of **polyA.1** is shown in Figure A.5B. Like the absorption, the emission is also red shifted from monomer to polymer, although the emission is not as

broadened. The aluminum complex **A.2** and the metallopolymer **polyA.2** also display red-shifted emission from monomer to polymer.

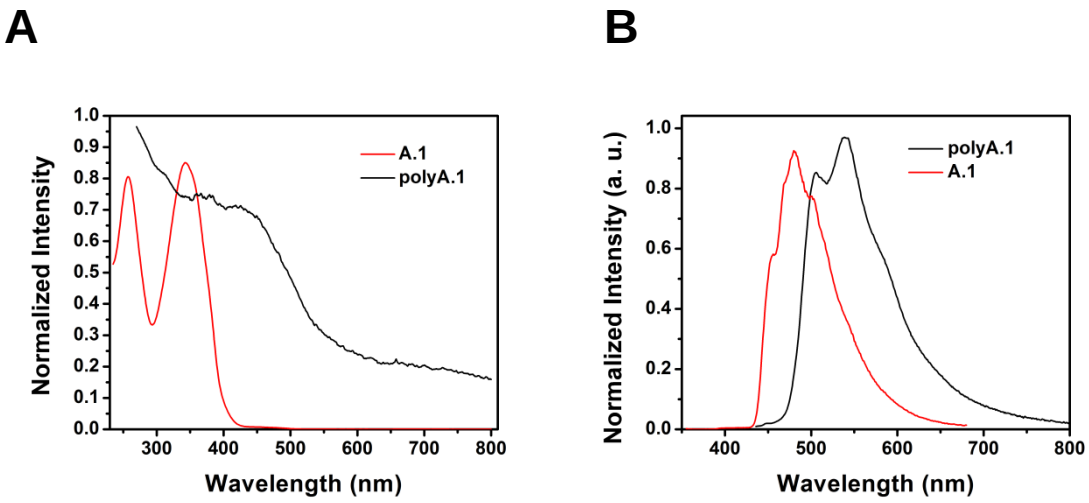

Figure A.5: (A) Absorbance spectra of **A.1** in CH_2Cl_2 and **polyA.1** suspended in DMF. (B) Emission spectra of **A.1** in CH_2Cl_2 and **polyA.1** taken as a suspension in DMF.

EXPERIMENTAL

General Methods

All chemicals were purchased from chemical suppliers and were used without further purification. All dry reactions were performed using standard Schlenk techniques and were performed under an inert atmosphere of nitrogen. Toluene was dried by allowing the solvent to sit over freshly activated 3Å molecular sieves for 24 hrs, followed by sparging with N_2 for 1 hr, as described by Williams and coworkers.[111] X-ray photoelectron spectroscopy (XPS) was carried out on a PHI 5700 XPS system equipped with dual Mg X-ray source and monochromatic Al X-ray source complete with depth profile and angle-resolved capabilities. The preparation of **A.1** is given by Sarah Swingle in her thesis.[114]

Electrochemistry

All electrochemical syntheses and studies were performed in a dry-box under a nitrogen atmosphere using a GPES system from Eco. Chemie B.V and an autolab potentiostat. All the electrochemical experiments were carried out in a three-electrode cell with $Ag/AgNO_3$ reference electrode (silver wire suspended in a 0.01 M silver nitrate solution with 0.1 M $[(n\text{-}Bu)_4N][PF_6]$ in dry CH_3CN), a Pt wire coil counter electrode, and a platinum working electrode. Potentials were measured relative to the $Ag/AgNO_3$ reference electrode. Ferrocene was purified by sublimation at 95 °C and was used as an external reference to calibrate the reference electrode before and after experiments were performed and that value was used to correct the measured potentials. All electrochemistry was performed in CH_2Cl_2 solutions using 0.1 M $[(n\text{-}Bu)_4N][PF_6]$ as the supporting electrolyte. $[(n\text{-}Bu)_4N][PF_6]$ was purified by recrystallization three times from hot ethanol before being dried for 3 days at 100 °C under reduced pressure prior to use. Electrosyntheses of the polymer films were performed from dilute monomer solutions by continuous cycling between -1.3 V and 1.7 V (vs. Fc/Fc^+) at 100 mVs^{-1}. The films obtained were then washed with fresh CH_2Cl_2 before performing further experiments.

Spectroscopy

Absorption spectra were recorded on a Varian Cary 6000i UV-Vis-NIR spectrophotometer with starna quartz fluorometer cells with a pathlength of 10 mm. Luminescent measurements were recorded on a Photon Technology International QM 4 spectrophotometer equipped with a 6-inch diameter K Sphere-B integrating sphere.

Synthesis of A.2

A.1 (0.038 g, 0.036 mmol) was fully dissolved in 150 mL dry toluene under nitrogen. Heating to 80 °C was necessary to achieve complete dissolution. A 1 M solution of dimethylaluminum chloride in hexanes (0.1 mL, 0.1 mmol) was added. The solution was stirred overnight at 80 °C under nitrogen. A yellow precipitate was isolated by filtration and was rinsed with hot toluene. **A.2** was introduced as a solution in MeOH for HRMS (ESI+), calculated for $C_{63}H_{57}AlN_2O_7S_4$: $[M + H]^+$ 1109.29370, found 1109.29570. IR: ν = 1729.98 cm^{-1} (C=O), ν = 1618.96 cm^{-1} (C=N). ^1H NMR ($CDCl_3$) δ: 9.55 (s, 2H), 8.67 (d, 2H, J = 2.1), 8.20 (dd, 2H, J = 8.9, 2.3), 8.03 (s, 2H), 7.78 (d, 4H, J = 8.7), 7.55 – 7.52 (m, 2H), 7.38 – 7.34 (m, 8H), 7.14 – 7.11 (m, 4H), 2.71 (t, 4H, J = 7.2), 1.632 (m, 4H),1.41 – 1.22 (m, 12H), 0.87 (t, 6H, J = 7.2).

Appendix B: Alternative Platinum Ligand

INTRODUCTION

When designing ligands for electropolymerization, one must consider where to append electropolymerizable moieties. The electropolymerizable ethylenedioxythiophene groups were attached in at the 1 and 5 positions for complex **5.6**. This yields a polymerized structure in which the emitter dangles from the polymer backbone. An alternative scheme was designed, see Scheme B.1, where ethylenedioxythiophene was attached at the 3 position to give a more symmetric and sterically hindered structure. The polymerized structure of complex **B.6** would place the emitter directly in the backbone of the polymer. Attempts were made to synthesize the alternate complex. Compounds **B.1** – **B.4** were synthesized and characterized. Complex **B.1** was synthesized through a Stille coupling between 4-iodonitrobenzene and tributyl(2,3-dihydrothieno[3,4-*b*][1,4]dioxin-5-yl)stannane. The nitro group is reduced to the aniline using sodium borohydride and charcoal following a procedure derived from Zeynizadeh and Setamdideh.[118] A Buckwald-Hartwig amination was utilized to synthesize **B.3** and **B.4**. The reactions to form complexes **B.3** and **B.4** are low yielding and result in monosubstituted compounds as the major product. Because appreciable amounts of these starting materials could not easily be synthesized efforts were no longer focused on the synthesis of these compounds.

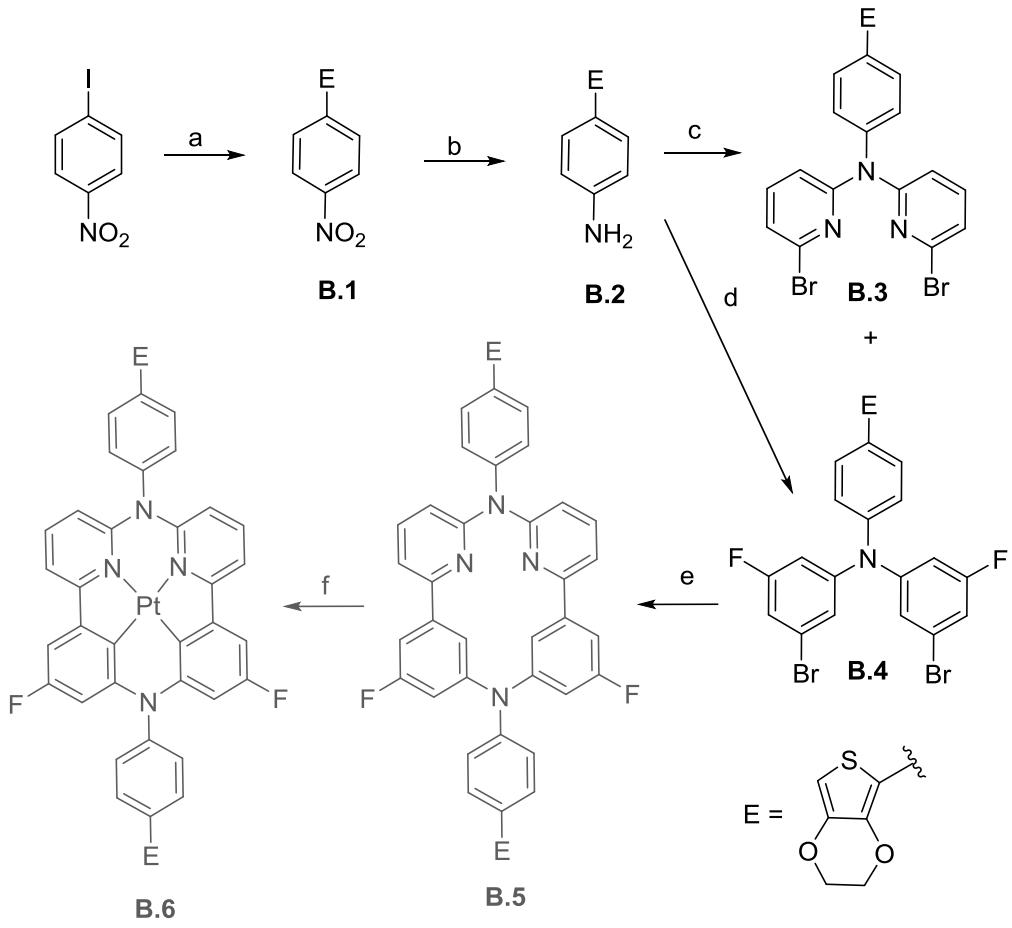

Scheme B.1: Synthesis of platinum complex precursors, **B.1 – B.4**.

(a) EDOTSnBu$_3$, PdCl$_2$(PPh$_3$)$_2$, CuI, Toluene, 110 °C, 18 h, 98.5% (b) NaBH$_4$, Charcoal, THF, H$_2$O, 50 °C, 18h, 65.3% (d) 2,6-dibromopyridine, Pd$_2$(dba)$_3$, DPPF, NaO*t*Bu, Toluene, 110 °C, 18 h, 21.8% (e) 1,3-dibromo-5-fluorbenzene, Pd$_2$(dba)$_3$, DPPF, NaO*t*Bu, Toluene, 110 °C, 18 h, 10.3%

EXPERIMENTAL

General Methods

All chemicals were purchased from chemical suppliers and were used without further purification. All dry reactions were performed using standard Schlenk techniques

and were performed under an inert atmosphere of nitrogen. Toluene was dried by allowing the solvent to sit over freshly activated 3Å molecular sieves for 24 hrs, followed by sparging with N_2 for 1 hr, as described by Williams and coworkers.[111] ^{1}H and $^{13}C\{^{1}H\}$ spectra were obtained on a Varian Unity+ 300 and were referenced to the residual solvent peaks. All coupling constants are listed in Hertz (Hz). Melting points are not corrected. Elemental analysis was performed by QTI, Whitehouse, NJ (www.qtionline.com). High resolution mass spectra were obtained with a Micromass Autospec Ultima. Tributyl(2,3-dihydrothieno[3,4-*b*][1,4]dioxin-5-yl)stannane was prepared according to Swager and coworkers.[112]

X-ray Crystallography

Crystals of **B.2** suitable for X-ray diffraction were obtained by slow evaporation from a saturated solution of **B.2** in dichloromethane that was layered with hexanes. Crystals of **B.3** suitable for X-ray diffraction were obtained by slow evaporation from a 45% ethyl acetate, 55% hexanes solution (*v/v*). The single–crystal diffraction data was collected at 100 K on a on a Rigaku AFC12 with Saturn 724+ CCD using a graphite monochromator. The complex was collected using a graphite monochromator with MoKα radiation (λ = 0.71073Å). Absorption corrections were applied using multi-scan. Data reduction was performed using the Rigaku Americas Corporation's Crystal Clear version 1.40.[39] The structures were solved by direct methods and refined anisotropically using full-matrix least-squares methods with the SHELX-97 program package.[40] The amine and amide H atoms were located in a difference Fourier map and both positional and isotropic displacement parameters were refined. All other H atoms were positioned geometrically and refined using a riding model, with C—H = 0.93–0.99 Å and $U_{iso}(H) = 1.2\ U_{eq}(C)$.

Neutral atom scattering factors and values used to calculate the linear absorption coefficient are from the International Tables for X-ray Crystallography (1992).[41]

Synthesis

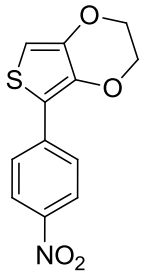

[B.1] 5-(4-nitrophenyl)-2,3-dihydrothieno[3,4-*b*][1,4]dioxine

To a solution of dry toluene under N_2 was added tributyl(2,3-dihydrothieno[3,4-*b*][1,4]dioxin-5-yl)stannane (21.4 g, 49.5 mmol), 4-iodonitrobenzene (7.7 g, 30.9 mmol), *trans*dichloro*bis*triphenylphosphine palladium (II) (0.3 g, 0.5 mmol), and copper (I) chloride (0.2 g, 1.1 mmol). The solution was refluxed at 110 °C overnight. The black solution exposed to atmosphere and conc. under reduced pressure. The solid was dissolved in dichloromethane and filtered over a bed of silica. The filtrate was conc. and recycrystallized in a dichloromethane/hexanes mixture to yield a bright yellow solid (98.5 %) m.p. 185 °C (decomp.). ^{1}H NMR ($CDCl_3$) δ 8.17 (d, 2H, J = 9.0), 7.83 (d, 2H, J = 9.3), 6.45 (s, 2H), 4.33-4.37 (m, 2H), 4.25 – 4.27 (m, 2H). $^{13}C\{^1H\}$ NMR ($CDCl_3$) δ: 145.4, 142.5, 140.6, 139.8, 125.7, 124.0, 115.1, 101.0, 65.9, 64.3, HRMS (CI+) calc for $C_{12}H_9NO_4S$ $(M+H)^+$ 264.0331 , found 263.0327.

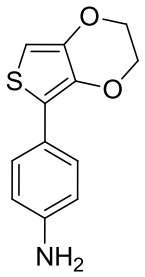

[B.2] 4-(2,3-dihydrothieno[3,4-*b*][1,4]dioxin-5-yl)aniline

B.1 (8.01 g, 30.43 mmol) and charcoal (8.39 g) were added to a round bottom and dissolved in THF. 5 mL of H_2O was added and the mixture was heated to 50 °C. Sodium borohydride (2.66 g, 70.5 mmol) was added in four portions over 1 hr. The reaction was heated for an additional 30 min after the last addition. The mixture was cooled to room temp and filtered, washing with THF. The solution was conc., the re-dissolved in CH_2Cl_2 and washed with H_2O. The organic layer was conc. to a third the original volume and mixed with an equal volume of hexanes. The solution was left in a fridge overnight and the precipating orange crystals were collected by vacuum filtration (4.63 g, 65.3% yield). m.p. 103 °C. ^{1}H NMR ($CDCl_3$) δ 7.51 (dt, J = 8.7, J = 2.1, 2 H), 6.66 (dt, J = 8.7, J = 2.4, 2H), 6.19 (s, 1H), 4.25 – 4.18 (m, 4H), 3.64 (b, 2H). ^{13}C{^{1}H} NMR ($CDCl_3$) δ: 145.2, 142.1, 136.6, 127.2, 123.5, 117.9, 115.0, 95.5, 64.5, 64.4. Anal Calcd for $C_{12}H_{11}NO_2S$: C, 61.78; H, 4.75; N, 6.00. Found: C, 61.67; H, 4.07; N, 5.90.

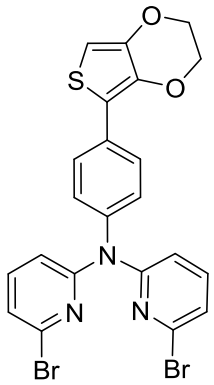

[B.3] 6-bromo-*N*-(6-bromopyridin-2-yl)-*N*-(4-(2,3-dihydrothieno[3,4-*b*][1,4]dioxin-5-yl)phenyl)pyridin-2-amine

In an air-free glovebox *tris*(dibenzylideneacetone)dipalladium(0) (0.488 g, 0.5 mmol) was added to a dry schlenk. The schlenk was pumped out, dry toluene was transferred into the flask by cannula and **B.2** (4.508 g, 19.3 mmol), 2,6-dibromopyridine (9.387 g, 39.6 mmol), 1,1'-*bis*(diphenylphosphino)ferrocene (0.632 g, 1.1 mmol), and sodium *tert*-butoxide (3.989 g, 41.5 mmol) were added to the solution. The solution was refluxed at 120 °C for 20 hours. The solution was cooled to room temperature and the toluene was removed by rotoevaporation. The product was extracted into CH_2Cl_2 (x3) washing with H_2O. The crude solid was purified by silica gel column chromatography with 45% ethyl acetate: 55% hexanes by volume ($R_f = 0.59$) to yield a bright yellow solid (2.298 g, 21.8 %). m.p. 160 °C. ^{1}H NMR ($CDCl_3$) δ 7.72 (d, 2H, J = 8.4), 7.36 (t, 2H, J = 7.9), 7.15 (d, 2H, J = 8.4), 7.09 (d, 2H, J = 5.1), 6.93 (d, 2H, J = 8.4), 6.30 (s, 1H), 4.31 – 4.25 (m, 4H), ^{13}C{^{1}H} NMR ($CDCl_3$) δ: 156.9, 142.2, 141.5, 139.6, 139.4, 138.3, 131.51, 127.2, 122.1, 116.6, 114.9, 97.9, 64.8, 64.4. Anal. calcd. for $C_{22}H_{15}Br_2N_3O_2S$: C, 48.46; H, 2.77; N, 7.71. Found: C, 48.63; H, 2.51; N, 7.59.

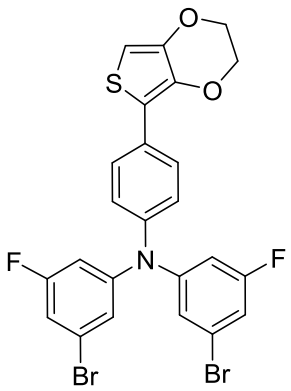

[B.4] 3-bromo-*N*-(3-bromophenyl)-*N*-(4-(2,3-dihydrothieno[3,4-*b*][1,4]dioxin-5-yl)phenyl)aniline

B.4 was prepared in accordance with **B.3**. **B.2** (1.282, 5.5 mmol), 1,3-dibromo-5-fluorbenzene (2.2 mL, 19.0 mmol), sodium *tert*butoxide (0.680 g, 7.1 mmol), *tris*(dibenzylideneacetone)dipalladium(0) (0.149 g, 0.2 mmol), and 1,1'-*bis*(diphenylphosphino)ferrocene (0.396 g, 0.7 mmol). Purified by silica gel column chromatography with 30% CH_2Cl_2: 70% hexanes by volume (R_f = 0.81) to yield a yellow solid (0.205 g, 10.3 %). m.p. 85 °C (decomp). ^{1}H NMR ($CDCl_3$) δ: 7.69 (d, *J* = 8.7, 2H), 7.06 (d, *J* = 8.7, 2H), 6.98 (s, 2H), 6.91 (dt, *J* = 7.8, *J* = 1.9, 2 H), 6.71 (dt, *J* = 10.20, *J* = 2.1, 2H), 6.30 (s, 1H), 4.22 – 4.31 (m, 4 H). ^{13}C{^{1}H} NMR ($CDCl_3$) δ: 164.8, 161.5, 148.8 (d, *J* = 42.6), 143.4, 138.18, 130.5, 127.3, 125.1, 123.1 (d, *J* = 47.4), 122.0, 116.4, 113.8 (d, *J* = 98.4), 109.4 (d, *J* = 97.2), 97.8, 64.7, 64.3.

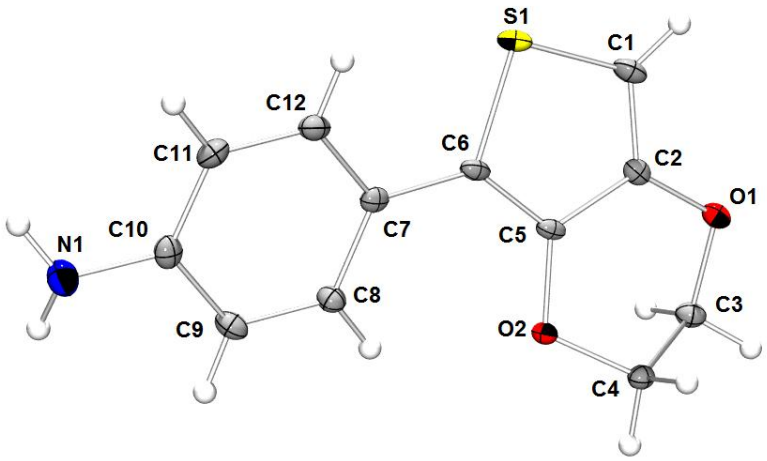

Figure B.1: Molecular structure of **B.2** showing the atom labeling scheme. Displacement ellipsoids are shown at the 30% probability level.

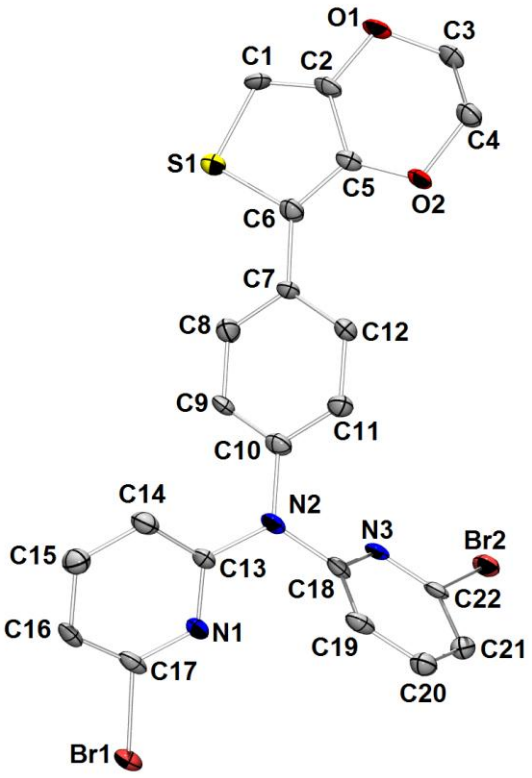

Figure B.2: Molecular structure of **B.3** showing the atom labeling scheme. Displacement ellipsoids are shown at the 50% probability level.

Crystallographic Data

Table B.1: Crystal data and structure refinement for **B.2**

Empirical formula	$C_{12}H_{11}NO_2S$	
Formula weight	233.28	
Temperature	100(2) K	
Wavelength	0.71075 Å	
Crystal system	Orthorhombic	
Space group	$P2_12_12_1$	
Unit cell dimensions	a = 6.9117(6) Å	α = 90 °
	b = 7.0898(6) Å	β = 90 °
	c = 21.4784(16) Å	γ = 90 °
Volume	1052.50(15) $Å^3$	
Z	4	
Density (calculated)	1.472 Mg/m^3	
Absorption coefficient	0.289 mm^{-1}	
F(000)	488	
Crystal size	0.29 x 0.27 x 0.08 mm^3	
θ range for data collection	3.03 to 25.00 °	
Index ranges	h = -8→8	
	k = -8→8	
	l = -22→25	
Reflections collected	11854	
Independent reflections	1853 [$R_{(int)}$ = 0.0470]	
Completeness to theta = 25.00°	99.9 %	
Max. and min. transmission	1.0000 and 0.858	
Refinement method	Full-matrix least-squares on F^2	
Data / restraints / parameters	1853 / 0 / 154	
Goodness-of-fit on F^2	0.864	
Reflections with [$I>2\sigma(I)$]	R_1 = 0.0286, wR_2 = 0.0754	
R indices (all data)	R_1 = 0.0292, wR_2 = 0.0759	
Largest diff. peak and hole	0.441 and -0.209 e.$Å^{-3}$	

Table B.2: Crystal data and structure refinement for **B.3**

Empirical formula	$C_{22}H_{15}Br_2N_3O_2S$	
Formula weight	545.25	
Temperature	100(2) K	
Wavelength	0.71075 Å	
Crystal system	Triclinic	
Space group	$P\bar{1}$	
Unit cell dimensions	a = 4.483(4) Å	α = 75.807(18) °
	b = 12.151(9) Å	β = 87.67(3) °
	c = 18.958(13) Å	γ = 89.62(2) °
Volume	1000.3(13) $Å^3$	
Z	2	
Density (calculated)	1.810 Mg/m^3	
Absorption coefficient	4.183 mm^{-1}	
F(000)	540	
Crystal size	0.22 x 0.03 x 0.03 mm^3	
θ range for data collection	1.73 to 25.00 °	
Index ranges	h = -5→5	
	k = -14→14	
	l = -22→22	
Reflections collected	13439	
Independent reflections	3521 [$R_{(int)}$ = 0.0793]	
Completeness to theta = 25.00°	99.6 %	
Max. and min. transmission	1.0000 and 0.5628	
Refinement method	Full-matrix least-squares on F^2	
Data / restraints / parameters	3521 / 0 / 271	
Goodness-of-fit on F^2	0.999	
Reflections with [$I>2\sigma(I)$]	R_1 = 0.0505, wR_2 = 0.1203	
R indices (all data)	R_1 = 0.0652, wR_2 = 0.1278	
Largest diff. peak and hole	1.059 and -0.827 e.$Å^{-3}$	

Appendix C: Key Findings and Future Directions

SEPARATION OF *F*-ELEMENTS

Key Findings

- Four previously undiscovered small molecules were synthesized and characterized (**2.3**, **2.4**, **2.8**, and **3.3**).
- Two novel homopolymers (**2.9** and **3.5**) in varying molecular weights were synthesized and characterized.
- Two novel block copolymers (**3.7** and **3.8**) in varying block ratios were synthesized and characterized.
- It was determined that variations in molecular weight influence the chelation properties of the polymeric materials.
- It was demonstrated that additional blocks in the polymeric materials had significant influences on the chelation properties even in the case where additional blocks were not in direct contact with chelating blocks.
- Efficient extractions were demonstrated without the use of organic solvents.
- Selectivity for thorium(IV) over europium(III), cerium(III), and lanthanum(III) was demonstrated for the homopolymers (**2.9a-c**) and the triblock polymers (**3.8a-b**).

Future Directions

- By testing the extraction properties of a wider range of molecular weights and a wider range of ratios of blocks in the copolymers, the trends in the data could be better understood.

- The chelation properties for block copolymers with a wider range of non-chelating blocks could be investigated. For instance the addition of alkyl chains verses the addition of the glycol chains could be compared in liquid-liquid and solid-liquid extractions.
- The influence of variations in the polydispersity index on the chelation properties of homopolymers could be investigated.
- Many ligands exist which have been shown to chelate actinides. It would be interesting to study other ligands in polymeric systems to determine if variations in molecular weight have similar trends in the extraction data and if there are discernible trends between varying ligand systems.
- The polymer could be hydrogenated to increase the flexibility of the system and test the chelation mechanism.

LUMINESCENT MATERIALS

Key Findings

- Seven previously undiscovered small molecules were synthesized and characterized (**5.3**, **5.4**, **5.5**, **5.6**, **5.7**, **B.3**, and **B.4**).
- Electropolymerizable groups were attached to the system without altering the emission wavelength of the original complex.
- Both the ligand (**5.6**) and the platinum complex (**5.7**) were electropolymerized into thin films.
- Light emission in the blue-green region was observed for the ligand, **5.6**, the platinum monomer, **5.7**, and the metallopolymer, **poly5.7**.
- Polymer emission was observed to be primarily ligand-centered.

Future Directions

- The influence on the optical and electronic properties of spacing out luminescent centers by electropolymerizing with excess 3,4-ethylenedioxythiophene could be studied.
- The optical and electronic properties of **5.3** and **5.4** could be studied and compared to a similar study by Pepitone and coworkers.[119]
- Complexes **B.3** and **B.4** are promising precursors to branched electroactive polymers, the materials could be synthesized and investigated following work similar to Hicks and coworkers.[120]

References

(1) Alley, W. M.; Alley, R. The Growing Problem of Stranded Used Nuclear Fuel. *Enviorn. Sci. Technol.* **2014**, *48*, 2091–2096.

(2) Worrall, A. Utilization of Used Nuclear Fuel in a Potential Future US Fuel Cycle Scenario. In *WM2013 Conference Proceedings*; Phoenix, AZ, 2013; pp. 1–13.

(3) *Separatiosn for the Nuclear Fuel Cycle in the 21st Century; ACS Symposium Series 933*; Lumetta, G. L.; Nash, K. L.; Clark, S. B.; Friese, J. I., Ed.; ACS Sympos.; American Chemical Society: Washington, D.C., 2006; Vol. 933.

(4) Salvatores, M. Nuclear Fuel Cycle Strategies Including Partitioning and Transmutation. *Nucl. Eng. Des.* **2005**, *235*, 805–816.

(5) Horwitz, E. P.; Kalina, D. G.; Diamond, H.; Vandergrift, G. F. The TRUEX Process - A Process for the Extraction of the Transuranic Elements from Nitric Acid Wastes Utilizing Modified PUREX Solvent. *Solv. Extr. Ion Exch.* **1985**, *3*, 75–109.

(6) Vandegrift, G. F.; Leonard, R. A.; Steindler, M. J.; Horwitz, E. P.; Basile, L. J.; Diamond, H.; Kalina, D. G.; Kaplan, L. *Transuranic Decomtamination of Nitric Acid Solutions by the TRUEX Solvent Extraction Process - Preliminary Development Studies*; ANL-84-45, Argonne, IL, 1984; pp. 1–115.

(7) Horwtiz, E. P.; Muscatello, A. C.; Kalina, D. G.; Kaplan, L. The Extraction of Selected Transplutonium(III) and Lanthanide(III) Ions by Dihexyl-N,N-Diethylcarbamoylmethylphonate from Aqueous Nitric Acid Media. *Sep. Sci. Technol.* **1981**, *16*, 417–437.

(8) Arnaud-Neu, F.; Böhmer, V.; Dozol, J.-F.; Grüttner, C.; Jakobi, R. A.; Kraft, D.; Mauprivez, O.; Rouquette, H.; Simon, N.; Vogt, W. Calixarenes with Diphenylphosphoryl Acetamide Functions at the Upper Rim. A New Class of Highly Efficient Extractants for Lanthanides and Actinides. *J. Chem. Soc., Perkin Trans. 2* **1996**, 1175–1182.

(9) Kornelia, M.; Sah, A. K.; Peters, M. W.; Srinivasan, P.; Gelis, A. V.; Regalbuto, M. R.; Scott, M. J. CMPO-Functionalized C3-Symmetric Tripodal Ligands in Liquid/Liquid Extractions: Efficient, Selective Recognition of Pu(IV) with Low Affinity for 3+ Metal Ions. *Inorg. Chem.* **2007**, *46*, 10549–10563.

(10) Matthews, S. E.; Saadioui, M.; Böhmer, V.; Barboso, S.; Arnaud-Neu, F.; Schwing-Weill, M. J.; Carrera, A. G.; Dozol, J. F. Conformationally Mobile Wide Rim Carbamoylmethylphosphine Oxide (CMPO)-Calixarenes. *J. Prakt. Chem.* **1999**, *341*, 264–273.

(11) Hoorn, W. P. Van; Briels, W. J.; Duynhoven, J. P. M. Van; Veggel, F. C. J. M. Van; Reinhoudt, D. N. Conformational Distribution of Tetramethoxycalix[4]arenes by Molecular Modeling and NMR Spectroscopy : A Study of Apolar Solvation. *J. Org. Chem.* **1998**, *3263*, 1611–1620.

(12) Gutsche, C. D. *Calixarenes Revisited*; The Royal Society of Cambridge: Cambridge, 1998.

(13) Wang, P.; Saadioui, M.; Schmidt, C.; Böhmer, V.; Host, V.; Desreux, J. F.; Dozol, J.-F. Dendritic Octa-CMPO Derivatives of Calix[4]arenes. *Tetrahedron* **2004**, *60*, 2509–2515.

(14) Schmidt, C.; Saadioui, M.; Böhmer, V.; Host, V.; Spirlet, M.; Desreux, J. F.; Brisach, F.; Arnaud-neu, F.; Dozol, J. Modification of Calix[4]arenes with CMPO-Functions at the Wide Rim . Synthesis , Solution Behavior , and Separation of Actinides from Lanthanides. *Org. Biomol. Chem.* **2003**, *1*, 4089–4096.

(15) Barboso, S.; Carrera, A. G.; Matthews, S. E.; Arnaud-Neu, F.; Böhmer, V.; Dozol, J.-F.; Rouquette, H.; Schwing-Weill, M.-J. Calix[4]arenes with CMPO Functions at the Narrow Rim. Synthesis and Extraction Properties. *J. Chem. Soc., Perkin Trans. 2* **1999**, 719–723.

(16) Reinoso-García, M. M.; Verboom, W.; Reinhoudt, D. N. Solvent Extraction of Actinides and Lanthanides by CMP(O)- and N-Actyl(thio)urea-Tetrafunctionalized Cavitants: Strong Synergistic Effect of Cobalt Bis(dicarbollide) Ions. *Solv. Extr. Ion Exch.* **2005**, *23*, 425–437.

(17) Babain, V. A.; Alyapyshev, M. Y.; Karavan, M. D.; Böhmer, V.; Wang, L.; Shokova, E. A.; Motornaya, A. E.; Vatsouro, I. M.; Kovalev, V. V. Extraction of Americium and Europium by CMPO-Substituted Adamantylcalixarenes. *Radiochim. Acta* **2005**, *93*, 749–756.

(18) Dam, H. H.; Reinhoudt, D. N.; Verboom, W. Influence of the Platform in Multicoordinate Ligands for Actinide Partitioning. *New J. Chem.* **2007**, *31*, 1620.

(19) Zimmermann, H.; Tolstoy, P.; Limbach, H.-H.; Poupko, R.; Luz, Z. The Saddle Form of Cyclotriveratrylene. *J. Phys. Chem. B* **2004**, *108*, 18772–18778.

(20) Boerrigter, H.; Verboom, W.; Reinhoudt, D. N. Novel Resorcinarene Cavitand-Based CMP(O) Cation Lgands: Synthesis and Exraction Properties. *J. Org. Chem.* **1997**, *62*, 7148–7155.

(21) Dinger, M. B.; Scott, M. J. Extended Structures Built on a Triphenoxymethane Platform - C3 -Symmetric , Conformational Mimics of Calix[n]arenes. *Eur J. Org. Chem.* **2000**, 2467–2478.

(22) Peters, M. W.; Werner, E. J.; Scott, M. J. Enhanced Selectivity for Actinides over Lanthanides with CMPO Ligands Secured to a C(3)-Symmetric Triphenoxymethane Platform. *Inorg. Chem.* **2002**, *41*, 1707–1716.

(23) Jańczewski, D.; Reinhoudt, D. N.; Verboom, W.; Malinowska, E.; Pietrzak, M.; Hill, C.; Allignol, C. Tripodal (N-Alkylated) CMP(O) and Malonamide Ligands : Synthesis , Extraction of Metal Ions , and Potentiometric Studies. *New J. Chem.* **2007**, *31*, 109.

(24) Reinoso-García, M. M.; Jańczewski, D.; Reinhoudt, D. N.; Verboom, W.; Malinowska, E.; Pietrzak, M.; Hill, C.; Báča, J.; Grüner, B.; Selucky, P.; Grüttner, C. CMP(O) Tripodands: Synthesis, Potentiometric Studies and Extractions. *New J. Chem.* **2006**, *30*, 1480.

(25) Reinoso-García, M. M; Verboom, W.; Reinhoudt, D. N.; Brisach, F.; Arnaud-Neu, F.; Liger, K. Solvent Extraction of Actinides and Lanthanides by CMP(O)- and N-Acyl(thio)urea-Tetrafunctionalized Cavitands: Strong Synergistic Effect of Cobalt Bis(dicarbollide) Ions. *Solv. Extr. Ion Exch.* **2005**, *23*, 425–437.

(26) Galletta, M.; Maceratea, E.; Mariani, M.; Giola, M. A Study on Synergistic Effects and Protonation of a Selected Calixarene Based Picolonamide Ligand Used in the An/Ln Separation. *Czech. J. Phys.* **2006**, *56*, D453–D467.

(27) Grüner, B.; Kvíčalová, M.; Plešek, J.; Šícha, V.; Císařová, I.; Lučaíková, M.; Selucky, P. Cobalt Bis(dicarbollide) Ions Functionalized by CMPO-like Groups Attached to Boron by Short Binds; Efficient Extraction Agents for Separation of Trivalent F-Block Elements from Highy Acidic Nuclear Waste. *J. Organomet. Chem.* **2009**, *694*, 1678–1689.

(28) Choppin, G.; Liljenzin, J.-O.; Rydberg, J.; Ekberg, C. *Radiochemistry and Nuclear Chemistry*; 4th ed.; Academic Press: Amsterdam, 2013.

(29) Grimes, T. S.; Nilsson, M. a.; Nash, K. L. Lactic Acid Partitioning in TALSPEAK Extraction Systems. *Sep. Sci. Technol.* **2010**, *45*, 1725–1732.

(30) Diamond, H.; Howrtiz, E. P.; Danesi, P. R. Activity Coefficients of Carbamoylmethylphosphoryl Extractants in Toluene. *Solvent Extr. Ion Exch.* **1986**, *4*, 1009–1027.

(31) Horwitz, E. P.; Diamond, H.; Martin, K. A. The Extraction of Selected Actinides in the (III) (IV) and (VI) Oxidation States from Hydrochloric Acid by OφD(iB)CMPO: The TRUEX-Chloride Process. *Solv. Extr. Ion Exch.* **1987**, *5*, 447–470.

(32) Nuñez, L.; Vandergrift, G. F. *Separation of F Elements*; Nash, K. L.; Choppin, G. R., Ed.; Plenum Press: New York, NY, 1995; pp. 241–256.

(33) Odian, G. *Principles of Polymerization*; 4th ed.; Wiley Interscience: Hoboken, NJ, 2004.

(34) Heath, W. H.; Palmieri, F.; Adams, J. R.; Long, B. K.; Chute, J.; Holcombe, T. W.; Zieren, S.; Truitt, M. J.; White, J. L.; Willson, C. G. Degradable Cross-Linkers and Strippable Imaging Materials for Step-and-Flash Imprint Lithography. *Macromolecules* **2008**, *41*, 719–726.

(35) Neubert, B. J.; Snider, B. B. Synthesis of (+/-)-Phloeodictine A1. *Org. Lett.* **2003**, *5*, 765–768.

(36) Kiełbasiński, P.; Mikołajczyk, M. Novel Approach to the Synthesis of Alkoxycarbonylmethyl- and Bis(alkoxycarbonylmethyl)phosphine Oxides Based on a Reformatsky-Type Reaction. *Synthesis (Stuttg).* **1994**, 144–146.

(37) Pollino, J. M.; Stubbs, L. P.; Weck, M. Living ROMP of Exo-Norbornene Esters Possessing Pd(II) SCS Pincer Complexes or Diaminopyridines. *Macromolecules* **2003**, *36*, 2230–2234.

(38) Trnka, T. M.; Grubbs, R. H. The Development of L_2X_2RuCHR Olefin Metathesis Catalysts: An Organometallic Success Story. *Acc. Chem. Res.* **2001**, *34*, 18–29.

(39) Rigaku. *Crystal Clear*; Rigaku Americas Corporation: The Woodlands, Texas, USA, 2008.

(40) Sheldrick, G. M. A Short History of SHELX. *Acta Cryst.* **2008**, *A64*, 112–122.

(41) *International Tables for X-Ray Crystallography*; Wilson, A. J. C., Ed.; Kluwer Academic Press: Boston, 1992; p. Vol C, Tables 4.2.6.8 and 6.1.1.4.

(42) *Handbook of Nuclear Chemistry*; Vertés, A.; Nagy, S.; Klencsár, Z.; Lovas, R. G.; Rösch, F., Ed.; 2nd ed.; Springer: New York, 2011.

(43) Wiese, H. W. Actinide Transmutation Properties of Thermal and Fast Fission Reactors Including Multiple Recycling. *J. Alloys Compd.* **1998**, *271-273*, 522–529.

(44) Bowman, C. D. Accelerator-Driven Systems for Nuclear Waste Transmutation. *Annu. Rev. Nucl. Part. Sci.* **1998**, *48*, 505–556.

(45) Cotton, S. *Lanthanide and Actinide Chemistry*; John Wiley & Sons, Ltd.: West Sussex, 2007.

(46) Dam, H. H.; Reinhoudt, D. N.; Verboom, W. Multicoordinate Ligands for Actinide / Lanthanide Separations. *Chem. Soc. Rev.* **2007**, *36*, 367–377.

(47) Sankaran, N. B.; Rys, A. Z.; Nassif, R.; Nayak, M. K.; Metera, K.; Chen, B.; Bazzi, H. S.; Sleiman, H. F. Ring-Opening Metathesis Polymers for Biodetection and Signal Amplification: Synthesis and Self-Assembly. *Macromolecules* **2010**, *43*, 5530–5537.

(48) Trenor, S. R.; Shultz, A. R.; Love, B. J.; Long, T. E. Coumarins in Polymers: From Light Harvesting to Photo-Cross-Linkable Tissue Scaffolds. *Chem. Rev.* **2004**, *104*, 3059–3077.

(49) Maddipatla, M. V. S. N.; Wehrung, D.; Tang, C.; Fan, W.; Oyewumi, M. O.; Miyosji, T.; Joy, A. Photoresponsive Coumarin Polyesters That Exhibit Cross-Linking and Chain Scission Properties. *Macromolecules* **2013**, *46*, 5133–5140.

(50) Ren, B.; Zhao, D.; Liu, S.; Liu, X.; Tong, Z. Synthesis and Characterization of Poly(ferrocenylsilanes) with Coumarin Side Groups and Thier Photochemical Reactivity and Electrochemical Behavior. *Macromolecules* **2007**, *40*, 4501–4508.

(51) Oyaizu, K.; Ando, Y.; Konishi, H.; Nishide, H. Nernstain Adsorbate-like Bulk Layer of Organic Radical Polymers for High-Density Charge Storage Purposes. *J. Am. Chem. Soc.* **2008**, *130*, 14459–14461.

(52) Altomare, A.; Cascarano, G.; Giacovazzo, C. Guagliardi, A.; Burla, M. C.; Polidori, G.; Camalli, M. SIR92 - a Program for Automatic Solution of Crystal Structures by Direct Methods. *J. Appl. Cryst* **1994**, *27*, 435–436.

(53) Spek, A. L. Structure Validation in Chemical Crystallography. *Acta Cryst.* **2009**, *D65*, 148–155.

(54) Farrugia, L. J. WinGX and ORTEP for Windows: An Update. *J. Appl. Cryst* **2012**, *45*, 849–854.

(55) Mydlak, M.; Mauro, M.; Polo, F.; Felicetti, M.; Leonhardt, J.; Diener, G.; De Cola, L.; Strassert, C. A. Controlling Aggregation in Highly Emissive Pt(II) Complexes Bearing Tridentate Dianionic N^N^N Ligands. Synthesis, Photophysics, and Electroluminescence. *Chem. Mater.* **2011**, *23*, 3659–3667.

(56) Kui, A. C. F.; Chow, P. K.; Tong, G. S. M.; Lai, S.-L.; Cheng, G.; Kwok, C.-C., Low, K.-H.; Ko, M. Y.; Che, C.-M. Robust Phosphorescent Platinum(II) Complexes Containing Tetradentate O^N^C^N Ligands: Excimeric Excited State and Application in Organic White-Light-Emitting Diodes. *Chem. Eur. J.* **2013**, *19*, 69–73.

(57) Wolfbeis, O. S. Materials for Fluorescence-Based Optical Chemical Sensors. *J. Mater. Chem.* **2005**, *15*, 2657–2669.

(58) Liu, C.; Song, X.; Rao, X.; Xing, Y.; Wang, Z.; Zhao, J.; Qiu, J. Novel Triphenylamine-Based Cyclometalated Platinum(II) Complexes for Efficient Luminescent Oxygen Sensing. *Dye. Pigment.* **2014**, *101*, 85–92.

(59) De Haas, R. R.; Van Gijlswijk, R. P. M.; Van Der Tol, E. B.; Zijlmans, H. J. M. A. A. .; Bakker-Schut, T.; Bonnet, J.; Verwoerd, N. P.; Tanke, H. J. Platinum Porphyrins as Phosphorescent Label for Time-Resolved Microscopy. *J. Histochem. Cytochem.* **1997**, *45*, 1279–1292.

(60) Lo, K. K.-W.; Chung, C.-K.; Lee, T. K.-M.; Lui, L.-H.; Tsang, K. H.-K.; Zhu, N. New Luminescent Cyclometalated Iridium(III) Diimine Complexes as Biological Labeling Reagents. *Inorg. Chem.* **2003**, *42*, 6886–6897.

(61) Baldo, M. A.; Thompson, M. E.; Forrest, S. R. Excitonic Singlet-Triplet Ratio in a Semiconducting Organic Thin Film. *Phys. Rev. B* **1999**, *60*, 422–428.

(62) Yersin, H. Triplet Emitters for OLED Applications. Mechanism of Exciton Trapping and Control of Emission Properties. *Top. Curr. Chem.* **2004**, *241*, 1–26.

(63) Williams, J. A. G. Photochemistry and Photophysics of Coordination Compounds: Platinum. *Top. Curr. Chem.* **2007**, *281*, 205–268.

(64) Chassot, L.; Von Zelewsky, A.; Sandrini, D.; Maestri, M.; Balzani, V. Photochemical Preparation of Luminescent Platinum(IV) Complexes via Oxidative Addition on Luminescent Platinum(II) Complexes. *J. Am. Chem. Soc.* **1986**, *108*, 6084–6085.

(65) Russel, M. D.; Gouterman, M.; Van Zee, J. A. Excitation-EmissionLlifetime Analysis of Multicomponent Systems - III. Platinum, Palladium and Rhodium Porphryins. *Spectrochim. Acta A* **1988**, *44A*, 873–882.

(66) Vezzu, D. A. K.; Deaton, J. C.; Jones, J. S.; Bartolotti, L.; Harris, C. F.; Marchetti, A. P.; Kondakova, M.; Pike, R. D.; Huo, S. Highly Luminescent Tetradenate Bis-Cyclometalated Platinum Complexes: Design, Synthesis, Structure, Photophysics, and Electroluminescence Application. *Inorg. Chem.* **2010**, *49*, 5107–5119.

(67) Treibs, A. Metal Complexes of Porphyrins. *Justus Liebigs Ann. Chem.* **1969**, *728*, 115–143.

(68) Callis, J. B.; Knowles, J. M.; Gouterman, M. Porphyrins. XXVI. Triplet Excimer Quenching of Free Base, Zinc, Palladium, and Platinum Complexes. *J. Phys. Chem.* **1973**, *77*, 154–157.

(69) Kwong, R. C.; Sibley, S.; Dubovoy, T.; Baldo, M.; Forrest, S. R.; Thompson, M. E. Efficient, Saturated Red Organic Light Emitting Devices Based on Phosphorescent Platinum(II) Porphyrins. *Chem. Mater.* **1999**, *11*, 3709–3713.

(70) Lai, S.-W.; Hou, Y.-J.; Che, C.-M.; Pang, H.-L.; Wong, K.-Y.; Chang, C. K.; Zhu, N. Electronic Spectroscopy, Photophysical Properties, and Emission Quenching Studies of an Oxidatively Robust Perfluorinated Platinum Porphyrin. *Inorg. Chem.* **2004**, *43*, 3724–3732.

(71) Waskitoaji, W.; Hyakutake, T.; Watanabe, M.; Nishide, H. Pt-Porpholactone- and -Porphyrin-Based Luminescent Sensory Polymer Coating for Visualization of Oxygen Pressure Distribution on Biplanar Surface. *React. Funct. Polym.* **2010**, *70*, 669–673.

(72) Xiang, H.; Zhou, L.; Feng, Y.; Cheng, J.; Wu, D.; Zhou, X. Tunable Fluorescent/Phosphorescent Platinum(II) Porphyrin-Fluorene Copolymers for Ratiometric Dual Emissive Oxygen Sensing. *Inorg. Chem.* **2012**, *51*, 5208–5212.

(73) Lin, Y.-Y.; Chan, S.-C.; Chan, M. C. W.; Hou, Y.-J.; Zhu, N., Che, C.-M.; Liu, Y.; Wang, Y. Structural, Photophysical, and Electrophosphorescent Properties of Platinum(II) Complexes Supported by Tetradenate N_2O_2 Chelates. *Chem. Eur. J.* **2003**, *9*, 1264–1272.

(74) Che, C.-M.; Chan, S.-C.; Xiang, H.-F.; Chan, M. C. W.; Liu, Y.; Wang, Y. Tetradentate Schiff Base Platinum(II) Complexes as New Class of Phosphorescent Materials for High-Efficiency and White-Light Electroluminescent Devices. *Chem. Commun.* **2004**, 1484–1485.

(75) Xiang, H.-F.; Chan, S.-C.; Wu, K., K.-Y.; Che, C.-M.; Lai, P. T. High-Efficiency Red Electrophosphorescence Based on Neutral Bis(pyrrole)-Diimine Platinum (II) Complex. *Chem. Commun.* **2005**, 1408–1410.

(76) Feng, K.; Zuniga, C.; Zhang, Y.-D.; Kim, D.; Barlow, S.; Marder, S. R.; Brédas, J. L.; Weck, M. Norbornene-Based Copolymers Containing Platinum Complexes and Bis(carbazolyl)benzene Groups in Their Side-Chains. *Macromolecules* **2009**, *42*, 6855–6864.

(77) Elsegood, M. R. J.; Lake, A. J.; Smith, M. B. A Noval Fluorene-Containing κ4-P2N2-Tetradetnate Platinum(II) Complex. *Dalton Trans.* **2009**, 30–32.

(78) Kui, S. C. F.; Chow, P. K.; Cheng, G.; Kwok, C.-C.; Kwong, C. L.; Low, K.-H.; Che, C.-M. Robust Phosphorescent Platinum(II) Complexes with Tetradentate O^N^C^N Ligands: Highly Efficiency OLEDs with Excellent Efficiency Stability. *Chem. Commun.* **2013**, *49*, 1497–1499.

(79) Turner, E.; Bakken, N.; Li, J. Cyclometalated Platinum Complexes with Luminescent Quantum Yields Approaching 100%. *Inorg. Chem.* **2013**, *52*, 7344–7351.

(80) Li, K.; Guan, X.; Ma, C.-W.; Lu, W.; Chen, Y.; Che, C.-M. Blue Electrophosphorescent Organoplatinum(II) Complexes with Dianionic Tetradentate Bis(carbene) Ligands. *Chem. Commun.* **2011**, *47*, 9075–9077.

(81) Saucedo, H. F.; Cortes-Llamas, S. A.; Vengoechea-Gómez, F. A.; Rufino-Felipe, E.; Crespo-Velasco, N. T.; Muñoz-Hernández, M.-A. Synthesis and Characterization of Aluminum Complexes Incorporating Schiff Base Ligands Derived from Pyrrole-2-Carboxaldehyde. *Main Gr. Chem.* **2011**, *10*, 127–140.

(82) Ganjali, M. R.; Ravanshad, J.; Hosseini, M.; Salavati-Niasari, M. Novel Dy(III) Sensor Based on a New Bis-Pyrrolidene Schiff's Base. *Electroanalysis* **2004**, 1771–1776.

(83) Reza, M.; Ghesmi, A.; Hosseini, M. Novel Terbium(III) Sensor Based on a New Bis-Pyrrolidene Schiff 's Base. *Sensors Actuators B* **2005**, *105*, 334–339.

(84) Adamovich, V.; Brooks, J.; Tamayo, A.; Alexander, A. M.; Djurovich, P. I.; D'Andrade, B. W.; Adachi, C.; Forrest, S. R.; Thompson, M. E. High Efficiency Single Dopant White Electrophosphorescent Light Emitting Diodes. *New J. Chem.* **2002**, *26*, 1171–1178.

(85) Lai, S.; Chan, M. C. W.; Cheung, K.; Che, C. Spectroscopic Properties of Luminescent Platinum (II) Complexes Containing 4,4',4"-Tri-Tert-Butyl-2,2':6',2'-Terpyridine (^{t}Bu$_3$tpy). Crystal Structures of [Pt(^{t}Bu$_3$tpy)Cl]ClO$_4$ and [Pt(^{t}Bu$_3$tpy){CH$_2$C(O)Me}]ClO$_4$. *Inorg. Chem.* **1999**, *38*, 4262–4267.

(86) Lü, X.; Wong, W.-Y.; Wong, W.-K. Self-Assembly of Luminescent Platinum-Salen Schiff-Base Complexes. *Eur J. Inorg. Chem.* **2008**, 523–528.

(87) Che, C.-M.; Kwok, C.-C.; Lai, S.-W.; Rausch, A. F.; Finkenzeller, W. J.; Zhu, N.; Yersin, H. Photophysical Properties and OLED Applications of Phosphorescent Platinum(II) Schiff Base Complexes. *Chem. Eur. J.* **2010**, *16*, 233–247.

(88) Borisov, S. M.; Saf, R.; Fischer, R.; Klimant, I. Synthesis and Properties of New Phosphorescent Red Light-Excitable Platinum(II) and Palladium(II) Complexes with Schiff Bases for Oxygen Sensing and Triplet-Triplet Annihilation-Based Upconversion. *Inorg. Chem.* **2013**, *52*, 1206–1216.

(89) Katsuki, T. Catalytic Asymmetric Oxidations Using Optically Active (Salen)Manganese(III) Complexes as Catalysts. *Coord. Chem. Rev.* **1995**, *140*, 189–214.

(90) Mejía, M. L.; Agapiou, K.; Yang, X.; Holliday, B. J. Seeded Growth of CdS Nanoparticles within a Conducting Metallopolymer Matrix. *J. Am. Chem. Soc.* **2009**, *131*, 18196–18197.

(91) Béreau, V.; Jubéra, V.; Arnaud, P. Kaibe, A.; Guionneau, P.; Sutter, J.-P. Modulation of the Luminescent Quantum Efficiency for Blue Luminophor {Al(saophen)}+ by Ester-Substituents. *Dalton Trans.* **2010**, *39*, 2070–2077.

(92) Hang, X-C.; Fleetham, T.; Turner, E.; Brooks, J.; Li, J. Highly Efficient Blue-Emitting Cyclometalated Platinum(II) Complexes by Judicious Molecular Design. *Angew. Chem. Int. Ed.* **2013**, *52*, 6753–6756.

(93) Sajoto, T.; Djurovich, P. I.; Tamayo, A.; Yousufuddin, M.; Bau, R.; Thompson, M. E.; Holmes, R. J.; Forrest, S. R. Blue and Near-UV Phosphorescence from Iridium Complexes with Cyclometalated Pyrazolyl or N-Heterocyclic Carbene Ligands. *Inorg. Chem.* **2005**, *44*, 7992–8003.

(94) Haneder, S.; Da Como, E.; Feldmann, J.; Lupton, J. M.; Lennartz, C.; Erk, P.l; Fuchs, E.; Molt, O.; Münster, I.; Schildknecht, C.; Wagenblast, G. Controlling the Radiative Rate of Deep-Blue Electrophosphorescent Organometallic Complexes by Singlet-Triplet Gap Engineering. *Adv. Mater.* **2008**, *20*, 3325–3330.

(95) Sasabe, H.; Takamatsu, J.; Motoyama, T.; Watanabe, S.; Wagenblast, G.; Langer, N.; Molt, O.; Fuchs, E.; Lennartz, C.; Kido, J. High-Efficiency Blue and White Organic Light-Emitting Devices Incorporating a Blue Iridium Carbene Complex. *Adv. Mater.* **2010**, *22*, 5003–5007.

(96) Wong, K.-H.; Chan, M. C.-W.; Che, C.-M. Modular Cyclometalated Platinum(II) Complexes as Luminescent Molecular Sensors for pH and Hydrophobic Binding Regions. *Chem. Eur. J.* **1999**, *5*, 2845–2849.

(97) Yoon, M. S.; Dowook, R.; Kim, J.; Ramesh, R. . A. K. H. Cyclometalated Platinum(II) Complexes Derived from a Chiral Pyridine Ligand: Synthesis, Structure, and Catalytic Activity. *Bull. Korean Chem. Soc.* **2007**, *28*, 2045–2050.

(98) Vezzu, D. A. K.; Lu, Q.; Chen, Y.-H.; Huo, S. Cytotoxicity of Cyclometalated Platinum Complexes Based on Tridentate NCN and CNN-Coordinating Ligands: Remarkable Coordination Dependence. *J. Inorg. Biochem.* **2014**, *134*, 49–56.

(99) Kido, J.; Okamoto, Y. Organo Lanthanide Metal Complexes for Electroluminescent Materials. *Chem. Rev.* **2002**, *102*, 2357–2368.

(100) Yang, C.-H.; Mauro, M.; Polo, F.; Wantanabe, S.; Muenster, I.; Fröhlich, R. De Cola, L. Deep-Blue-Emiting Heteroleptic Iridium(III) Complexes Suited for Highly Efficient Phosphorescent OLEDs. *Chem. Mater.* **2012**, *24*, 3684–3695.

(101) Gu, J.-F.; Xie, G.-H.; Zhang, L.; Chen, S.-F.; Lin, Z.-Q.; Zhang, Z.-S.; Zhao, J.-F.; Xie, L.-H.; Tang, C.; Zhao, Y.; Liu, S.-Y.; Huang, W. Dumbbell-Shaped Spirocyclic Aromatic Hydrocarbon to Control Intermolecular $\pi-\pi$ Stacking Interaction for High-Performance Nondoped Deep-Blue Organic Light-Emitting Devices. *J. Phys. Chem. Lett.* **2010**, *1*, 2849–2853.

(102) Gong, J.-R.; Wan, L.-J.; Lei, S.-B.; Bai, C.-L.; Zhang, X.-H.; Lee, S.-T. Direct Evidence of Molecular Aggregation and Degradation Mechanism of Organic Light-Emitting Diodes under Joule Heating: An STM and Photoluminescence Study. *J. Phys. Chem. B* **2005**, *109*, 1675–1682.

(103) Shi, Y.; Luo, S.-C.; Fang, W.; Zhang, K.; Ali, E. M.; Boey, F. Y. C.; Ying, J. Y.; Wang, J.; Yu, H.; Li, L.-J. Work Function Engineering of Electrodes via Electropolymerization of Ethylenedioxythiophenes and Its Derivatives. *Org. Electron.* **2008**, *9*, 859–863.

(104) Segura, L.; Go, R.; Reinold, E.; Băuerle, P. Synthesis and Electropolymerization of a Perylenebisimide-Functionalized 3,4-Ethylenedioxythiophene (EDOT) Derivative. *Org. Lett.* **2005**, *7*, 2345–2348.

(105) Luo, S.; Ali, E. M.; Tansil, N. C.; Yu, H.; Gao, S.; Kantchev, E. A. B.; Ying, J. Y. Poly(3,4-Ethylenedioxythiophene) (PEDOT) Nanobiointerfaces: Thin, Ultrasmooth, and Functionalized PEDOT Films with in Vitro and in Vivo Biocompatibility. *Langmuir* **2008**, *24*, 8071–8077.

(106) Luo, J.; Li, X.; Hou, Q.; Peng, J. B.; Yang, W.; Cao, Y. High-Efficiency White-Light Emission from a Single Copolymer: Fluorescent Blue, Green, and Red Chromophores on a Conjugated Polymer Backbone. *Adv. Mater.* **2007**, *19*, 1113–1117.

(107) Hesterberg, T. W. Phosphorescent Cyclometalated Iridium(III) Complexes and Corresponding Conducting Metallopolymers, Ph.D. Thesis, The University of Texas at Austin, 2012.

(108) Chen, X. Luminescent and Magnetic Materials Based on Conducting Metallopolymers, Ph.D. Thesis, The University of Texas at Austin, 2011.

(109) Rausch, A. F.; Murphy, L.; Williams, J. a G.; Yersin, H. Probing the Excited State Properties of the Highly Phosphorescent Pt(dpyb)Cl Compound by High-Resolution Optical Spectroscopy. *Inorg. Chem.* **2009**, *48*, 11407–11414.

(110) Bérubé, M.; Poirier, D. Synthesis of Simplified Hybrid Inhibitors of Type 1 17B-Hydroxysteroid Dehydrogenase via Cross-Metathesis and Sonogashira Coupling Reactions. *Org. Lett.* **2004**, *6*, 3127–3130.

(111) Williams, D. B. G.; Lawton, M. Drying of Organic Solvents: Quantitative Evaluation of the Efficiency of Several Desiccants. *J. Org. Chem.* **2010**, *75*, 8351–8354.

(112) Zhu, S. S.; Swager, T. M. Conducting Polymetallorotaxanes: Metal Ion Mediated Enhancements in Conductivity and Charge Localization. *J. Am. Chem. Soc.* **1997**, *119*, 12568–12577.

(113) Kubiczak, G. A.; Oesch, F.; Borlakoglu, J. T.; Kunz, H.; Robertson, L. W. A Unique Approach to the Synthesis of 2,3,4,5-Substituted Polybrominated Biphenyls: Quantitation in FireMaster FF-1 and FireMaster BP-6. *J. Agric. Food. Chem.* **1989**, *37*, 1160–1164.

(114) Swingle, S. F. Main Group Semiconducting Materials: Boron Arsenide and an Ester-Functionalized Salophen Aluminum Polymer, Ph.D. Thesis, The University of Texas at Austin, 2013.

(115) Beraeu, V.; Duhayon, C.; Sournia-Saquet, A.; Sutter, J. Tuning of the Emission Efficiency and HOMO − LUMO Band Gap for Ester-Functionalized {Al(salophen)(H_2O)$_2$}+ Blue Luminophors. *Inorg. Chem.* **2012**, *51*, 1309–1318.

(116) Milum, K. M.; Kim, Y. N.; Holliday, B. J. Pt-[NCN] Pincer Conducting Metallopolymers That Display Redox-Attenuated Metal-Ligand Interactions. *Chem. Mater.* **2010**, *22*, 2414–2416.

(117) *Handbook of Advanced Electronic and Photonic Materials and Devices*; Nalwa, H. S., Ed.; Academic Press: San Diego, 2001.

(118) Zeynizadeh, B.; Setamdideh, D. NaBH4/Charcoal: A New Synthetic Method for Mild and Convenient Reduction of Nitroarenes. *Synth. Commun.* **2006**, *36*, 2699–2704.

(119) Pepitone, M. F.; Eaiprasertsak, K.; Hardaker, S. S.; Gregory, R. V. Synthesis of bis[(3,4-ethylenedioxy)thien-2-Yl]-Substituted Benzenes. *Tetrahedron Lett.* **2004**, *45*, 5637–5641.

(120) Chahma, M.; Gilroy, J. B.; Hicks, R. G. Linear and Branched Electroactive Polymers Based on ethylenedioxythiophene–Triarylamine Conjugates. *J. Mater. Chem.* **2007**, *17*, 4768.